Enclosure 4

MFN 08-419

NEDO-33082, Revision 2
ESBWR Scaling Report, April 2008

Non-Proprietary Information

NEDO-33082
Revision 2
Class I
neDRF Section 0000-0082-9695, Rev 1
April 2008

ESBWR Scaling Report

Authors

Revision 2: Dr. P. Saha

Revision 1: Dr. R. E. Gamble
A. F. Fanning
B. Vaishnavi

NON-PROPRIETARY INFORMATION NOTICE

This is a non-proprietary version of the document NEDC-33082P, which has the proprietary information removed. Portions of the document that have been removed are indicated by open and closed double brackets as shown here [[ ]].

IMPORTANT NOTICE REGARDING CONTENTS OF THIS REPORT

Please read carefully

The information contained in this document is furnished **for the purpose of supporting the NRC review of the certification of the ESBWR.** The only undertakings of GE Hitachi with respect to information in this document are contained in contracts between GE Hitachi and any participating utilities, and nothing contained in this document shall be construed as changing those contracts. The use of this information by anyone other than those for which it is intended is not authorized; and with respect to **any unauthorized use**, GE Hitachi makes no representation or warranty, and assumes no liability as to the completeness, accuracy, or usefulness of the information contained in this document.

REVISION 2

Revision 2 incorporates the information provided to NRC via GE letter MFN 06-225, "Response to NRC Request for Additional Information Letter No. 4 Related to ESBWR Design Certification Application – ESBWR Scaling Analysis – RAI Number 6.3-1," July 18, 2006. Specifically, this revision addresses the scaling issues related to ESBWR core power increase from 4000 MWt to 4500 MWt (12.5 percent) and change of configuration (GDCS gas space connected to the drywell instead of the wetwell). Simplified confirmatory scaling analysis, as requested by the NRC in RAI Number 6.3-1 and responded to by GE in MFN 06-225, is also included in a new Section 10.

Revision 2 still shows the RAI responses related to Rev. 0 in footnotes. The details are in NEDC-33083P-A (In section: NRC RAI and Responses – ESBWR Scaling Report NEDC-33082P), March 2005.

Technical contributions made by Mike Cook, Dr. James R. Fitch and Dr. Bharat S. Shiralkar to Revision 2 are gratefully acknowledged.

REVISION 1

Revision 1 incorporates changes requested to respond to NRC Requests for Additional Information (RAIs) related to Rev. 0. All changes between Rev 0 and Rev 1 are accompanied by left side vertical change bars. Errors in Tables (A1 to A14) have been corrected. These do not affect any conclusions reached in the reports.

Table of Contents

Table of Contents (cont'd)

List of Tables

List of Figures

List of Figures

Nomenclature and Abbreviations

Symbols	Description	Units
A	Surface area	m^2
a	Cross-sectional area	m^2
c_p	Specific heat at constant pressure	J/kg-K
c_v	Specific heat at constant volume	J/kg-K
d	Characteristic length	m
D	Diameter	m
E	Internal energy	J
e	Specific internal energy	J/kg
f	Darcy friction factor	*
F_n	Loss coefficient for pipe segment (Eq. 3.2-2b)	*
F/a^2	Sum of loss coefficients divided by area^2 (Eq. 3.2-4b)	$1/m^4$
H	Height or submergence	m
h	Heat transfer coefficient	W/m^2-K
h	Specific enthalpy	J/kg
h_{fg}	Latent heat of vaporization	J/kg
G	Mass flux	kg/m^2-s
g	Acceleration of gravity	9.81 m/s^2
j, J	Volumetric flow rate	m^3/s
k	Ratio of specific heats, c_p/c_v	*
k	Thermal conductivity	W/m-K
k_n	Local loss coefficient of segment n	*
ℓ_n	Length of segment n	m
L/a	Sum of lengths divided by areas (Eq. 3.2-4c)	1/m
L	Length	m
M	Mass	kg
$\dot{m}$	Mass flow rate	kg/s
P	Pressure	Pa
$\wp$	Perimeter	m
$\dot{Q}$	Heat rate	W
R	Gas constant	J/kg-K
R	System scale (prototype to model)	*
T	Temperature	K

* = dimensionless

Nomenclature and Abbreviations (cont'd)

t	Time	s
u	Velocity	m/s
V	Volume	m^3
v	Specific volume	m^3/kg
W	Mass flow rate	kg/s
y	Mass fraction	*
z	Axial coordinate along flow path	m
Fo	Fourier number	*
Nu = h d/k	Nusselt number	*

Greek Letters

Symbols	Description	Units
Δ	Change in reference parameter	
α	Void fraction	*
μ	Viscosity	kg/m-s
Π	Nondimensional group	*
ρ	Density	kg/m^3
τ	Time constant	s
ω	Characteristic frequency	s^{-1}
∂	Partial differential operator	
Γ	Net vaporization rate	kg/m^3-s
ψ	Vapor mass function	*
Σ	Summation	

Subscripts

Symbols	Description
Decay	Decay heat
e	Energy equation PI group
g	Gas
g	Gravity
h	Submergence or hydrostatic head term
hp	Enthalpy-pressure
IC	Isolation condenser
i	Mass flow path (for summations)
in	Inertia
j	Constituent (for summations)
k	Sensible energy flow path (for summations)

* = dimensionless

Nomenclature and Abbreviations (cont'd)

L, ℓ	Liquid
LG	Change from liquid to gas
loss	Friction and form loss
M	Mass
M	Mass equation PI group
MV	Main Vent
mech	Mechanical compression due to mass addition term
mod	Model or test facility
m	Generic junction pipe
n	Pipe segment
nv	Vertical portion of pipe segment
o	Initial value
P	Pressure rate equation PI group
PCC	Passive Containment Cooling Condenser
PCCS	Passive Containment Cooling System
$\dot{P}$	Flashing term
$\dot{P}1$	Flashing term
$\dot{P}2$	Flashing term
p	Pipe
pch	Phase change
pd	Pressure difference
prot	Prototype or ESBWR
R	Reactor pressure vessel, scale factor between prototype and model
RPV	Reactor Pressure Vessel
r	Reference parameter
sub	Subcooling or submergence
v	Refers to vertical distance
VB	Vacuum breaker
W	Flow
Wh	Energy flow due to enthalpy
$\dot{Q}$	Energy rate
$\dot{V}$	Volume change

Additional subscripts are defined in the text.

Nomenclature and Abbreviations (cont'd)

Superscripts

Symbols	Description
'	Denotes derivative with respect to pressure
•	Denotes derivative with respect to time
+	Nondimensional variable

Abbreviations

Symbols	Description
ADS	Automatic Depressurization System
BAF	Bottom of Active Fuel
CHF	Critical Heat Flux
DBA	Design Basis Accident
DPV	Depressurization Valve
DW	Drywell
FWLB	Feedwater Line Break
GDCS	Gravity-Driven Cooling System
GDLB	GDCS line break
GE	General Electric Company
GEH	GE Hitachi Nuclear Energy
GIST	GDCS Integrated Systems Test
H2TS	Hierarchical Two-Tier Scaling
h.t.c.	Heat transfer coefficient
IC	Isolation Condenser
ICS	Isolation Condenser System
LOCA	Loss-of-Coolant Accident
MIT	Massachusetts Institute of Technology
MSL	Main Steam Line
MSLB	Main Steam Line Break
NB	No-Break
NRC	Nuclear Regulatory Commission
PCC	Passive Containment Condenser
PCCS	Passive Containment Cooling System
PIRT	Phenomena Identification and Ranking Table
PSI	Paul Scherrer Institute
RPV	Reactor Pressure Vessel
SBWR	Simplified Boiling Water Reactor
SC	Pressure Suppression Chamber
SIT	Systems Interaction Tests
SLCS	Standby Liquid Control System

Nomenclature and Abbreviations (cont'd)

SP	Suppression Pool
SRV	Safety/Relief Valve
TAF	Top of Active Fuel
TAPD	Test and Analysis Program Description
UCB	University of California at Berkeley
WW	Wetwell
Π	Refers to nondimensional group

EXECUTIVE SUMMARY

The **objective** of this scaling report is to show that the test facilities properly "scale" the important phenomena and processes identified in the ESBWR PIRT and/or provide assurance that the experimental observations from the test programs are sufficiently representative of ESBWR behavior for use in qualifying TRACG for ESBWR licensing calculations. This objective is met through a series of steps described below.

Section 2 provides an overview of the methodology used. The scaling methodology follows the hierarchical two-tiered scaling methodology composed of top-down scaling, which identifies processes important to the system behavior and a bottom-up, or phenomena level, scaling that looks at the characteristics of the processes identified as important from the top-down scaling

Section 3 describes the equations that govern the behavior of parameters important to the behavior and safety of the ESBWR, namely: RPV liquid mass, pressure and void fraction; containment pressure; and suppression pool energy. These equations are normalized in subsequent sections to provide scaling laws and evaluate the ESBWR and test facilities.

In **Section 4** the system governing equations are normalized using general reference parameters in order to arrive at a set of **general scaling criteria** that can be used for test facility design. These are the criteria that were used for the design of the test facilities included in this report. Brief **descriptions of the test facilities** are provided in **Section 5** as well as references to where the details of the test facilities can be found. In general the design of the experimental facilities and the conduct of the various tests were guided by consideration of the proper modeling and simulation of the key phenomena governing the performance of the passive safety systems. The implications of the scaling adjustments for the ESBWR are minimized by the fact that all of the tests were performed at prototypical temperature and pressure and with prototypical or near-prototypical elevations and elevation differences. These are the key variables and parameters governing the performance of the passive safety systems.

It should be noted that the general scaling criteria are very useful for facility design but do not provide a measure of what phenomena are important to the system behavior, nor are they useful in identifying distortions in the test facilities once they are completed. Instead this is accomplished with a more detailed nondimensionalization of the governing equations as described in **Section 6**. The nondimensionalization developed in Section 6 provides detailed scaling equations that can be used to identify which phenomena are important to the system behavior and therefore should be well scaled in the test facilities. Additionally these equations can be used to assess if this goal had been achieved in the tests.

In **Section 7** the detailed scaling equations from Section 6 are applied to the ESBWR (4500 MWt) to identify the processes important to the system behavior. The parameters important to safety are identified as: the RPV liquid mass that ensures that the core remains covered; the RPV pressure which is important in determining the timing of the GDCS injection; and the containment pressure which is important to assure that the containment is not breached during an accident. The LOCA transient is broken down into four temporal phases – late blowdown, GDCS transition, reflood, and long-term decay heat removal – within which the dominant phenomena remain unchanged and the phenomena magnitudes are relatively constant.

The **results for the ESBWR** indicate that a small number of processes are important to the behavior of the system parameters of interest (liquid mass and pressure). For the RPV liquid mass the important processes are flashing due to depressurization, boiling due to energy input from stored energy and decay heat, and GDCS flow (Figures 7-1 through 7-3). Although other parameters influence the behavior of the liquid mass during the short GDCS transition phase, the mass change during this phase is very small and therefore not very significant to the overall mass loss in the vessel. For the RPV pressure the dominant phenomena is energy flow through the ADS system (Figures 7-4 and 7-5).

The wetwell pressure controls the containment pressure and the drywell is found to be unimportant to the containment response during the transient period considered (late blowdown onward). The drywell is found to act in a manner similar to a large pipe that transfers steam from the RPV to the main vents and PCCs (Figure 7-6). The time constant for the DW pressure is very short compared to the wetwell and the pressure in the DW therefore rapidly adjusts to the boundary condition presented by the WW pressure. The primary contribution of the DW is that its volume determines the quantity of noncondensible gas that must be accommodated by the WW in the long term. The important process for the containment pressure is the movement of noncondensible gas from the DW to the WW (Figure 7-7).

In **Section 8**, the same scaling method is applied to the test facilities to evaluate if the phenomena identified as important to the ESBWR (4500 MWt and 4000 MWt) are scaled properly in the test facilities. Figures 8-1 through 8-7 show that all of the important phenomena magnitudes are well scaled in the test facilities.

Proper bottom-up scaling is a common problem with reduced scale facilities, where aspect ratio, surface to volume ratio and other geometric considerations make it difficult to simulate local effects. A review of the processes important to the system behavior concludes that they are either well scaled from the bottom-up perspective (ADS flow, PCC heat removal, SP mixing) or can be addressed through parametric studies and a bounding approach with TRACG (stratification in gas space, SP mixing). Much of the bottom-up results are borrowed from the SBWR scaling report rather than repeating them in this report.

Although it does not constitute scaling analyses, **absence of significant distortions is confirmed** by comparing key parameters from tests done at a wide variety of scales in **Section 9**. The comparisons shown in Figures 9-1 through 9-5 show a similar behavior at all scales indicating that the important processes were well represented in the tests and that no significant scale distortions occurred.

Results of confirmatory scaling analysis, based on continuous calculation in non-dimensional time domain, for short-term RPV behavior are presented in Section 10.1. The results are in agreement with those presented in Section 8.3. As discussed in Section 10.2, similar confirmatory analysis is not required for the long-term cooling phase; results presented in Section 8.4 are sufficient for the scaling purposes.

Overall the test facilities are demonstrated to adequately simulate the phenomena important to the ESBWR. Although there are distortions in the facilities, they are found to be in areas that do

not affect significant parameters for the system behavior. As such, the test data obtained from these facilities are suitable for qualification of TRACG.

1.0 INTRODUCTION

1.1 Background

In the 1980's, GE began a project to design and certify a new Boiling Water Reactor (BWR) design which incorporates advanced, passive safety features. The Simplified BWR (SBWR) experienced design evolution from its beginning until the mid 1990's.

The final design was a natural circulation reactor rated at 670 MWe with a typical BWR pressure suppression containment system. The major safety systems are:

- Gravity-Driven Cooling System (GDCS), which during a postulated loss-of-coolant accident (LOCA), supplies makeup water to the reactor core from a pool located above the core.
- Isolation Condenser System (ICS), which during an isolation transient, uses natural circulation to remove core decay heat from the reactor pressure vessel (RPV) by condensing steam from the RPV and returning condensate to the RPV.
- Passive Containment Cooling System (PCCS), which during a postulated LOCA, removes heat from the containment by condensing steam from the drywell and returns the condensate to the GDCS pool.

A comprehensive experimental program was carried out to demonstrate the thermal-hydraulic performance of these passive systems and their components. The philosophy of testing was to focus on those features and components that are SBWR-unique or performance-critical, and to test over a range that spans and bounds the SBWR parameters of importance. In addition to demonstrating the performance of these systems, these tests were conducted to provide test data to be used to qualify the TRACG computer code for SBWR application. TRACG is the GE version of TRAC-BWR.

Major SBWR test programs were conducted at the GIST, GIRAFFE, PANTHERS, and PANDA test facilities. GIST, GIRAFFE, and PANDA were integral systems tests focusing on different aspects of the SBWR response to LOCAs. Figure 1-1 shows the relationship of these tests to the LOCA phases. These facilities also simulated the SBWR at different system scales (1:500 for GIST, 1:400 for GIRAFFE and 1:25 for PANDA). PANTHERS tests were full-scale component tests of prototypical ICS and PCCS condensers.

In the mid 1990's, GE redirected the focus of SBWR programs from plants of the 670 MWe size to plants of 1000 MWe or larger. However, GE completed key ongoing test and analysis activities to make this data available for other applications of the SBWR technology.

The larger plant design evolved into the 4500 MWt ESBWR design. In this report, scaling data are presented for both the previous ESBWR [1-1] design value of 4000 MWt and the present ESBWR design value of 4500 MWt. The ESBWR is in general a first principles scale-up of the SBWR[1]. The testing done for the SBWR is still representative of the ESBWR, but at smaller scale (1:1000 for GIST, 1:800 for GIRAFFE and 1:50 for PANDA). To expand the experimental

[1] RAI 16

database, additional tests were run in the PANDA facility at a scale of 1:50, representative of the ESBWR.

The *ESBWR Test and Analysis Program Description* (TAPD) [1-2] describes a comprehensive integrated plan that addresses the testing elements needed for analysis of ESBWR performance. The TAPD provides the technical basis for determining the performance of the plant during transients and accidents. It provides the rationale for the diverse experimental and analytical efforts in support of ESBWR certification based on the Phenomena Identification and Ranking Tables (PIRT). These tables listed the phenomena and interactions between systems important to ESBWR transient and accident analysis.

This report goes on to provide an evaluation of the test facilities with respect to the scaling of the important phenomena and processes identified in the ESBWR PIRT. The study demonstrates that the experimental observations from the test programs were representative of ESBWR behavior and that the data are useful for TRACG qualification.

1.2 Objectives and Scope of Scaling Analysis

The scope of the scaling study reported here was to:

- Describe the scaling philosophy and strategy used in designing the various tests.
- Provide the applicable scaling laws.
- Identify important phenomena to ESBWR behavior and provide information for PIRT validation.
- Show that the test facilities properly "scale" the important phenomena and processes identified in the ESBWR PIRT and/or provide assurance that the experimental observations from the test programs are representative of ESBWR behavior.
- Identify scaling distortions and discuss their importance; in particular, identify the ways by which scaling distortions should be considered when the experimental data are used for code qualification.
- Provide the basis for showing that the experimental data cover the correct phenomena and ranges for qualifying TRACG for application to ESBWR accident analysis.

1.2.1 Accidents and Accident Phases Considered

The range of accidents considered includes the main steam line break (MSLB), as well as other breaks of the primary system, such as the GDCS line break and the bottom drain line break.

The scenario for these accidents can be roughly subdivided into four phases:

- The *blowdown phase* extending from the initiation of rapid depressurization by blowdown up to the time of GDCS initiation. The blowdown phase can be further subdivided into an *early* phase extending until the time the pressure reaches a level of about 0.8 MPa, and a *late* blowdown phase thereafter.

- A *GDCS Transition phase* covering the short period from when the RPV pressure has decreased enough that the GDCS flow to the RPV begins, to the time when the GDCS flow reaches it maximum value.

- An intermediate *GDCS phase* during which the GDCS is delivering its stored water inventory to the primary system.

- A *long-term cooling phase* beginning when the RPV inventory starts becoming replenished by the condensate flowing down from the PCCS (i.e., when the GDCS hydrostatic head necessary to drive flow into the core is made up by the PCCS condensate). At about the same time, the PCCS condensers become the dominant decay heat removal mechanism, replacing the heat sink provided by the water inventory initially stored in the GDCS pools.

The scaling analysis performed in this report is primarily directed at scaling the reactor and containment components and phenomena which are significant during the time period starting with the late blowdown phase and extending into the long-term cooling phase. As stated in Section 1.1, phenomena associated with the early stage of depressurization of a BWR vessel are well understood and are not considered to be part of the ESBWR testing program. Thus, this report deals with *post-LOCA performance* focusing on the phases of the transient following the early blowdown phase.

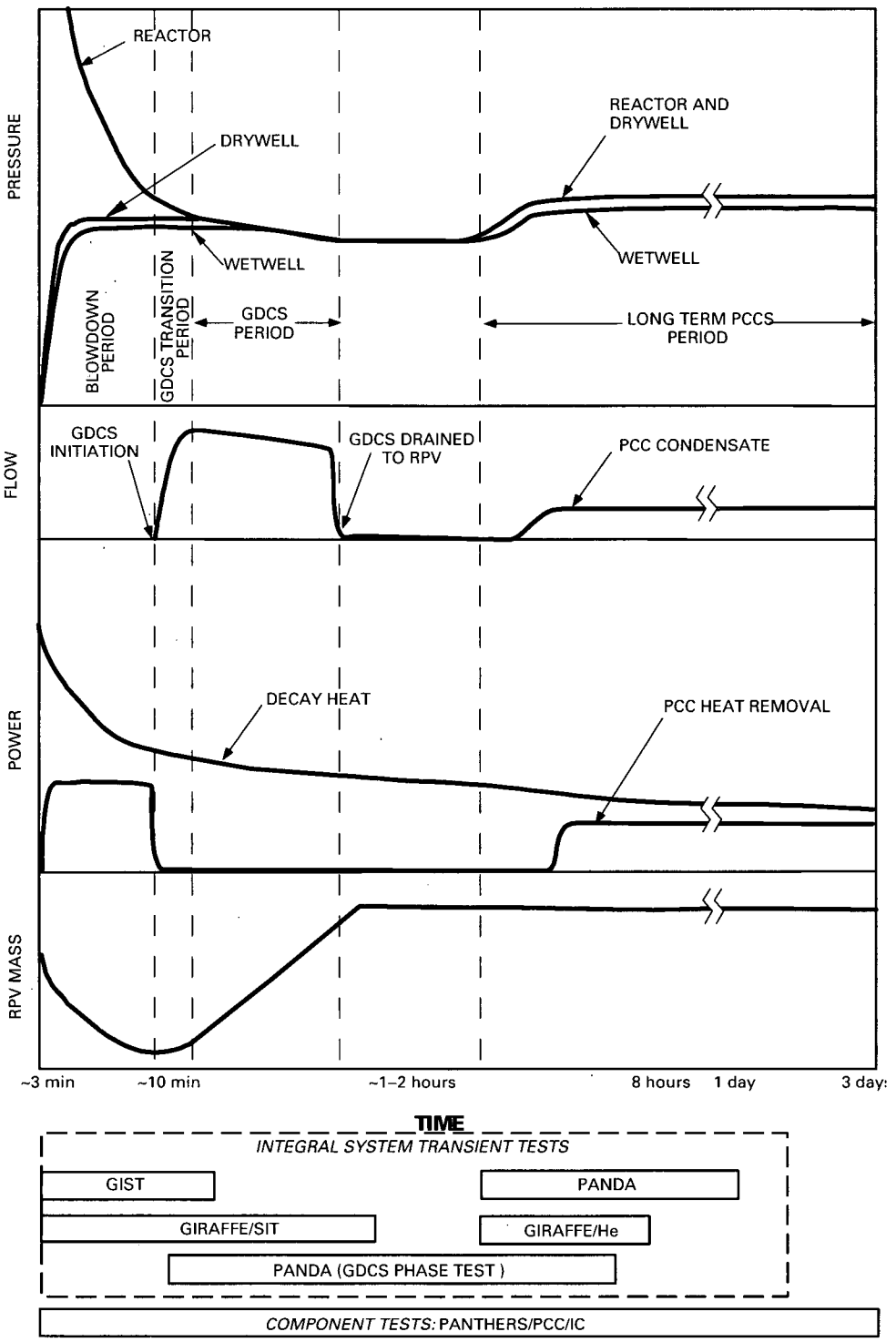

Figure 1-1 Key Variables and Test Coverage During ESBWR LOCA Phases

2.0 SCALING METHODOLOGY

2.1 The H2TS Scaling Methodology

The scaling methodology developed by an NRC Technical Program Group [2-1] was applied in this study for the purpose of evaluating the experiments and computer models in terms of how well they represent actual cooling systems and phenomena of the ESBWR.

Objectives of the NRC scaling methodology are summarized as follows:

- To provide a scaling methodology that is systematic and practical, auditable, and traceable.
- To provide the scaling rationale and similarity criteria.
- To provide a procedure for conducting comprehensive reviews of facility design, of test conditions and results.
- To ensure the prototypicality of the experimental data.
- To quantify biases due to scaling distortions or due to nonprototypical conditions.

The scaling methodology embraces the behavior of integrated subsystems and components (top-down approach), and specific processes which may occur within the subsystems (bottom-up approach).

A subsystem in the ESBWR is defined as a volume, such as the reactor vessel, drywell, wetwell air space, wetwell pool, the PCC condenser, and the isolation condenser. Global properties of a given subsystem include the pressure or the hydraulic head which drives mass flow rate, the bulk temperature differences which drive heat transfer, and the total mass and energy inflows, outflows, and storage rates. Furthermore, flow paths connecting the various volumes are included in the subsystem category because associated flow rates depend on global properties of connected volumes and resistance and inertia properties of the flow paths. Similarity laws for the ESBWR subsystems were obtained from top-down considerations.

The state within a volume may depend on phenomena that cause spatial nonuniformity in properties, such as bubble and droplet formation, density stratification of steam and noncondensibles in the drywell, or thermal plumes and stratification in both the pools and drywell. If stratification in two well-mixed superimposed layers occurs within a volume, two distinct volumes with uniform global properties will exist for the top and bottom layer subsystems formed. If complete mixing and spatial uniformity occurs within a volume, one subsystem and one global state is appropriate. If the degree of component or phase stratification varies throughout a volume, and the properties of the mass being discharged from a given location is important, it is desirable to satisfy bottom-up similarity laws which govern the stratification. Heat transfer and condensation processes in the PCCS are determined by fine-structure, local heat and mass transfer phenomena, which involve bottom-up considerations.

The magnitude of the nondimensional Π groups resulting from top-down and bottom-up scaling considerations depends on the particular LOCA phase; namely, Blowdown, GDCS Transition, Reflood and PCCS. The scaling procedure yields a unique set of Π groups for each phase, because properties at the beginning of each phase (initial states) and the dominant time responses are different.

The H2TS procedure involves writing the equations that govern the property behavior of each subsystem in the ESBWR. One set of equations gives the rates of pressurization in each volume, expressed in terms of mass and energy flow rates, and current state properties. A second set of equations provides the energy rate of change in each volume. A set of momentum equations provides the flow rate in each connecting path, ranging from transient flow when driving pressures or hydraulic heads are changing, to steady state. The details of this are shown in Section 3.

Scaling is performed by nondimensionalizing the equations governing a particular process or phase of an accident. This is accomplished classically by dividing the (dimensional) values by reference values or scales to make them nondimensional. The nondimensional variables and the various scales are then separated in two groups: (1) groups of reference scales, and (2) the so-called Π groups or Π numbers, which appear and multiply the nondimensional terms. Two parallel approaches are used for nondimensionalizing the governing equations. The first is appropriate for test facility design and results in a set of general scaling criteria that can be used in the design of test facilities. The second approach is appropriate for confirming the adequacy of test data for use in representing a specific plant system. This second approach results in an identification of important phenomena and a measure of distortions between the tests and prototype. These two approaches are summarized below and described in detail in Sections 4 and 6, respectively.

2.2 Scaling Laws for Test Design

If a test facility is perfectly scaled, then the values of all Π numbers for the prototype and the model should be perfectly matched[2]. By considering a priori perfect matching of all the Π numbers for all system components, one can obtain guidance regarding *general scaling criteria.* In deriving such general scaling criteria, one does not have to worry in particular about the magnitude of the *nondimensionalized* terms, since everything should in principle be perfectly matched. This is the analysis described in Section 4. It leads to the *general* criteria that govern scaling of the models.

The test facilities for the ESBWR test program have been designed following this basic philosophy. The resulting test facilities, as well as the ESBWR are summarized in Section 5.

2.3 Scaling for PIRT Validation and Confirmation of Test Validity

In practical cases, the model cannot be perfectly scaled. One then needs to evaluate the importance of scaling distortions. These appear as differences in the values of the pairs of Π groups calculated for the various components of the system (prototype and model). Since, for a given system and a specific Π number, several pairs of Π values may need to be calculated, the range of magnitudes that pairs of a *particular* Π group may take may be broad. For example, when Π groups containing the various flow rates entering into a control volume are considered, the magnitude of a *component* Π group will depend on the magnitude of the corresponding flow rate. To properly evaluate the magnitude of scaling distortions, in defining the Π numbers, one should use reference scales making the magnitude of all the *nondimensional* terms of order one.

[2] RAI 253

The Π numbers multiplying the various nondimensional terms specify then their relative importance in the governing equation. In addition comparing corresponding Π numbers between the test and prototype result in a measure of the distortion for the related phenomenon. The scaling groups developed in Section 6 for this purpose are related to, but different from, the relationships developed for the general scaling criteria in Section 4. The general scaling criteria are general relations used to design a test facility while the equations developed in Section 6 are used to identify the important phenomena in the ESBWR and quantify distortions present in test facilities. The equations in Section 4 result in the minimum number of scaling groups that must be maintained in order to adequately scale the prototype with a test facility. There is no attempt to minimize the groups developed in Section 6 although many of them are combinations of other scaling groups. The application is much clearer if each scaling group is spelled out as a new group. The equations in Section 6 satisfy two purposes: first, identifying the important phenomena to the ESBWR behavior provides information for validating the PIRT rankings; second, the method can be applied to the test facilities after they are designed to show that the phenomena important to the ESBWR behavior have been represented adequately in the test facility. The application of these equations to the ESBWR for important phenomena identification is found in Section 7. The confirmation of test facility scaling is performed in Section 8.

2.4 Time Scales – Closure with H2TS

One possible response time during a given LOCA phase consists of a volume filling or emptying time, based on initial or other reference flow rates. Another response time is associated with the transient acceleration of an open flow loop between the reactor and wetwell, the pressure source and sink. One other response time involves the vessel decompression, and is significantly different from the water mass emptying time of that vessel.[3]

Another process for comparing relative time responses in an integrated system is provided in the H2TS, which involves both the time constant of subsystems and a corresponding transport frequency. That is, if a flow transient response occurs in a pipe between two volumes, the system response time would correspond to either the filling or emptying time of the controlling volume (e.g., the GDCS pool). The transport frequency would correspond to the number of purges per unit time of the GDCS pool drain line. The product of frequency and response time gives the number of purges during the filling or emptying process. When a high number of purges occurs, it is not necessary to preserve the acceleration time response of the flow path, but only the quasi-steady flow properties. When a small number of purges occurs, the flow path inertia would influence the system behavior, and it would be desirable to preserve the Π groups involving inertia.

The same result is obtained by comparing the volume fill times to the transit times of the connected piping. When the fill time is much longer than the transit time, then the flow path inertia is not important. This is the approach taken in this report, as described in Section 2.4.

[3]RAI 254

3.0 SYSTEM MODELING EQUATIONS

3.1 Vessel Pressurization Rate Equation for a Control Volume

Consider the control volume V of Figure 3-1[4] containing a mass M with internal energy E at a pressure P and a temperature T[5]. The volume contains a number of constituents (noncondensible gases, steam, etc.), each denoted by the subscript j. Any changes in the kinetic and potential energy of the mass M are much smaller than changes in its intrinsic internal energy and therefore are neglected. The system is well mixed (i.e., the distributions of constituents and of the temperature are uniform), and at thermodynamic equilibrium. The conservation equations for mass and energy are used to derive an equation for the rate of pressure change in this control volume. The conservation equations and the final result are given in this section; the details of the derivation can be found in Appendix B of reference [3-1][6].

The *total-mass* continuity equation for this volume is:

$$\frac{dM}{dt} - \sum_i W_i = 0 \tag{3.1-1}$$

where W_i are the total (steam, noncondensibles, etc.) mass flow rates entering the volume. The mass conservation equation for *constituent j* is

$$\frac{dM_j}{dt} - \sum_i W_{i,j} = 0 \tag{3.1-2}$$

Here a constituent is either steam-water or a noncondensible gas.
The energy conservation equation is:

$$\frac{dE}{dt} = -P\frac{dV}{dt} + \dot{Q} + \sum_i W_i h_{o,i} \tag{3.1-3}$$

where $\dot{Q}$ is the heat added to the system (e.g., by conduction through the wall), and $h_{o,i}$ is the total specific enthalpy of stream i. The total enthalpy (subscript o) includes the kinetic and potential energy. The specific internal energy of the system,

$$e = \frac{E}{M} \tag{3.1-4}$$

is a function of two thermodynamic variables, namely, the pressure and the specific volume v = V/M; and of the mass fractions y_j of the various constituents:

$$e = e(P,v,y_j) \tag{3.1-5}$$

[4] RAI 257
[5] RAI 255
[6] RAI 256

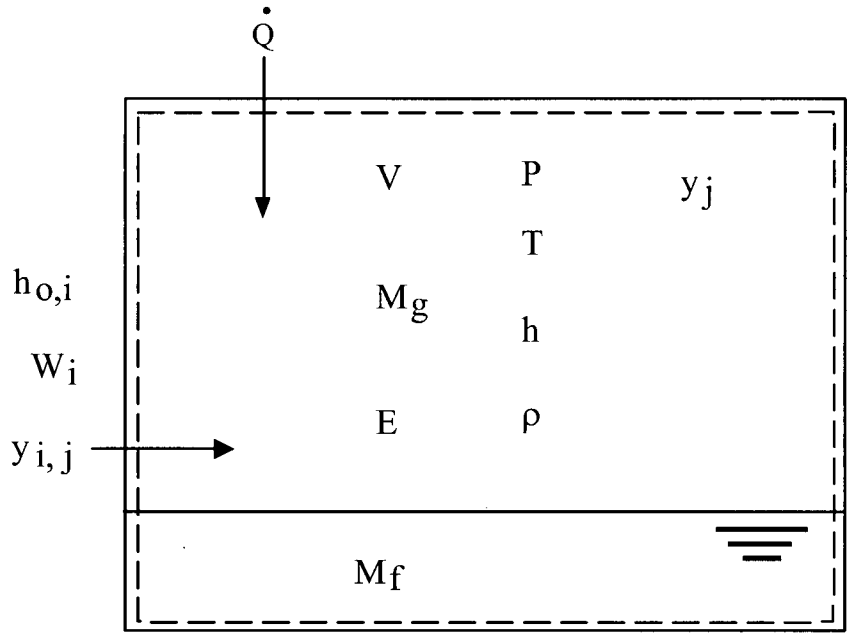

$$e = \frac{E}{M} = e(P, v, y_j)$$

A containment volume receiving mass flow rates W_i with corresponding total enthalpies $h_{o,i}$, and heat at rate Q

Figure 3-1 Control Volume Receiving Mass Flow Rates W_i with Corresponding Total Enthalpies h_{oi} and Heat at Rate Q

The conservation equations and state equation listed above can be combined to derive an equation for the rate of change of the internal specific energy of the volume and an equation for the rate of pressurization, dP/dt, of a control volume. These equations were derived in Ref [3-1] and can be written in compact form as follows:

$$M\frac{de}{dt} = -P\frac{dV}{dt} + \sum_k \dot{Q}_k + \sum_i W_i(h_{o,i} - h) + P/\rho \sum_i W_i \qquad (3.1\text{-}6)$$

$$Vf_2 \frac{dP}{dt} = \sum_i [W_i(h_{o,i} - h)] + \sum_i W_i P^* v + \sum_k \dot{Q}_k - P^* \frac{dV}{dt} - V\sum_j \left[f_{l,j} \frac{dy_j}{dt} \right] \qquad (3.1\text{-}7)^7$$

[7] RAI 258

where the following short–hand notations were made:

$$P^* \equiv P + \left.\frac{\partial e}{\partial v}\right|_{P,y_j} \tag{3.1-8}$$

$$f_{1,j} \equiv \frac{1}{v}\left.\frac{\partial e}{\partial y_j}\right|_{P,v,y} \quad \text{(units of energy per unit volume)}$$

$$f_2 \equiv \frac{1}{v}\left.\frac{\partial e}{\partial P}\right|_{v,y_j} \quad \text{(Nondimensional)}$$

where y_j constant means all y_j are held constant and y constant means all y_j except the one in the derivative are held constant.

For containment vapor volumes, the quantities P^*, $f_{i,j}$ and f_2 denote thermodynamic properties of the mixture, which are functions of P, v, and y_j. When prototypical fluids under prototypical thermodynamic conditions are used, these thermodynamic properties are identical for prototype and model.

We note that Equation 3.1-7 yields the rate of change of the pressure in terms of heat addition, mass and enthalpy fluxes into the volume, and changes of volume *composition*. The rate of change of volume dV/dt (e.g., due to phase change at the boundary) is also considered.

The system compliance in Equation 3.1-7 is a function of the vapor mass fraction in vessels containing liquid such as the RPV. The equation for the vapor fraction is obtained by combining the vapor phase continuity equation and net vapor generation equation[8]:

$$\rho_g \frac{d\alpha}{dt} = \frac{1}{V}\Sigma W_g + \frac{\Sigma(h_\ell - h_f)W_\ell}{h_{fg}V} + \frac{\dot{Q}}{h_{fg}V} + \frac{\psi}{h_{fg}}\frac{dP}{dt} \tag{3.1-9}$$

where

$$\psi = 1 - (1-\alpha)\rho_f h'_f - \alpha\rho_g h'_g - \alpha h_{fg}\rho'_g \tag{3.1-10}$$

This can also be written in terms of the liquid mass equation[9]; as developed in Appendix A of [3-2] as

$$\frac{dM_l}{dt} = -\sum_k \frac{\dot{Q}_k}{h_{fg}} + \sum_i W_{l,i} + \sum_i \frac{\Delta h_{sub} W_{l,i}}{h_{fg}} - \frac{1}{h_{fg}}\left[V_{RPV}(1-\rho_g h'_g) + M_l\left(\frac{\rho_g}{\rho_l}h'_g - h'_f\right)\right]\frac{dP_R}{dt} \tag{3.1-11}$$

[8] RAI 259. The vapor generation equation is derived in Section 2.4.3 of "Two-Phase Flow in Complex Systems", by Salomon Levy, and reproduced in Appendix B of "SBWR Scaling Report", NEDC-32288P.
[9] RAI 262

3.2 Generic Junction Flow Rate Equation

The general equation governing the pressurization rate in control volumes was developed in Section 3.1. In this section, the equation governing the flows of mass in junctions between control volumes is developed.

Mass transfers between control volumes (i.e., at flow junctions) are driven by pressure differences; these could be due to differential buildup of pressure in the two volumes attached to a junction or may be hydrostatically driven. In this section the generic equation governing junction flow rates is presented.

The general cases (Figure 3-2) of pipes connecting two volumes at pressure P_1 and P_2 are considered. The pipe in the receiving vessel may be immersed in a pool of liquid at a submergence H; this configuration is referred to as a "vent". The case of an open vent is considered here. When the vent is closed, the column of liquid in the vent line balances the hydrostatic pressure difference between the two volumes. The case of single-phase incompressible flow is considered here, since this is the case for the majority of the junction flows in the ESBWR containment system. The case of two-phase flows can be obtained by specifying appropriate two-phase friction multipliers.

The detailed derivation of the junction flow rate equation of length ℓ_n starts by considering the momentum equation for time-dependent flow in a *segment* of the piping. By adding the momentum equations in different segments constituting a *flow path,* the following equation is obtained:

$$\sum_n \frac{\ell_n}{a_n}\frac{dW}{dt} = \Delta P_{12} + \rho g \sum_n \ell_{nv} - \rho_L g H - \sum_n \frac{F_n}{a_n^2}\frac{W^2}{2\rho} \tag{3.2-1}$$

where,

$$\Delta P_{12} = P_1 - P_2 \tag{3.2-2a}$$

and

$$F_n = \frac{f_n \ell_n}{D_n} + k_n \tag{3.2-2b}$$

The various symbols are defined in Figure 3-2, and k_n and f_n are the local loss coefficient and friction factor, respectively, in segment n. Equation 3.2-1 can be symbolically written for junction flow path m as

$$\left(\frac{L}{a}\right)_m \frac{dW_m}{dt} = \Delta P_m + \rho_m g L_m - \rho_L g H_m - \left(\frac{F}{a^2}\right)_m \frac{W_m^2}{2\rho_m} \tag{3.2-3}$$

where,

$$L_m = \sum_n \ell_{nv} \tag{3.2-4a}$$

$$\left(\frac{F}{a^2}\right)_m = \sum_n \frac{F_n}{a_n^2} = \sum_n \left(\frac{f_n \ell_n}{D_n} + k_n\right)\frac{1}{a_n^2} \tag{3.2-4b}$$

and

$$\left(\frac{L}{a}\right)_m = \sum_n \frac{\ell_n}{a_n} \tag{3.2-4c}$$

For the gas-filled line indicated schematically in Figure 3-2a, the gas density is very small compared to that of the liquid and the gas gravity head $\rho_m g L_m$ can be neglected and the submergence $H_m = H_{sub}$. For the liquid-filled line shown in Figure 3-2b, the net gravity head is $L_m = L_1 - L_2$ and the density ρ_m equals that of the average liquid density ρ_L for flow path m. Also, in this case H_m is set equal to zero.

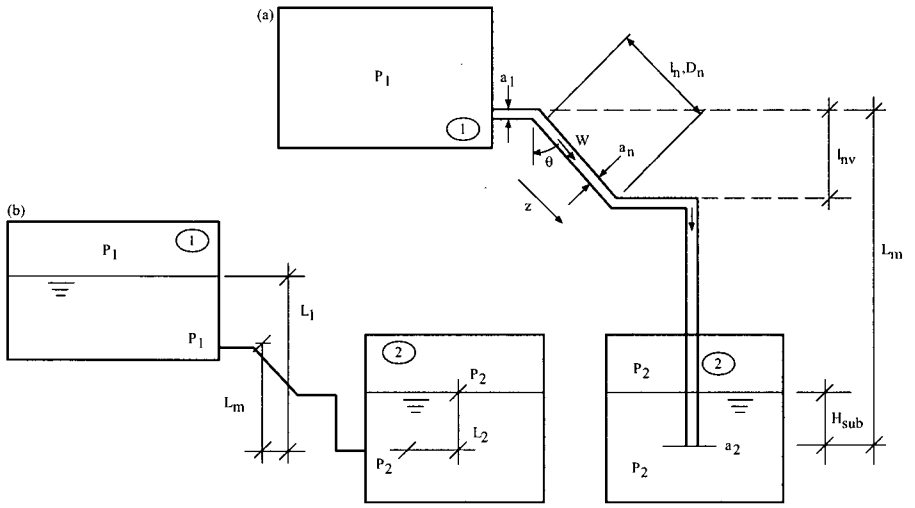

(b) Pipe Connecting Two Pools; $L_m = L_1 - L_2$, $H_m = 0$

(a) Pipe Connecting Two Volumes and Submerged in Volume 2: $H_m = H_{sub}$, $\rho_m g L_m = 0$

Figure 3-2 Junction Pipes

3.3 Summary

The generic equations governing the flow rates between junctions (Equation 3.2-3), total and component mass conservation (Equations 3.1-1 and 3.1-2), the pressurization rates of volumes (Equation 3.1-7) and the volume internal energy (Equation 3.1-6) were presented in Sections 3.1 and 3.2.

The enthalpies h_o appearing in Equations 3.1-6 and 3.1-7 were *total* specific enthalpies (i.e., the sum of the intrinsic specific enthalpy of the fluid plus its kinetic and potential energies). Consequently, the exact scaling of these would have required separate consideration of specific enthalpy, velocity and elevation scales. Since changes in kinetic and potential energy are very

small or totally negligible, this complication is avoided here and the h_o are replaced by h in the following.

The equations that will be nondimensionalized in subsequent sections are repeated here for convenience:

$$\frac{dM}{dt} - \sum_i W_i = 0 \tag{3.1-1}$$

$$\frac{dM_j}{dt} - \sum_i W_{ij} = 0 \tag{3.1-2}$$

$$\left(\frac{L}{a}\right)\frac{dW}{dt} = \Delta P - \frac{1}{\rho}\left(\frac{F}{a^2}\right)\frac{W^2}{2} + \rho g H^* \tag{3.1-3}$$

$$M\frac{de}{dt} = -P\frac{dV}{dt} + \sum_k \dot{Q}_k + \sum_i W_i\left(h_{o,i} - h\right) + P/\rho\sum_i W_i \tag{3.1-6}$$

$$Vf_2\frac{dP}{dt} = \sum_i\left[W_i\left(h_{o,i} - h\right)\right] + \sum_i W_i P^* v + \sum_k \dot{Q}_k - P^*\frac{dV}{dt} - V\sum_j\left[f_{l,j}\frac{dy_j}{dt}\right] \tag{3.1-7}$$

$$\rho_g\frac{d\alpha}{dt} = \frac{1}{V}\sum_i W_g + \frac{\sum_i\left(h_\ell - h_f\right)W_\ell}{Vh_{fg}} + \frac{\dot{Q}}{V} + \frac{\psi}{h_{fg}}\frac{dP}{dt} \tag{3.1-9}$$

$$\frac{dM_l}{dt} = -\sum_k\frac{\dot{Q}_k}{h_{fg}} + \sum_i W_{l,i} + \sum_i\frac{\Delta h_{sub}W_{l,i}}{h_{fg}} - \frac{1}{h_{fg}}\left[V_{RPV}\left(1 - \rho_g h'_g\right) + M_l\left(\frac{\rho_g}{\rho_l}h'_g - h'_f\right)\right]\frac{dP_R}{dt} \tag{3.1-11}$$

* The hydrostatic head and submergence terms are of the same form and have been combined into one generic term, ρgH.

4.0 SCALING FOR TEST DESIGN

The general scaling criteria applicable to the ESBWR System with its various subsystems and components and their counterparts in the related tests under consideration are derived in this section by a top-down approach. General scaling criteria have been derived by several authors ([4-1], [4-2], [4-3], [4-4]. Generally, these are not specific to the combined thermodynamic and thermal-hydraulic phenomena taking place inside containments and therefore are not directly applicable here. To arrive at general scaling criteria applicable to the ESBWR System, the controlling processes in generic subsystems having the essential characteristics of classes of ESBWR systems (e.g., containment volumes, pipes, etc.) are considered. These lead to generic governing equations for the rate of pressurization of volumes (the "pressure rate equations") and for the flow rates between volumes (the "flow rate equations"). These equations are cast in nondimensional form and various nondimensional groups controlling component or system behavior appear. This has been summarized previously in references 3-1 and 4-5.

The ESBWR System consists of a number of volumes (RPV, DW, SC, etc.) connected via junctions (i.e., openings, piping, vents, heat exchanging equipment such as the ICS and PCCS condensers, etc.). Mass and energy transfers take place between these volumes through their junctions. Heat may also be exchanged by conduction with the structures. These exchanges lead to changes in the thermodynamic condition of the various volumes; this, in particular leads to changes of the volume pressures. The junction flows (flows between volumes) are driven by the pressure differences between volumes. Thus, the thermodynamic behavior of the system (essentially, its pressure history) is linked to its thermal-hydraulic behavior (the flows of mass and energy between volumes). Proper global scaling of these processes is important for the ESBWR-related tests considered here and the topic addressed in this section.

Global scaling is based on the mathematical formulations of the basic physical principles which govern top-down phenomena. Dependent variables like pressure, velocity, mass flow rates, and enthalpies are normalized with respect to either their initial values, or other limiting values, which cause the normalized variables to have an order of magnitude unity; that is, O(1). Only quantities which can be controlled in an experiment are chosen for the normalizing values. The normalizing time scale for top-down phenomena is determined for each LOCA phase; namely, Blowdown, GDCS transition, reflood and PCCS.

Prototypical fluids under prototypical thermodynamic conditions were used in all the ESBWR-related tests. The fact that the fluids are expected (by design and operation of the test facilities) to be in similar states in the prototype and the models, will be used to simplify the following analyses.

4.1 Top down Scaling

These equations will be nondimensionalized using the following reference quantities (denoted by the subscript r):

- For time: t_r
- For volume: Vr
- For mass flow rates: Wr

- For heat addition: $\dot{Q}_r$
- For densities: ρ_r
- For pressure, a reference pressure difference: ΔP_r
- For properties involving vapor mass function: Ψ_r
- For enthalpies and internal energies, a reference specific enthalpy difference: Δh_r

To derive the general scaling criteria, the equations will be nondimensionalized by dividing the dimensional variables z by the reference values z_r above; this produces the nondimensional variables z^+:

$$z^+ \equiv \frac{z}{z_r} \tag{4.1-1}$$

In particular, note that:

$$h_{o,i} - h_o \approx h_i - h = h_i^+ \Delta h_r \tag{4.1-2}$$

where h^+ denotes a nondimensional enthalpy difference for flow i (enthalpy of stream entering h_i, minus average volume enthalpy, h).

Also

$$f_{l,j} = f_{l,j}^+ \frac{\rho_r \Delta h_r}{y_{j,r}} \tag{4.1-3}$$

and

$$f_2 = f_2^+ \rho_r \frac{\Delta h_r}{\Delta P_r} \tag{4.1-4}$$

The details of the derivations can be found in Appendices A and B of Ref [3-1]. The resulting nondimensional equations are:

Conservation Equations:

$$\frac{d}{dt^+}\left(V^+ e^+\right) - \Pi_t \sum_i W_i^+ = 0 \tag{4.1-5}$$

$$\frac{d}{dt^+}\left(V^+ \rho_j^+\right) - \Pi_{t,j} \sum_i W_i^+ y_{i,j}^+ = 0 \tag{4.1-6}$$

Momentum Equation:

$$\Pi_{in} \frac{dW^+}{dt^+} = \Pi_{pd} \Delta P^+ - \Pi_{loss} \frac{W^{+2}}{\rho^+} - \Pi_h \rho^+ H^+ \tag{4.1-7}$$

Energy Equation:

$$V^+\rho^+\frac{de^+}{dt^+} = -\frac{1}{\Pi_{hp}}\rho^+\frac{dV^+}{dt^+} + \sum_k \Pi_t \Pi_{pch}\dot{Q}_k{}^+ + \Pi_t \sum_i W_i^+ h_i^+ + \frac{\Pi_t}{\Pi_{hp}}\frac{P^+}{\rho^+}\sum_i W_i^+ \quad (4.1\text{-}8)$$

Pressure Rate Equation:

$$\frac{dP^+}{dt^+} = \frac{1}{V^+ f_2^+}\left\{\Pi_t \sum_i W_i^+ h_i^+ + \frac{\Pi_t}{\Pi_{hp}}\frac{P^{*+}}{\rho^+}\sum_i W_i^* + \sum_k \Pi_t \Pi_{pch}\dot{Q}_k{}^+ - \frac{1}{\Pi_{hp}}P^{*+}\frac{dV^+}{dt^+} - V^+\sum_j f_{l,j}^+\frac{dy_j^+}{dt^+}\right\} \quad (4.1\text{-}9)$$

Vapor Fraction Equation:

$$\rho_g^+\frac{d\alpha}{dt^+} = \Pi_t \sum_i W_{g,i}^+ + \Pi_t \frac{\sum_i h_{sub,i}^+ W_{\ell,i}^+}{h_{fg}^+} + \sum_k \Pi_t \Pi_{pch}\frac{\dot{Q}_k{}^+}{h_{fg}^+} + \frac{\Pi_\psi}{\Pi_{hp}}\psi^+\frac{dP^+}{dt^+} \quad (4.1\text{-}10)$$

The Π groups which appear above are defined below:

In the conservation equations:

- The nondimensional time numbers for total flow;

$$\Pi_t \equiv \frac{t_r}{V_r\rho_r / W_r} \quad (4.1\text{-}11)$$

- and for component j,

$$\Pi_{t,j} \equiv \frac{t_r}{\rho_r V_r / W_r y_{r,j}} \quad (4.1\text{-}12)$$

In the Momentum Equation:

- The inertial pressure drop number

$$\Pi_{in} \equiv \frac{W_r\left(\frac{L}{a}\right)_r}{\Delta P_r t_r} \quad (4.1\text{-}13)$$

- The pressure difference number,

$$\Pi_{pd} \equiv \frac{\Delta P_o}{\Delta P_r} \tag{4.1-14}$$

- The pressure loss number,

$$\Pi_{loss} \equiv \frac{W_r^2 \left(\frac{F}{a^2}\right)_r}{2\Delta P_r \rho_r} \tag{4.1-15}$$

- The submergence or hydrostatic level difference number,*

$$\Pi_h \equiv \frac{\rho_r g H_r}{\Delta P_r} \tag{4.1-16}$$

In the Energy and Pressure Rate Equations:

- The enthalpy-pressure number,

$$\Pi_{hp} \equiv \frac{\Delta h_r}{\Delta P_r / \rho_r} \tag{4.1-17}$$

- The phase change number,

$$\Pi_{pch} \equiv \frac{\dot{Q}_r}{W_r \Delta h_r} \tag{4.1-18}$$

In the Vapor Fraction Equation:

- The flashing number,

$$\Pi_\psi = \psi_r \tag{4.1-19}$$

- The reference component fraction scales $y_{j,r}$. Considering the fact that the $y_{j,r}$ must be conserved, there is no need to consider $\Pi_{t,j}$. The time number Π_t suffices, since $\Pi_{t,j} = \Pi_t / y_{j,r}$. We are thus left with the following eight Π numbers to match between prototype and model:

$$\Pi_t, \Pi_{in}, \Pi_{pd}, \Pi_{loss}, \Pi_{sub}, \Pi_{hp}, \Pi_{pch} \text{ and } \Pi_\psi$$

4.2 Phase Changes at Interfaces

The phase changes at interfaces involve the latent heat of vaporization and the inerfacial mass flow rates and mass fluxes. The reference enthalpy scale Δh_r used above can, in principle, be

* A separate hydrostatic level difference number Π_{hyd} is used later, using a level difference in place of the submergence.

selected arbitrarily. A [10]rational definition for Δh_r arises, however, when phase changes at interfaces are scaled. In this case, the natural choice is $\Delta h_r = h_{fg,r}$, the reference latent heat of vaporization.

Although it is generally difficult to scale exactly phase changes taking place by condensation on structures and walls it is relatively straightforward to scale phase changes at the free pool surfaces. The flow rates due to phase change at the surface of a pool are given by the product of the pool surface area A_{LG} times the mass flux due to phase change $\dot{m}_{LG}$. The latter, in general, [11]depends on the fluid conditions on both sides of the interface (P, T, partial densities of constituents ρ_j) and on hydrodynamic parameters controlling mass transfer (i.e., the Grashoff, Reynolds and Prandtl numbers of the fluids). The hydrodynamic dependence is considered in the bottom-up analysis of Section 7.6. Here we derive the scaling of the surface areas.

The vapor flow rate due to vaporization

$$W_{LG} = A_{LG}\dot{m}_{LG} \tag{4.2-1}$$

must scale the same way as the other flow rates in the system. Assuming that with prototypical fluids and well scaled local conditions at the interface, the phase-change mass fluxes $\dot{m}_{LG}$ in the prototype and the model are identical, one concludes that the pool areas A_{LG} must scale like the flow rates.

4.3 General Scaling Criteria

The nondimensional numbers identified above will now be used to derive general scaling criteria for the experimental facilities.

The analysis of this section considers a single individual flow path and a single volume and derives the general scaling laws applicable to these. These general criteria are applied then to each flow path and volume in the system. The resulting scaling of the entire system, any possible interactions between subsystems[12], and the identification of scaling distortions are considered in Sections 7 and 8.

Although several other choices are also possible, the *system scale R* can be defined as the ratio of prototype to test facility power input:

$$R \equiv \frac{\dot{Q}_{prot}}{\dot{Q}_{mod}} = \dot{Q}_R \tag{4.3-1}$$

where the subscript R denotes the ratio between the corresponding scales of prototype and model. For a variable Z:

[10] RAI 265
[11] RAI 266
[12] Supp. RAI 259 & Supp RAI 286

$$z_R \equiv \frac{z_{prot}}{z_{mod}} \tag{4.3-2}$$

Nine nondimensional groups were identified by the analysis of Section 4.1 (Equations 4.1-11 to 4.1-19). In addition, it was shown that the pool surface areas A_{LG} must scale like the flow rates.

By dividing Π_t by $\Pi_{t,j}$, it becomes evident that the reference component fraction scales $y_{j,r}$ must be conserved; with this constraint there is no need to further consider $\Pi_{t,j}$; instead

$$(y_j)_R = 1 \tag{4.3-3}$$

Also, from consideration of the vapor mass equation $(\alpha)_R = 1$.

For a given flow path, the reference ΔP_r scale can be chosen to be the initial driving pressure difference ΔP_o; this makes $\Pi_{pd} = 1$. Furthermore, for all of the ESBWR related tests considered here the facilities were designed to have pressure differences and elevations conserved*. This leads to

$$(H)_R = (\Delta P)_R = 1 \tag{4.3-4}$$

and Π_{pd} needs no longer be considered.

Thus, we are left with the following six Π numbers to match between prototype and model components:

$$\Pi_t, \Pi_{in}, \Pi_{loss}, \Pi_h, \Pi_{hp} \text{ and } \Pi_{pch}$$

in addition to

$$(\alpha)_R = (y_j)_R = (\Delta P)_R = (H)_R = 1 \tag{4.3-5}$$

and

$$(A_{LG})_R = W_R \tag{4.3-6}$$

The minimum set of not-yet specified independent reference scales appearing in the remaining Π numbers listed above is

$$t_r, \rho_r, V_r, W_r, \left(\frac{L}{a}\right)_r, \left(\frac{F}{a^2}\right)_r, \Delta h_r \text{ and } \dot{Q}_r$$

* Other choices may be possible, but are not considered here.

In Section 4.2, it was shown that a [13]rational choice for Δh_r was

$$\Delta h_r = h_{fg,r} \tag{4.3-7}$$

Thus, where prototypical fluids are used and the test facilities are designed to operate under prototypical thermodynamic conditions,

$$(\Delta h)_R = (h_{fg})_R = \rho_R = 1 \tag{4.3-8}$$

The pressure evolution resulting from the thermodynamics of the system and the pressure drops between volumes must clearly be scaled in an identical fashion. Considering the fact that prototypical fluids are used, this requirement links the properties of the fluid (in particular, the latent heat and the specific volumes of water and steam) to the pressure differences between volumes (and to the submergence depths of vents or water levels), resulting in 1:1 scaling for pressure drops.

The choice of a proper time scale t_r will be discussed in Section 4.6. To arrive at the general scaling criteria, one can specify $\Pi_t = 1$; this leads to the definition of t_r as the volume residence time,

$$t_r = \frac{V_r \rho_r}{W_r} \tag{4.3-9}$$

Having decided to use 1:1 scaling for pressure drops and elevations and prototypical fluids, matching of the submergence of hydrostatic level difference number Π_h, and of the enthalpy-pressure number Π_{hp} is automatically satisfied.

Matching of the phase change number requires that, for prototypical fluids, the ratio $\dot{Q}/W$ be preserved. Having already defined $\dot{Q}_R = R$, this leads to

$$\dot{Q}_R = W_R = (A_{LG})_R = R \tag{4.3-10}$$

Matching of the remaining inertial pressure drop number and frictional pressure loss numbers,

$$\Pi_{in} = \frac{W_r \left(\frac{L}{a}\right)_r}{\Delta P_r t_r} \tag{4.3-11}$$

and

[13] RAI 267

$$\Pi_{loss} = \frac{W_r^2\left(\frac{F}{a^2}\right)_r}{2\Delta P_r \rho_r} \tag{4.3-12}$$

leads to

$$(\Pi_{in})_R = \frac{R\left(\frac{L}{a}\right)_R}{1} = R\left(\frac{L}{a}\right)_R = 1 \tag{4.3-13}$$

and

$$(\Pi_{loss})_R = \frac{R^2\left(\frac{F}{a^2}\right)_R}{1} = R^2\left(\frac{F}{a^2}\right)_R = 1 \tag{4.3-14}$$

These two requirements can be satisfied if

$$L_R = F_R = 1 \tag{4.3-15}$$

and

$$a_R = R \tag{4.3-16}$$

Since W = uρa, u being the flow velocity in a pipe, with $\rho_R = 1$ and $W_R = R$, the requirement a_R = R leads to identical velocities in the prototype and the model. The scaling of the flow velocities is discussed in Section 4.4.

Although it may be relatively easy to have prototypical lengths of piping in the test facilities (i.e., L_R=1), the requirement F_R=1 is more difficult to match, since the $f\ell/D$ components of F (Equation 2.1-2a) cannot be matched when a_R=R and $D_R = \sqrt{a_R} = \sqrt{R}$. The practical scaling of the frictional pressure losses is discussed in Section 4.4.

Instead of conserving F_R and a_R separately, for given F it is clearly sufficient to conserve the ratio $(F/a^2)_R$. However, this will lead to a somewhat different scale for a_R and may lead to distortions of $(L/a)_R$. However, for systems such as the ESBWR containment, where inertial effects play a minor role, the distortion of the inertial effects is usually not important.

The vapor mass continuity equation applied to the two-phase region inside the RPV leads to the need to match Π_ψ in addition to Π_t, Π_{hp} and Π_{pch}. Π_ψ is matched by setting $(\alpha)_R = 1$ and using prototypical pressures and thermodynamic conditions in the experiment. The other Π groups have already been discussed and shown to be matched by scaling $\dot{Q}_R = W_R = A_R = R$ and maintaining $L_R = 1$.

The axial void distribution and level swell are also matched by setting $L_R = 1$ (Section 3.8 of [3-1]). The two-phase level $L_{2\phi}$ is given by

$$L_{2\phi} = \frac{V_f}{(1-\overline{\alpha})A} \tag{4.3-17}$$

where V_f is the volume below the level. Level swell will be matched by using the scale of $(V_f)_R = A_R = R$ (i.e., $L_R = 1$).

Since the volume scale V_r appears only in the time constant t_r, one could, in principle, conduct tests at a different time scale (not 1:1) by modifying the volume scale ratio V_R. This is possible as long as t_r is *the* controlling time scale, as already discussed in Section 4.1. Accelerated tests can, for instance, be conducted by decreasing V_R or increasing equally the other scales, $\dot{Q}_R = W_R = (A_{LG})_R$. Conservation of the time scale t_r also implies (in any case) preservation of the ratio V_r/W_r.

4.4 Scaling of the Piping[14]

The scaling of the piping is determined by the already defined pressure drop and reference flow rate scales. The relevant Π number is

$$\Pi_{loss} \equiv \frac{(F/a^2)_r W_r^2}{2\Delta P_r \rho_r} = 1 \tag{4.4-1}$$

The factor F/a^2 (Equation 3.2-4b) depends on both the frictional losses in the pipes (i.e., on the groups $f_n \ell_n / D_n$) and on the local losses k_n. The latter are generally insensitive to scale. Since the model diameters D_n are smaller, however, the F/a^2 factors of the models tend to be larger. Thus, conservation of Π_{loss} leads to reduced velocities in the models. This is not important, as long as the transit times between volumes are small compared to the volume fill times t_r, and the velocities do not become so low as to introduce new phenomena in the models.[15]

In practice, pipe scaling is performed according to the following procedure: the pipe cross-sectional areas in the scaled facilities are oversized for convenience; this leads to somewhat lower flow velocities in the pipes. Thus, considering only the *local losses* (for which the loss coefficients are only weakly dependent on flow velocity or Reynolds number), the total Δp's in the models would be *lower* than prototypical. On the contrary, *wall friction* in the scaled facilities is *larger* (due to larger values of the $f\ell/D$ values produced by the smaller pipe diameters), as it cannot be compensated in general by the decrease in velocity. Usually (and fortunately), the total pressure drops in the piping are dominated by local losses, so that the total ΔP's in the scaled facilities end up being somewhat smaller. They can therefore be matched by introducing additional losses by local orificing.

[14] RAI 264
[15] RAI 268

The pipe flow areas determined in this fashion result in velocities that do not lead to matching pipe transit times. This is, however, of secondary importance, as already noted.

In summary, matching of the total pressure drops is accomplished by using orifices in conjunction with convenient choices for pipe diameters.

4.5 Compressibility of the Gas Flowing in Pipes

The gases flowing in pipes connecting containment volumes were treated as incompressible; this assumption is justified in this section.

We start from the continuity equation, written for the pipe segment of Figure 3-2,

$$\frac{dM}{dt} = W_1 - W_2 \tag{4.5-1}$$

where W_1 and W_2 are the mass flow rates at Sections 1 and 2, respectively; in general

$$W = A_p \rho u$$

M is the mass contained in the pipe of volume $V_P=A_PL_P$ and average density $\bar{\rho}$. We nondimensionalize Equation 4.5-1 by defining

$$t^+ \equiv \frac{t}{t_{\rho,r}}$$

and

$$W^+ \equiv \frac{W}{W_r}$$

with

$$W_r = \rho_r A_p u_r$$

and

$$\rho^+ \equiv \frac{\rho}{\rho_r}$$

and a pipe transit time

$$t_{tr,r} \equiv \frac{L_P}{u_r}$$

Equation 4.5-1 takes the nondimensional form

$$\frac{t_{tr,r}}{t_{\rho,r}}\frac{d\bar{\rho}^{+}}{dt^{+}} = W_1^{+} - W_2^{+} \tag{4.5-2}$$

It is evident that if $t_{\rho,r} >> t_{tr,r}$ (i.e. rate of change of the average density is small), the mass flow rates at the inlet and the exit of the pipe will be approximately equal, $W_1^{+} \approx W_2^{+}$, or $W_1 \approx W_2$. So clearly, the pipe transit time $t_{tr,r}$ must be compared to the other time constants of the system

4.6 Time Scales

Several time scales appeared during the general scaling considered in this section. These are briefly discussed here.

Volume fill time

This first time constant is related to mass continuity and is the volume fill time [16] for mass flowing into the volume V_r at the mass flow rate W_r [2-1]:

$$t_{m,r} = \frac{V_r \rho_r}{W_r} \tag{4.6-1}$$

The volume fill time t_r is the [17]reference time for subsystems and processes where volume emptying or filling due to mass flows takes place.[18]

Pressurization Time Constant

Another time scale comes from the pressure rate equation and is related to the time for a volume to depressurize due to enthalpy flows. For a volume V_r with flow W_r leaving at an enthalpy Δh_r greater than the average enthalpy, the time constant for blowdown is:

$$t_r = \frac{V_r \rho_r}{W_r}\frac{\Delta P_r}{\Delta h_r}\left(\frac{\partial e}{\partial p}\right)_r \tag{4.6-2}$$

This is related to the volume fill time constant by

$$t_r = t_{m,r}\frac{\Delta P_r}{\Delta h_r}\left(\frac{\partial e}{\partial p}\right)_r \tag{4.6-3}$$

This is the natural time constant for subsystems and processes where volume pressurization due to enthalpy flows takes place.

Flashing Time Constant

[16] RAI 270
[17] RAI 271
[18] RAI 263

When a saturated volume depressurizes, there is a time constant associated with the swelling of the liquid region to reach a quasi-steady void fraction:

$$t_{flash,r} = \frac{\rho_{g,r}}{\Gamma_r} \tag{4.6-4}$$

This is the time constant associated with the beginning of a blowdown event such as those at the initiation of the GIST and GIRAFFE/SIT tests.

Inertial Time Constant

Another time scale is needed in scaling the inertial effects in the momentum equation, written in nondimensional form as Equation 4.1-7:

$$\Pi_{in}\frac{dW^+}{dt^+} = \Pi_{pd}\Delta P^+ - \Pi_{loss}\frac{W^{+2}}{\rho^+} - \Pi_h \rho^+ H^+ \tag{4.6-5}$$

where the *inertial pressure drop number*

$$\Pi_{in} \equiv \frac{W_r\left(\frac{L}{a}\right)_r}{\Delta P_r t_{in,r}}$$

appeared. The inertia time scale is obtained by comparing the inertial Π group, Π_{in}, with the dominant Π group driving the flow on the right hand side of equation 4.6-5 (i.e. either Π_{pd} or Π_h). For liquid filled pipes driven by hydrostatic head such as the condenser drain lines this yields

$$\Pi_{in}\left(=\frac{W_r\left(\frac{L}{a}\right)_r}{\Delta P_r t_{in,r}}\right) = \Pi_h\left(=\frac{\rho_r g_r H_r}{\Delta P_r}\right) \tag{4.6-6}$$

or

$$t_{in,r} = \frac{W_r\left(\frac{L}{a}\right)_r}{\rho_r g_r H_r} \tag{4.6-7}$$

but $W_r = \rho_r a_r u_r$ and $L_r \approx H_r$ so that

$$t_{in,r} = \frac{u_r}{g} \tag{4.6-8}$$

When the process is dominated by a sudden imposed pressure differential, a balance between the inertial and pressure difference terms controls the flow so that:

$$\Pi_{in}\left(=\frac{W_r\left(\frac{L}{a}\right)_r}{\Delta P_r t_{in,r}}\right)=\Pi_{pd}\left(=\frac{\Delta P_o}{\Delta P_r}\right) \tag{4.6-9}$$

This leads to the alternate definition of the inertial time constant:

$$t_{in,r}=\frac{W_r\left(\frac{L}{a}\right)_r}{\Delta P_o}=\frac{\rho_r u_r L_r}{\Delta P_o}=\frac{u_r}{g}\frac{\rho_r g L_r}{\Delta P_o} \tag{4.6-10}$$

Thus, the inertial time scale $t_{in,r}$ can be thought of as the time roughly needed to accelerate the fluid from zero to u_r as a result of the dominant driving force.

Pipe Transit Time[19]

Finally, *a pipe transit time* was defined in Section 4.5 as

$$t_r \equiv \frac{L_p}{u_r} \tag{4.6-11}$$

Comparison of the Time Scales

The five time scales produced by this analysis (t_r, $t_{m,r}$, $t_{flash,r}$, $t_{in,r}$, and $t_{tr,r}$) scale the rates of pressurization, volume fill, flashing/redistribution, inertial effects, and pipe transfers, respectively. Clearly, the systems considered here are made of large volumes connected by piping of much lesser volumetric capacity. The pressure drops between these volumes are not expected to be dominated by inertial effects. Thus, the inertia and transit times, which are of the same order of magnitude, are much smaller than the volume fill times:

$$t_r \approx t_{m,r} >> t_{in,r} \approx t_{tr,r} \tag{4.6-12}$$

For this condition, the time behavior of the system will be controlled by the pressurization rates. The pipe transit times and the inertial time scale of the piping ($t_{tr,r}$ and $t_{in,r}$) are much shorter and the overall dynamics of the system will not be controlled by such effects. A discussion of the non-dimensional reference time (and other) Pi parameters is provided in Section 4.1.

[19] RAI 269

4.7 Specific Frequencies of the Process

Another way of viewing the processes taking place is by considering their specific frequencies which are given as ratios of a transfer intensity to capacity (amount) of the receiving volume [2-1]. In the particular case considered here, two specific frequencies involved are the ratio of heat addition $\dot{Q}_r$ and enthalpy addition $W_r\Delta h_r$ to the heat capacity of the receiving volume $V_r\rho_r\Delta h_r$:

$$\omega_{\dot{Q}_r} \equiv \frac{\dot{Q}_r}{V_r\rho_r\Delta h_r} \tag{4.7-1}$$

and

$$\omega_{\Delta h} \equiv \frac{W_r\Delta h_r}{V_r\rho_r\Delta h_r} \tag{4.7-2}$$

A *residence* or *fill* time t_r has already been defined as

$$t_r = \frac{V_r\rho_r}{W_r} \tag{4.7-3}$$

The product of $\omega_{\dot{Q}}$ and t_r results in the phase change number,

$$\omega_{\dot{Q}} \bullet t_r = \Pi_{pch} \tag{4.7-4}$$

as expected, while $\omega_{\Delta h} \bullet t_r = 1$; no new nondimensional number is derived.

A third specific frequency is the ratio between the intensity of enthalpy addition $W_r\Delta h_r$ and the "capacity of the volume to absorb work" $V_r\Delta p_r$:

$$\omega_{\Delta p} \equiv \frac{W_r\Delta h_r}{V_r\Delta p_r} \tag{4.7-5}$$

The product of $\omega_{\Delta p}$ with t_r produces, as expected, the enthalpy-pressure number Π_{hp},

$$\omega_{\Delta p} \bullet t_r = \Pi_{hp} \tag{4.7-6}$$

Consider now the specific frequency of the transfers of mass in the piping. Again, considering the ratio of an intensity of transfer (the volumetric flow rate) to the (volumetric) capacity of the piping, we obtain

$$\omega_{tr} \equiv \frac{W_r}{\rho_r L_V a_r} = \frac{u_r}{L_V} \tag{4.7-7}$$

where L_V is the equivalent volume-length of the piping. The pipe transit time (already used above) is the inverse of ω_{tr}:

$$t_{tr,r} \equiv \frac{1}{\omega_{tr}} = \frac{L_v}{u_r} \tag{4.7-8}$$

4.8 Summary

The analysis presented in this section has shown that when prototypical fluids under prototypical thermodynamic conditions are used:

Given a system scale R defined as the ratio of power input between model and prototype

$$R \equiv \dot{Q}_R \tag{4.8-1}$$

to obtain identical pressure differences and pressure evolution between prototype and model:

- The elevations in the prototype and in the model must be identical, especially the submergence depths of the vents and the water levels in vessels:

$$\Delta P_R = H_R = 1 \tag{4.8-2}$$

- The piping must satisfy the following two relations:

$$(L/a)_R = \frac{1}{R} \text{ and } (F/a^2)_R = \frac{1}{R^2} \tag{4.8-3}$$

If $L_R \approx 1$, and F can be chosen in the model so that $F_R \approx 1$, this leads to the scaling of flow areas like

$$a_R = R \tag{4.8-4}$$

If the condition $F_R \approx 1$ cannot be met, then the flow areas can be adjusted to keep

$$\left(\frac{F}{a^2}\right)_R = \frac{1}{R^2} \tag{4.8-5}$$

The factor F/a^2 determining the total pipe losses, can be adjusted by increasing the model pipe diameters and by introducing local losses in the model to match the pressure drops, if necessary.

- The pipe flow areas determined in this fashion result in velocities that do not match the pipe transit and inertial times; usually, the velocities in the model may be smaller than those of the prototype. This is, however, not important as long as the pipe transit and inertial times are small *compared to the volume* fill times t_r; the distortion of the inertial characteristics of the system is not important for relatively slow transients.

– The flow rates, heat inputs and horizontal pool areas must be scaled according to the system scale R,

$$\dot{Q}_R = W_R = (A_{LG})_R = R \tag{4.8-6}$$

– *If*, in addition, the volumes are also scaled with R,

$$V_R = R \tag{4.8-7}$$

the time scale between model and prototype is 1:1. In this case, we can speak of a vertical *slice* or vertical *section* model of the prototype.

5.0 SYSTEM DESCRIPTIONS

5.1 Introduction

The purpose of this section is to present a summary description of the test facilities that have been used to confirm the design adequacy of the ESBWR response to a LOCA and to qualify the TRACG computer code for the analysis of ESBWR post-LOCA performance. The focus of the tests and the TRACG qualification is the performance of the passive safety systems that maintain core cooling and remove decay heat from the primary system and the containment. The main systems performing these functions are the Gravity-Driven Cooling System (GDCS), the Isolation Condenser System (ICS), and the Passive Containment Cooling System (PCCS). Although the test facilities described herein were originally designed and built to confirm system performance and qualify the TRACG code for the original SBWR design [5-1], the test data and the TRACG qualification are directly applicable to the ESBWR. This update of the test facility descriptions is provided to keep the present document reasonably self-contained, and to clarify the application of the testing to the larger and higher-power ESBWR. The descriptions provided here are overviews. A full set of references describing details of the various test facilities can be found in the ESBWR TAPD [1-2].

A summary description of the post-LOCA response of the ESBWR with specific emphasis on the passive safety systems that perform the functions of core cooling and decay heat removal is presented in Section 5.2. In subsequent sections, the test facilities used to confirm ESBWR system performance and provide data for TRACG qualification are described. These descriptions include the major considerations that governed the design and scaling of the test facilities for the original SBWR and the scaling adjustments implied by the application of the test results to the ESBWR. The design of the experimental facilities and the conduct of the various tests were guided by consideration of the proper modeling and simulation of the key phenomena governing the performance of the passive safety systems. The implications of the scaling adjustments for the ESBWR are minimized by the fact that all of the tests were performed at prototypical temperature and pressure and with prototypical or near-prototypical elevations and elevation differences. These are the key variables and parameters governing the performance of the passive safety systems.

The test facilities included in the following discussion are listed in Table 5-1. They include the GIST and GIRAFFE/SIT facilities for integral systems testing of GDCS performance (core cooling); the PANDA and GIRAFFE/He facilities for integral systems performance of the PCCS and ICS (long-term containment heat removal); the PANTHERS passive containment condenser (PCC) and isolation condenser (IC) component tests; and the UCB and MIT laboratory tests that supported the development of correlations for PCC and IC condensation heat transfer that have been incorporated in TRACG. The PANDA test facility is described in greater detail than the others because it was specifically modified to include a containment design innovation of the ESBWR, and was subsequently used to perform a new series of long-term post-LOCA containment cooling tests, similar to the original SBWR test matrix. These tests provided further confirmation of the design adequacy of the ESBWR and enhanced the qualification basis for the TRACG code [5-2].

The integral test[20] facilities were designed according to the general scaling criteria summarized in Section 4.8. In addition, each test has some unique variations to these criteria either to take advantage of eliminating unnecessary cost or to enhance the capability of the facility. The specifics of these variations are[21] covered in subsequent sections.

To facilitate a common understanding of the use of the SBWR and ESBWR test programs for confirmation of ESBWR design adequacy and for TRACG qualification, the following convention has been adopted for the discussion of the test facilities: In the majority of cases, where a characteristic of the test facility was originally designed to represent the SBWR but is equally representative of the ESBWR, the notation E/SBWR will be used. In those cases where a facility characteristic is uniquely associated with the SBWR or (in the case of the modified PANDA facility) the ESBWR, those separate notations will be used.

5.2 Post-LOCA Response of the ESBWR

In the event of a break in the primary system, the ESBWR uses passive safety systems to cool the core and remove decay heat from the primary system and the containment. The main systems performing these functions are the GDCS, the ICS and the PCCS. Emergency core cooling water is provided by the GDCS. The GDCS consists of three water pools situated above the top of the core, from which makeup coolant flows by gravity to replenish the coolant lost from the reactor pressure vessel (RPV). Operation of the GDCS requires depressurization of the RPV and the ESBWR is equipped with an Automatic Depressurization System (ADS) that performs this function. The depressurization of the BWR primary system and the RPV phenomena associated with the early phase of a blowdown have been studied extensively for established BWR designs. A comprehensive set of test programs investigating these phenomena has been used for TRACG qualification [5-3]. The containment loads during early blowdown have also been extensively investigated and are evaluated by established procedures that relate them to the thermal-hydraulic conditions in the containment [5-4].

Decay heat removal from the ESBWR primary system is performed by the ICS, which consists of four Isolation Condensers (ICs) located in a set of interconnected IC and PCC pools high in the reactor building. When redundant condensate return valves are opened, steam from the RPV flows into the tubes of the ICs, condenses, and returns to the RPV, removing stored energy to the atmosphere. The behavior of the IC is well understood because ICs have been in operation for many years in older BWRs. Decay heat is removed from the drywell (DW) by the PCCS, which employs four PCC condensers located in the same set of interconnected pool compartments as the ICs. The PCC condenser tubes are permanently open to the DW so that no operator action is required to actuate the PCCS. A mixture of steam and a time-varying fraction of noncondensible gases (principally, nitrogen, which is used to inert the containment environment) enters the PCC condensers. The steam condenses and the noncondensible gases are vented to the Suppression Chamber (SC) beneath the surface of the suppression pool (SP).

In addition to the PCC vents, the DW volume is connected directly to the SP via the main pressure suppression vents. The PCCS is designed to minimize flow through the main vents by locating the PCCS vent discharges at a higher elevation in the SP than the uppermost main vent

[20] RAI 275
[21] RAI 276

discharges. This ensures that containment cooling can be accomplished by passive means and, specifically, eliminates the need for the SP to have an active safety-grade cooling system. The PCCS is designed to condense essentially all of the steam produced by decay heat and to vent any noncondensible gases and residual steam to the SP at a temperature close to saturation at atmospheric pressure (i.e., ~100°C). There is sufficient boiloff water inventory in the IC/PCC pools to ensure coverage of no less than 50% of the length of the condenser tubes for 72 hours from the start of the LOCA. This ensures that the PCCS has sufficient capacity to remove the decay heat throughout this time period with no replacement of pool inventory.

5.3 GIST

GE conducted the GDCS Integrated Systems Test (GIST) series in San Jose, California in 1988. The objectives and conditions for the 24 GIST tests are described in detail in the ESBWR TAPD [1-2]. Proof of the technical feasibility of the GDCS concept was a major test objective. Additionally, test data were obtained for E/SBWR TRACG qualification during the late blowdown and GDCS periods of LOCA transients.

5.3.1 Facility Description

The GIST facility (Figure 5-1) was a section-scaled simulation of the 1987 SBWR design configuration. The major difference between the 1987 SBWR design and the E/SBWR design is that the early design used a single pool of water to provide both the containment pressure suppression function and the water source for core cooling. The E/SBWR replaced this concept with separate GDCS and pressure suppression pools. The E/SBWR also increased the capacity of the GDCS injection lines and reconfigured the ADS relative to what was simulated in GIST. A prior evaluation of these differences concluded that the key GIST parameters (RPV and GDCS water levels and containment pressure) were either conservative or representative with respect to the final E/SBWR design [5-5].

GIST used cylindrical vessels to represent the regional volumes of the E/SBWR. Relative to the E/SBWR, the facility had a 1:1 vertical scale. The horizontal area scale of the RPV and containment volumes relative to the SBWR was 1:508. This translates to an ESBWR area/volume scale of approximately 1:1000. The same SBWR scaling (1:508) and ESBWR (4000 MWt) adjustment (~1:1000) applies to the GIST simulation of RPV decay power. The effect of the 12.5% higher decay power for the 4500 MWt ESBWR is addressed is subsequent sections of this report.

All significant plant features that could affect the performance of the GDCS were included in the design. GDCS activation is determined by the containment pressure in conjunction with the GDCS pool water level. Consequently, scaled representations of the DW and SC were part of the facility. The piping included simulations of the Automatic Depressurization System (ADS), the GDCS injection lines, and the broken line from the RPV. Capability was provided to simulate conditions at the break location for a range of break types [5-5]. The GIST scaling produced data at real time and at prototypical pressures and temperatures.

5.3.2 Initial Conditions and Test Control

The initial conditions for the GIST tests were determined from TRACG simulations of the initial blowdown behavior of the SBWR from 7 MPa. The facility was first depressurized from 1.03

MPa to 0.79 MPa by venting to the atmosphere. This initial depressurization, which was accomplished over a period of 30 to 50 seconds, created representative thermal-hydraulic conditions in the RPV[22] as it entered the later stages of the depressurization transient (Figure 5-2). The important RPV conditions are the water level and the void fraction distribution. The vessels representing the containment were pressurized and preheated to the TRACG calculated pressures and temperatures at the time the RPV pressure reached 0.79 MPa. The DW was purged of air with steam to simulate the air carryover to the SC during the initial blowdown. Initial SP water temperatures ranged from 42 to 69°C and encompassed the expected conditions in the E/SBWR. The initial RPV water level was increased to compensate for the inability of the GIST facility to represent the creation and sustenance of voids in the lower plenum by stored energy release from the walls of the RPV.[23]

When the RPV reached a pressure of 0.79 MPa, the blowdown flows through both the broken line and the ADS lines were switched from the atmosphere to the containment. With further depressurization of the RPV, the head of water in the GDCS eventually became sufficient to overcome the RPV pressure and open the GDCS check valves. This allowed GDCS flow to enter and reflood the vessel.

5.4 GIRAFFE

The GIRAFFE test facility was a full-height, reduced volume, integral system test facility built and operated by Toshiba at its Kawasaki City, Japan site. Test data were obtained for E/SBWR TRACG qualification during the late blowdown/early GDCS phase for liquid-line breaks (GIRAFFE/Systems Interaction Test (SIT)) and during the long-term post-LOCA containment cooling period (GIRAFFE/Helium Test). An important objective of the GIRAFFE/SIT series was confirmation of GDCS performance while operating in parallel with the ICS and PCCS. As the name suggests, the main objective of the GIRAFFE/Helium series was to investigate PCCS performance in the presence of helium as a stand-in for a lighter-than-steam noncondensible gas.

5.4.1 Facility Description

A schematic of the GIRAFFE facility, configured for the SIT series, is shown in Figure 5-3. (This figure minus the ICS and the piping used to simulate liquid line breaks is equally applicable to the GIRAFFE/Helium facility configuration.) Separate vessels represented the RPV, DW, SC, GDCS pools, and the pools that provide secondary-side heat removal for both the ICS and PCCS condensers. The scaled GIRAFFE heater power was based on the E/SBWR decay heat curve, adjusted to compensate for stored energy release in the prototype RPV, which was otherwise not scaled by the GIRAFFE facility. Elevations and submergences scaled the E/SBWR at 1:1 with minor variations as discussed below. Volume scaling relative to the SBWR was nominally 1:300 for the RPV and 1:400 for the other vessels. These ratios correspond to approximately 1:600 for the ESBWR RPV and 1:800 for the other ESBWR vessels. Similarly, power scaling was 1:400 for the SBWR, approximately 1:800 for the 4000 MWt ESBWR and approximately 1:900 for the 4500 MWt ESBWR. The same scaling ratios applied to the mass flow rates. Prototypical pressures, temperatures and pressure drops were preserved.

[22] RAI 277
[23] RAI 278

The ESBWR RPV was simulated in full height from the bottom of the core to the main steam line (MSL) and the RPV-to-PCC and RPV-to-GDCS pool elevation differences were preserved. The RPV regions below the bottom of the core and above the MSL were shortened but the overall volume of the RPV was preserved. The DW was approximately full-height, with some shortening of the regions above and below the region representing the E/SBWR annular DW (i.e., the portion of the DW surrounding the RPV). The variation of DW volume with height in the annular region was preserved so that the DW LOCA water level transient following a liquid break was similar to that expected in the E/SBWR. The lower drywell volume in the GIRAFFE facility was capable of retaining noncondensible gases and/or water as can occur in the E/SBWR.

The GIRAFFE scaling preserved the full height of the E/SBWR SC and GDCS. The configuration of the piping interconnecting the vessels corresponded to the SBWR and the 4500 MWt ESBWR design, i.e., the GDCS pool airspace and the DW were directly connected. This is different from the 4000 MWt ESBWR design (see [24]'ESBWR Design Description', NEDC-33084P, Rev 1, August 2003 for a discussion of the GDCS to containment connection in the 4000 MWt ESBWR). A vacuum breaker line connected the upper DW to the SC gas space as in the E/SBWR. The E/SBWR elevations of the three LOCA vent line discharge points and the PCC vent line discharge point were preserved. All lines interconnecting the vessels were sized and orificed to produce prototypical pressure drops at scaled mass flow rates.

The GIRAFFE PCC condenser was a three-tube representation of the E/SBWR PCCS condensers. The GIRAFFE PCC tubes were thicker than the E/SBWR tubes and, in consequence, on a purely geometric basis, the GIRAFFE PCCS scaling was about 1:690 for the SBWR. However, earlier steady-state GIRAFFE testing indicated that pure numeric and geometric scaling of the tubes relative to the prototype underestimated the heat removal capacity of the GIRAFFE condenser. It was concluded that significant heat transfer was occurring through the non-prototypical GIRAFFE headers. The net effect was to scale the PCCS at 1:430 for the SBWR (i.e., approximately 1:800 for the ESBWR), which, coincidentally, is consistent with the overall system scale. The three GIRAFFE condenser tubes were spaced so as to maintain a representative secondary-side per-tube cross-sectional flow area. A chimney surrounding the condenser unit was used to simulate the expected predominant circulation pattern in the E/SBWR condenser pools.

5.4.2 GIRAFFE/SIT Tests

The parameters of primary interest for the GIRAFFE/SIT tests were those associated with the RPV blowdown and transient water level and related systems interactions. Systems of primary interest in this regard are the GDCS, ICS, PCCS and the systems controlling RPV depressurization. The containment pressure response is important because the pressure adds to the driving head for the GDCS injection flow and impacts the blowdown flow rate once it is no longer choked. The important parameters for maintaining the correct drywell pressure are the hydraulic resistances and discharge submergences of the flow paths between the DW and the SC. These parameters were accurately represented in the GIRAFFE facility

[24] RAI 279

5.4.3 GIRAFFE/Helium Tests

The primary purpose of the GIRAFFE/Helium tests was to demonstrate the operation of the Passive Containment Cooling System (PCCS) in post-accident containment environments including both lighter and heavier-than-steam noncondensible gases. The test matrix included tests in which the DW was initially charged with nitrogen and/or helium and tests with helium addition over time to simulate the transient release of a lighter-than-steam noncondensible gas. These tests demonstrated E/SBWR containment thermal-hydraulic performance and PCCS heat removal in a wide range of potential containment accident environments. In addition, they provided data for TRACG qualification for prediction of containment response in the presence of lighter-than-steam noncondensible gases.

5.5 PANDA

The large-scale PANDA integral systems test facility at the Paul Scherrer Institute (PSI) in Switzerland provided a comprehensive set of test data for confirmation of the performance of E/SBWR passive safety systems for long-term post-LOCA containment cooling and for TRACG qualification. The issues addressed by PANDA testing included parallel operation of multiple PCC loops, parallel operation of the ICS and PCCS, DW-to-WW bypass leakage and the delayed release of noncondensible gas in the DW. The PANDA scaling of elevations, gravity heads and submergences was 1:1 for the E/SBWR. Volume/power scaling was 1:25 for the SBWR, which corresponds to approximately 1:50 for the ESBWR. The experiments were conducted under prototypical pressure and temperature conditions for the phase of the accident under considered.

Two sets of PANDA transient tests contribute to the ESBWR qualification basis. The first set (the "M-series") was performed in support of the original SBWR design which is similar to the 4500 MWt ESBWR design. From the standpoint of PCCS performance and TRACG qualification, the M-series data are also applicable to the 4000 MWt ESBWR. The second and more recent set of tests (the "P-series") were performed explicitly in support of the 4000 MWt ESBWR, as confirmatory tests. Prior to the execution of the P-series tests, the PANDA facility was reconfigured to incorporate the 4000 MWt ESBWR design change that connected the airspace of the GDCS pool to the WW instead of the DW as in the SBWR and 4500 MWt ESBWR. This change effectively increases the ratio of WW to DW volume and reduces the long-term containment pressure by providing a larger repository for the initial DW inventory of noncondensible gas. A detailed comparison between the P-series test data and TRACG test predictions is provided in Reference 5-2. In spite of some geometrical differences, both the "M-series" and "P-series" test data are valid for assessing the long-term PCCS performance of the 4500 MWt ESBWR design.

5.5.1 Facility Description

A schematic of the PANDA test facility is shown in Figure 5-4. Early in the conceptual design phase, it was concluded that it was not practical to preserve exact geometric similarity between the prototype containment volumes and the experimental facility. However, it is expected that multidimensional phenomena such as mixing of gases within large volumes and natural circulation between volumes will depend on the geometry of the containment building. The approach followed was to allow multidimensional effects to take place by representing both the DW and the SC with two vessels, and by providing a range of well-controlled boundary

conditions (e.g., RPV steam flow to one or both DW vessels) to study various system scenarios and alternative accident paths. In this way, the various phenomena could be studied under well-defined conditions and a behavior envelope of the system established. A corollary advantage of this approach is that carefully conducted parametric experiments provide the most useful data for code qualification.

As described above, the PANDA DW and SC are each represented by two interconnected cylindrical vessels (Figure 5-4). The RPV and GDCS pool were each represented by a single cylindrical vessel. The RPV contains an electrical heat source with a 1.5-MW capacity. There are three PCCS condensers representing the four units in the ESBWR. The PCC condensers are open to the two DW vessels, as shown in Figure 5-4. The fact that there are two PCC units connected to DW2 and one unit to DW1 produces a degree of asymmetric behavior between the two DWs even when they receive equal flow from the RPV. There is a single ICS condenser representing, in terms of heat removal capacity, approximately two of the four ESBWR units. The ICS is activated by opening the valve in the condensate return line to the RPV. The facility is heavily instrumented with approximately 560 sensors for temperature, pressure, pressure difference, level or void fraction, flow rate, gas concentration, electrical power, and conductivity (presence of phase) measurements.[25]

5.5.1.1 Vessels

Figure 5-5 shows the geometrical arrangement of PANDA in comparison to the E/SBWR and the relative elevations of the two systems. All the E/SBWR RPV elevations are represented except those below the top of the active fuel (TAF). The top of the PANDA RPV electric heaters is placed at the TAF location but the heaters are only about 1/2 the height of the E/SBWR core. The RPV liquid inventory above the bottom of the active fuel (BAF) is scaled according to the system scale. The RPV liquid inventory below BAF was eliminated because it is essentially inactive during the long-term cooling phase of the post-LOCA transient and is not required for the correct simulation of any gravity heads. The liquid volume between mid-core and BAF was included in the scaled PANDA RPV volume by a small adjustment of the vessel diameter. Eliminating and redistributing the water volume below mid-core and modifying the length of the heater elements does not significantly influence any natural circulation paths. The PANDA RPV includes a downcomer and a riser above the heater rods. The flow areas in the downcomer, the riser, and the core are scaled according to the system scale. The diameter of the PANDA riser is close to the hydraulic diameter of one partition of the E/SBWR riser. The PANDA facility did not include a steam separator and dryer because liquid entrainment and RPV-to-DW pressure drop are insignificant for the portion of the post-LOCA transient simulated by PANDA.

A portion of the lower SP was eliminated in PANDA to reduce vessel size. This is acceptable because the water at the bottom of the pool does not participate in the system thermal-hydraulic response during the long-term cooling phase of a LOCA. The important phenomena take place above the submergence depth of the top row of LOCA vents and, for the most part, above the discharge point for the PCCS vents. There is sufficient water below the main vent discharge in PANDA (~1.6 m) to ensure prototypical mixing during the LOCA period simulated. The effect of deeper mixing during the blowdown phase in the E/SBWR is represented by the setting of the

[25]RAI 272

test initial conditions. There is sufficient clearance between the PCC vent discharge elevation and the bottom of the SC vessel (~2 m) to ensure prototypical venting of noncondensibles and residual steam. Effects such as the convection of water to the bottom of the vessel by cold plumes running down the walls are of minor importance [5-6].

From Figure 5-5, it can be seen that the region of the DW surrounding the RPV (the annular DW) and the region below the RPV skirt (the lower DW) were not explicitly represented in PANDA. (The volume of the annular region was included in the scaled volume of the PANDA DW.) This was judged to be an acceptable simplification of the test facility because the only potentially important phenomenon taking place in these regions is retention and subsequent upward convection of a portion of the initial DW noncondensible inventory. This effect is considered in the test matrix by including tests with a delayed injection of noncondensible gas into the DW.

The PANDA GDCS vessel is roughly a factor of two smaller in relation to the E/SBWR than the system scale applied to the other vessel volumes. This is acceptable because the injection of the initial GDCS inventory to the RPV has been completed prior to the start of the portion of the LOCA transient simulated by PANDA. The GDCS volume is sufficient to hold the water inventory remaining at one hour from the start of the LOCA. During the subsequent long-term containment cooling phase, the main function of the GDCS is to provide a return path for the PCCS and ICS condensate to the RPV. Both the original M-series and the more recent P-series test matrices did, however, include one test that picked up the LOCA transient at a time when the GDCS pool is still draining its initial inventory to the RPV. It was recognized that the subscaled GDCS volume imposed a limitation on the degree to which these "early-start" tests could be expected to produce prototypical behavior. The early-start tests did, nonetheless, provide valuable information for TRACG qualification and assessment of PCCS performance with systems interactions suggestive of E/SBWR behavior during the transition from GDCS injection to PCCS operation in a noncondensible environment.

A final PANDA volumetric scaling compromise was the inventory of the PCCS/ICS pools. In the ESBWR, the boiloff volume is sufficient to maintain coverage of at least 50% of the condenser tube length for a period of 72 hours from the start of the LOCA. In PANDA, 50% of the tube length is exposed in about 18 hours from the start of a test with scaled prototypical decay heat. However, with the exception of one test that was run specifically to investigate the effect of pool boildown on PCCS performance, none of the PANDA tests was run long enough for pool boildown to play a role in the simulation.

5.5.1.2 PCCS/ICS

The PANDA facility includes a PCCS with three PCC loops and an ICS with one IC loop. For the SBWR, the three PCC loops corresponded to the three loops in the prototype PCCS, and the one IC loop represented one of the three IC loops in the prototype ICS. A key factor that led to the original PANDA SBWR system scale of 1:25 was the objective of simulating prototypical PCC and IC secondary-side behavior. The PANDA condensers are, effectively, vertical "slices" from the prototype condensers (Figure 5-6) and are fully prototypical with respect to tube height, pitch, diameter, and wall thickness. With the inclusion of baffles that prevent non-prototypical flow into the bundle in the direction of the header axis, the circulation of the secondary-side

water in a plane perpendicular to the axis of the headers is similar to that in the prototype condenser pools. Scaling is determined by the number of tubes included in the slice. The fundamental scaling consideration was to include enough tubes to have a good overall representation of secondary-side heat transfer while not enlarging the overall facility beyond practical limits. This led to the choice of five rows of tubes (i.e., twenty tubes in total).

For the SBWR, which had three PCC units with approximately 500 tubes per unit, the choice of twenty tubes for the PANDA condensers dictated a system scale of 1:25. For the ESBWR, the individual PCC units have about one-third more tubes than the SBWR units and the prototype PCCS has four PCC loops. The combination of these two factors results in a PANDA scale of 1:50 for the ESBWR PCCS. At a scale of 1:50, the one IC loop in PANDA represents approximately two of the four IC loops in the ESBWR. The scaling of the PANDA vessel volumes for the ESBWR adheres to the 1:50 ratio less stringently than the original 1:25 scaling for the SBWR but, on an overall basis, the characterization of PANDA ESBWR scaling as 1:50 is a good approximation.

5.5.1.3 Flow Paths Between Vessels

The PANDA piping is scaled according to the system scale. The pipe diameters were calculated to match the frictional and form losses of the E/SBWR at the scaled mass flow rates and the resulting pipe diameters were rounded to the next larger standard diameter. This process was facilitated by the fact that the actual pressure drops are dominated by form losses that depend weakly on flow velocity. The lines were provided with orifice plates that were used to adjust the pressure losses following calibration testing. The PANDA main steam lines (one to each DW from the RPV) were scaled to represent the combination of the E/SBWR MSLs and DPVs. To investigate asymmetric DW conditions, all of the RPV steam flow could be directed through one of the steam lines to one DW. The PANDA main vents have a cross-sectional area smaller than the one dictated by the system scale but the gas velocities in the main vents during the phase of the LOCA simulated in PANDA are small enough to produce negligible frictional loss. The vacuum breakers, which provide the flow path for potential redistribution of noncondensible gas between the SC and the DW, were simulated by control valves that were programmed to reproduce the characteristics of the E/SBWR vacuum breakers.

5.5.1.4 Vessel Heat Capacity and Heat Losses

The simulation of the heat capacity of the various SBWR structures was contemplated during the original design phase of the PANDA facility. The PANDA vessels have thin walls with limited heat capacity. The insertion of heat capacity "slabs" in the vessels to match the heat capacity of the E/SBWR structures, and the use of layers of different materials to simulate the response time of the prototype walls were considered. In the end, these concepts were not implemented because it was estimated that energy absorption in the E/SBWR boundary structures during the long-term containment cooling period was of the same order of magnitude as the PANDA facility heat losses. Facility characterization tests showed that heat losses were between 3% and 6.5% of the scaled decay heat [5-7]. The heat loss data were used to calibrate the TRACG model of the PANDA facility.[26]

[26] RAI 273

5.5.2 Establishment of Test Initial Conditions

The initial conditions for most of the PANDA M-series and P-series tests were representative of the state of the E/SBWR at the start of the long-term containment cooling period following a postulated guillotine rupture of a main steam line. Conditions at this time in the LOCA transient were derived from E/SBWR TRACG calculations. Unique sets of initial conditions were specified for tests simulating an earlier start in the LOCA transient or extreme conditions designed to challenge the performance of the PCCS (e.g., tests initiated with the DW filled with air). To establish the initial conditions, the PANDA vessels were first isolated and individually preconditioned. When the vessels were stabilized with conditions within a specified tolerance band, the connecting valves between them were opened. The PANDA RPV vessel was brought to its prescribed initial (saturated) state with the heater power close to zero. After the valves were opened, the power was quickly increased to the prescribed initial value for the test. Operator actions during specific tests included valving the IC in or out, delayed injection of DW noncondensible and opening and closing the DW-to-WW bypass leakage path.

5.6 PANTHERS

Thermal-hydraulic performance data for a PCC condenser (Figure 5-7) and an IC module (Figure 5-8) that were prototypical for the SBWR were obtained at the PANTHERS test facility in Piacenza, Italy. The IC module (half unit) tested at PANTHERS is also prototypical for the ESBWR but the PCC unit contained about 25% less tubes than the ESBWR PCC. Extrapolation of the PANTHERS PCC test data to the ESBWR is justified by the fact that the ESBWR PCC design is obtained by simply extending the upper and lower headers to accommodate the additional tubes in the exact geometric pattern of the SBWR unit. Since the PANTHERS tests were conducted with full-scale components, there are no scaling distortions to be addressed other than the issue of PCC extrapolation. There is no expected effect from testing only one IC module except, possibly, minor distortions in pool circulation that would have minimal effect on overall heat transfer

The PANTHERS tests were conducted with prototypical flow, pressure, temperature, and inlet noncondensible fractions. The purpose of the tests was to qualify the PCC and IC condenser designs with respect to thermal-hydraulic performance and structural integrity. Figures 5-9 and 5-10 show schematics of the PANTHERS test facility configured for the PCC and IC tests, respectively. A detailed description of the PANTHERS test objectives is given in the ESBWR TAPD [1-2].

The PANTHERS PCC heat transfer data were collected under steady-state conditions. This procedure was justified because the operation of the PCCS under postulated LOCA conditions can be described as a slow transient. Under certain conditions, PCCS operation may become cyclical but the period of the cycles will be long in comparison to the response time of the PCCS. The characteristic response time of a PCC condenser unit is primarily determined by the transit time of the fluid in the tubes and the time constant of the tube wall, both of which are on the order of a few seconds. Thus, the response of the PCC condenser units to changes in inlet and/or

boundary conditions is much faster than the response of the large E/SBWR containment volumes that set those conditions.[27]

5.7 UCB and MIT Condensation Heat Transfer Tests

The condensation of steam from a mixture of steam and noncondensible gases within a vertical tube under conditions expected in the PCC units was investigated in experimental programs conducted at the University of California-Berkeley (UCB) and the Massachusetts Institute of Technology (MIT). These tests encompassed tube geometries and thermodynamic conditions covering the E/SBWR conditions. Data from these tests were used to develop a model for condensation heat transfer in the presence of noncondensibles that was incorporated in TRACG [5-8].[28]

[27] RAI 274
[28] RAI 298

Table 5-1 The ESBWR Related Tests

Test	Purpose	Nominal ESBWR Scale
GIST	Integral GDCS system test	1:1000
GIRAFFE/SIT	Integral GDCS system test	1:800
GIRAFFE/He	Integral long-term containment heat removal tests with lighter-than-steam noncondensible gas	1:800
PANDA	Integral long-term containment heat removal tests	1:50
PANTHERS IC	Structural and heat transfer tests of the IC	Full-scale prototype (One module)
PANTHERS PCC	Structural and heat transfer tests of the PCC	Full-scale prototype (25% less tubes)
UCB MIT	Condensation in the presence of noncondensibles	Single-tube (near full-scale)

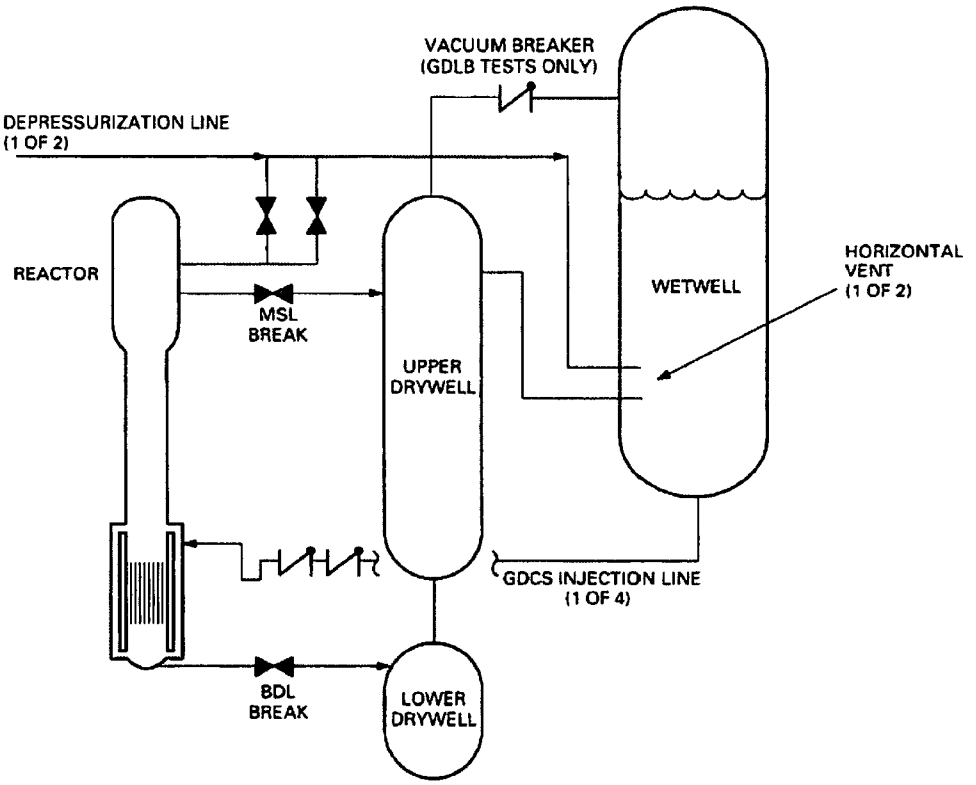

Figure 5.1. Main Components of the GIST Facility

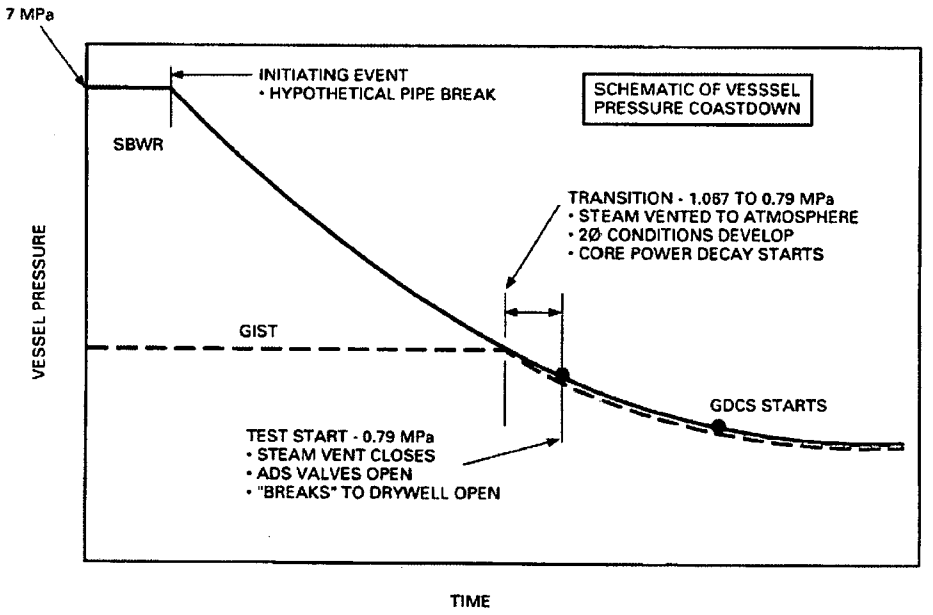

Figure 5.2. Vessel Pressure Coastdown During the SBWR and the GIST Depressurization Transients

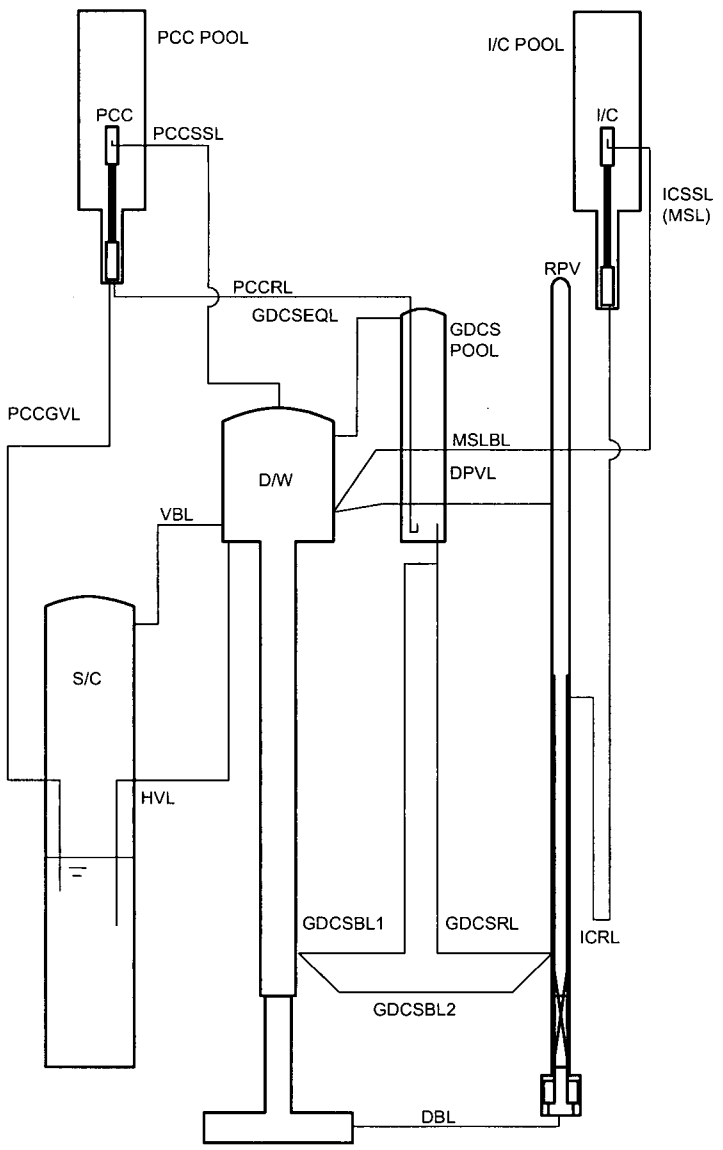

- PCCSSL
  PCC STEAM SUPPLY LINE
  D/W TOP - PCC STEAM BOX
- PCCRL
  PCC DRAIN WATER RETURN LINE
  PCC WATER BOX - GDCS POOL
  WITH U-TUBE
- PCCGVL
  PCC GAS VENT LINE
  PCC WATER BOX - S/C
- GDCSRL
  GDCS DRAIN RETURN LINE
  GDCS POOL - RPV
- GDCSEQL
  GDCS - D/W PRESSURE
  EQUALIZING LINE
  GDCS POOL - D/W
- MSLBL
  MAIN STEAM LINE BREAK LINE
  RPV - D/W
- DPVL
  DEPRESSURIZATION VALVE LINE
  RPV - D/W
- HVL
  LOCA (MAIN) VENT LINE
  D/W - S/C
- VBL
  VACUUM BREAKER LINE
  S/C - D/W
- ICSSL
  I/C STEAM SUPPLY LINE
  RPV - I/C STEAM BOX (MSL)
- ICRL
  I/C DRAIN WATER RETURN LINE
  I/C WATER BOX - RPV
  WITH U-TUBE
- GDCSBL1
  GDCSL BREAK LINE
  GDCS POOL - D/W
- GDCSBL2
  GDCSL BREAK LINE
  RPV - D/W
- DBL
  BOTTOM DRAIN BREAK LINE
  RPV BOTTOM - D/W

Figure 5-3. GIRAFFE Test Facility Schematic (GIRAFFE/SIT Test)

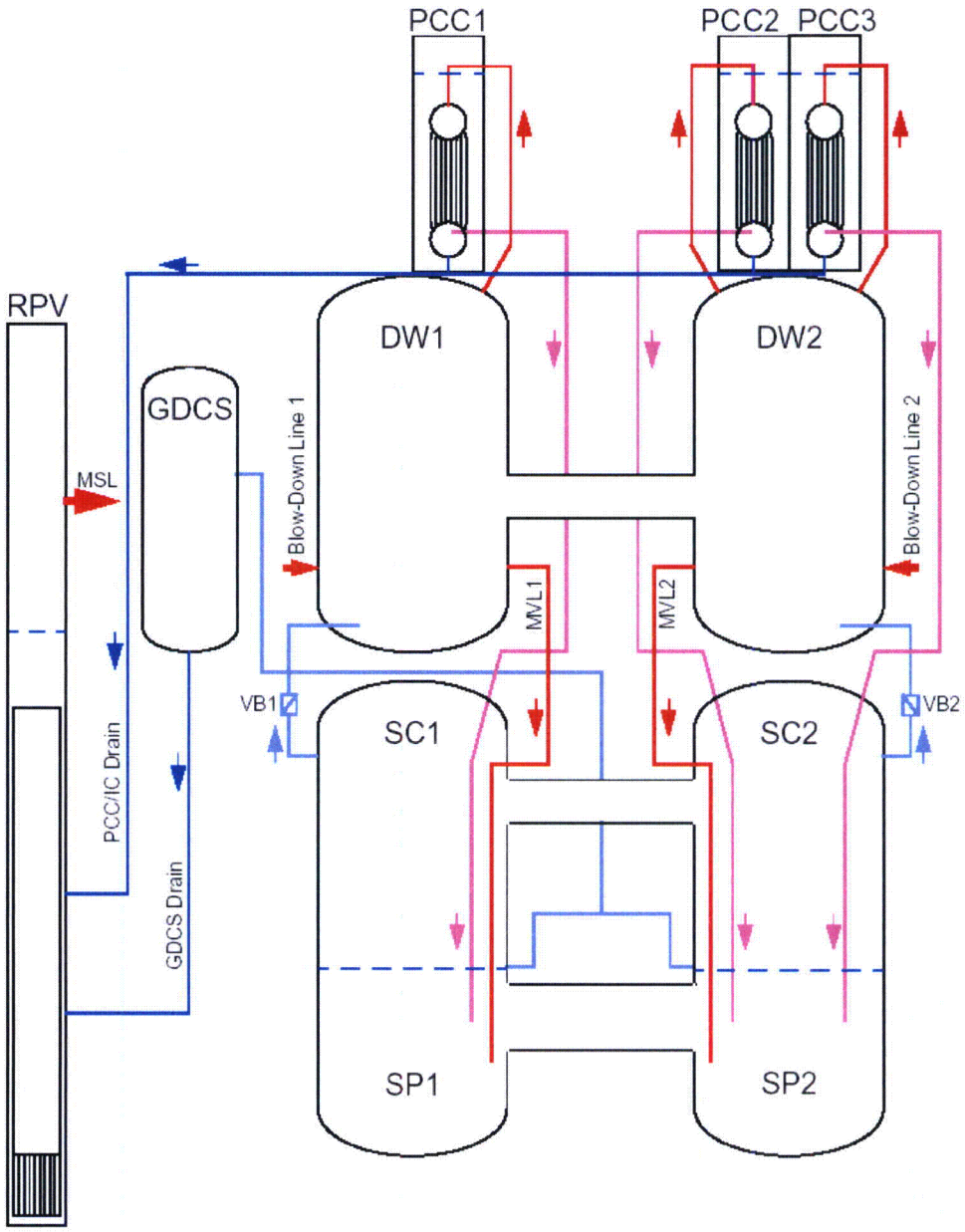

Figure 5-4. PANDA Test Facility Schematic

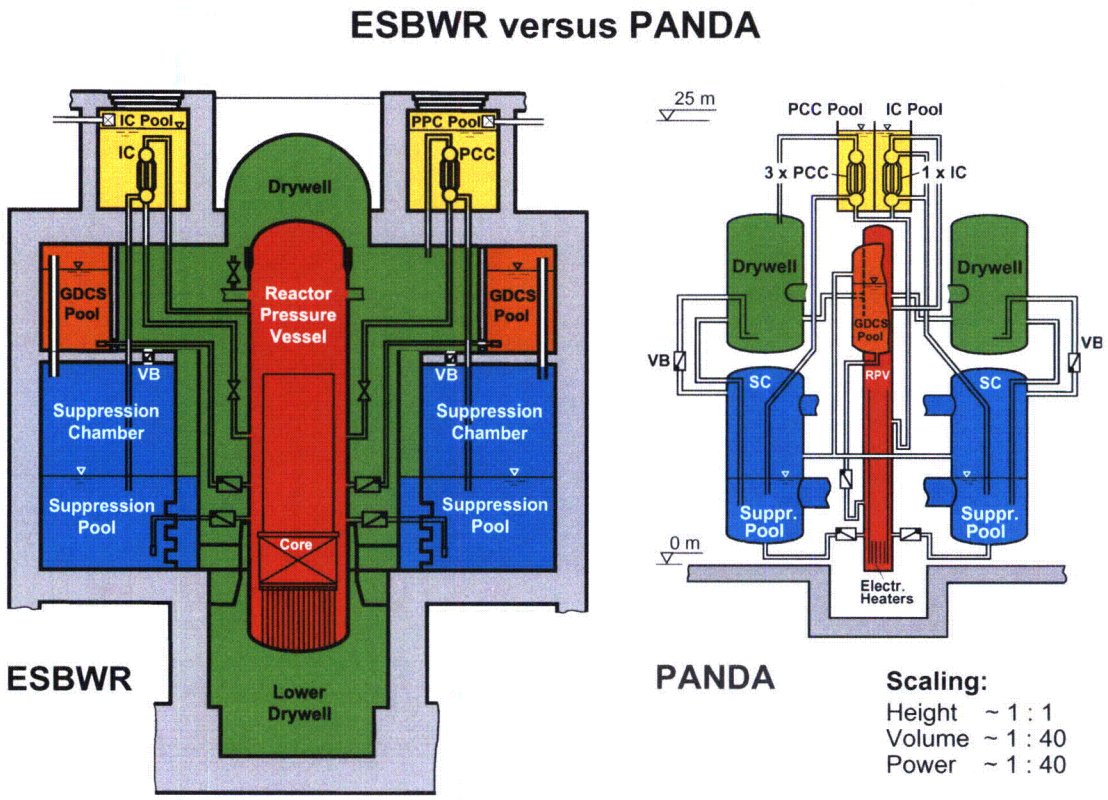

Figure 5-5. Comparison of the PANDA Elevations with the ESBWR

[[

]]

Figure 5-6. The PANDA PCCS and ICS Condenser Units

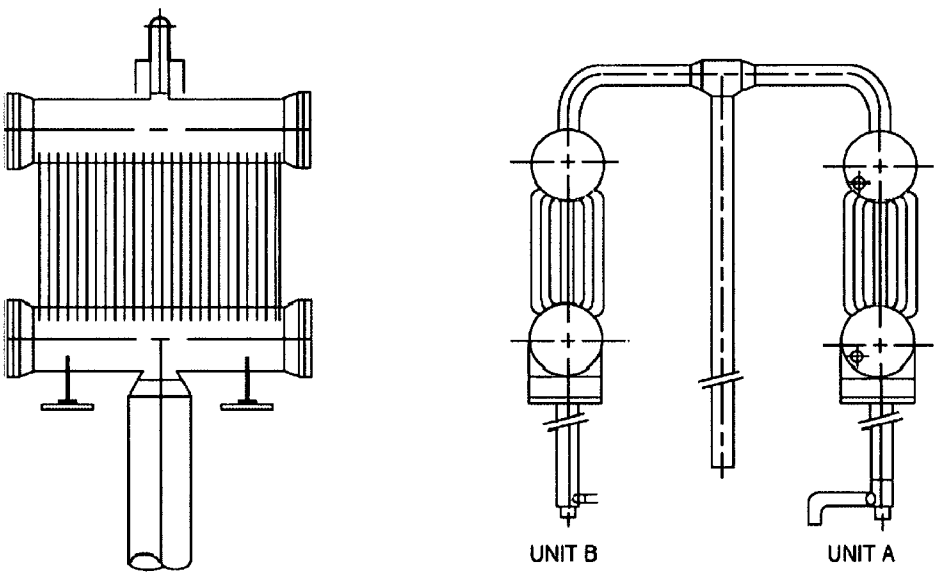

Figure 5-7. Passive Containment Condenser Tested at PANTHERS

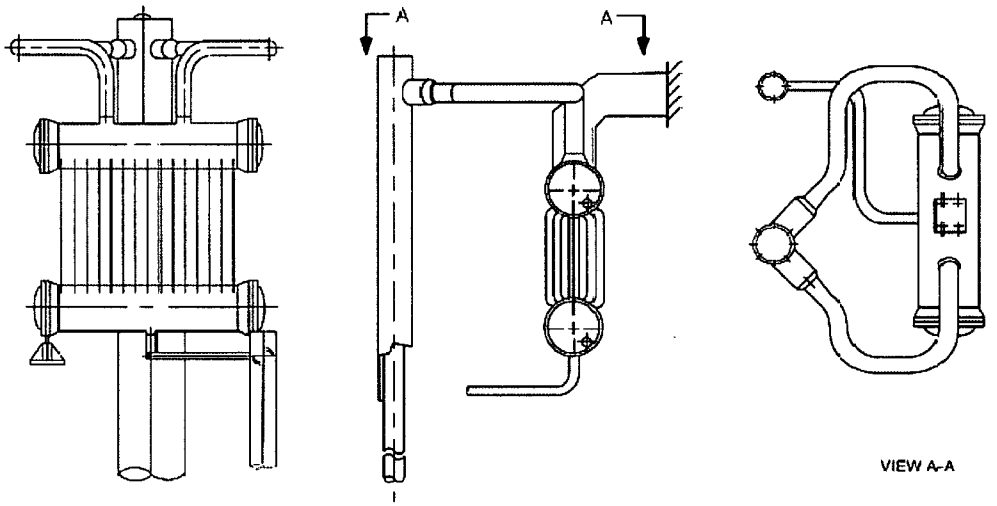

Figure 5-8. Isolation Condenser Module Tested at PANTHERS

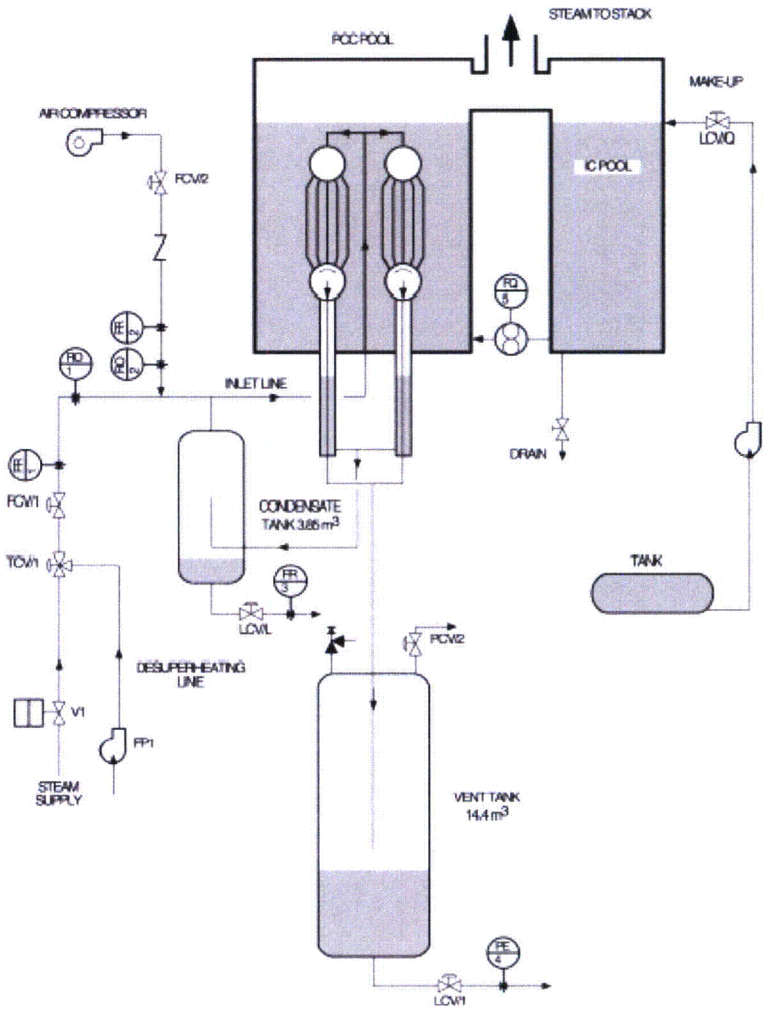

Figure 5-9. Schematic of the PANTHERS PCC Test Facility

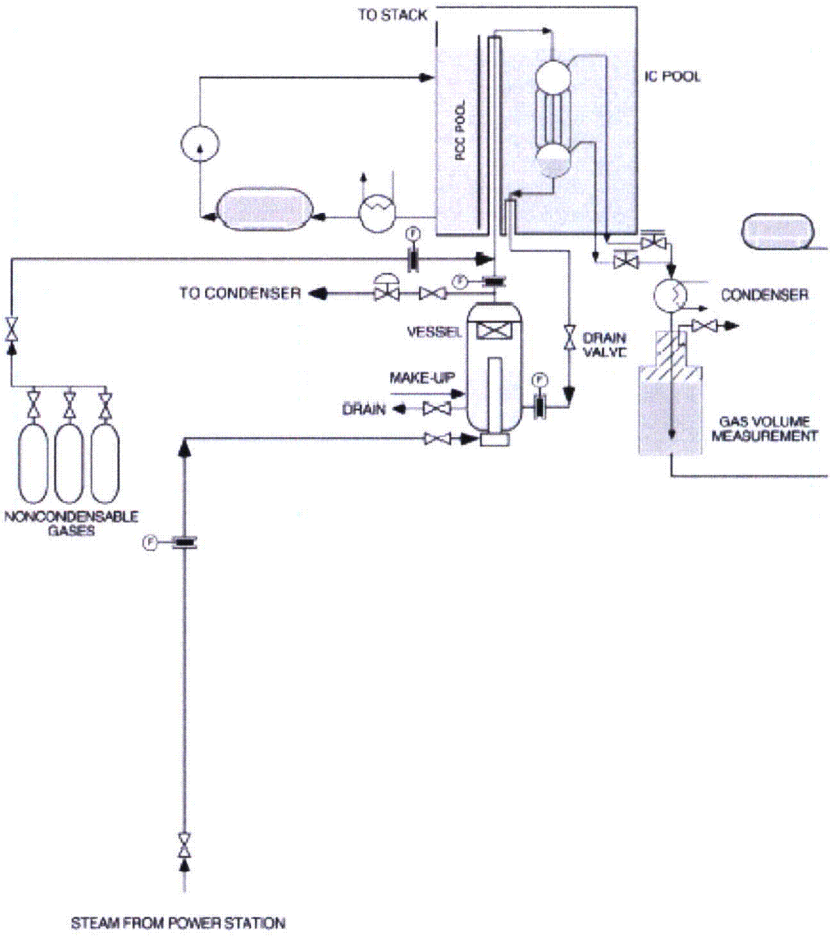

Figure 5-10. Schematics of the PANTHERS IC Test Facility

6.0 SCALING FOR PIRT VALIDATION AND TEST FACILITY EVALUATION

6.1 Scaling for Important Phenomena and Facility Distortions

In Section 4, nondimensionalization of the governing equations resulted in the general scaling criteria used to design the test facilities described in Section 5. However, in practical cases, the test facilities cannot be perfectly scaled. One then needs to evaluate the importance of scaling distortions. This section summarizes a system specific nondimensionalization method that provides the basis for identifying phenomena and processes important to system behavior and identifying distortions that may occur in test facilities.

To properly evaluate the magnitude of scaling distortions, in defining the Π numbers, one should use reference scales making the magnitude of all the *nondimensional* terms of order one. The Π numbers multiplying the various nondimensional terms will then specify their relative importance in the governing equation. This information is useful in assessing the effect of scaling distortions, and helps to ensure that (1) all important phenomena are preserved and (2) nonrepresentative effects have not been introduced. In addition, comparing corresponding Π numbers between the test and prototype results in a measure of the distortion for the related phenomenon.

In many systems, several Π groups of the same type appear in the governing equation (for example, several Π groups containing flow rates entering the control volume). It is necessary in these cases to use separate reference values for each term to adequately normalize the different flow rates. The relative magnitude of the resulting Π groups will show which system components should be scaled most carefully. Similarly, the relative magnitude of the Π terms containing the various flow rates will show which component flow rates should be matched most carefully.

Reference values for normalization are selected or carefully calculated using controlled parameters to assure that the nondimensional variables in the model equations will be of order one. For variables that are not differentiated, the reference values are selected as the value at the beginning of the phase. These are denoted by the subscript "o" in the equations below. For differentials, the reference change in the variable is selected using the estimated change resulting from the dominant causative process. These are denoted by the subscript "r" in the equations below. The selection of these reference values is covered in more detail in Section 7.3.

The governing equations summarized in Section 3.3 are normalized using reference variables as described above. The resulting nondimensionalized equations are summarized below.

Liquid Mass:

To assess the state of core coverage in the RPV the liquid mass equation (3.1-11) is used. This is similar to the void fraction equation used for the general scaling criteria but allows better quantitative assessment of the distortions in test facilities. The development of the equation is shown in Section 4.2.1 and Appendix A of the SBWR Testing Summary Report [3-2]. The right side of the equation contains terms for evaporation due to heat additions, change of mass by

liquid flows, reduction of evaporation or condensation due to entering subcooled liquid, and flashing due to depressurization. The nondimensional form of the equation is

$$h_{fg}^{+}\frac{d\Delta M_{\ell}^{+}}{dt^{+}} = -\sum_{k}\Pi_{M,\dot{Q},k}\dot{Q}_{k}^{+} + h_{fg}^{+}\sum_{i}\Pi_{M,W,i}W_{\ell,i}^{+} + \sum_{i}\Pi_{M,sub,i}h_{sub,i}^{+}W_{\ell,i}^{+} - \left[\Pi_{M,\dot{P}1}V_{RPV}^{+}f_{3}^{+} + \Pi_{M,\dot{P}2}f_{4}^{+}M_{\ell}^{+}\right]\frac{dP^{+}}{dt^{+}} \quad (6.1\text{-}1)$$

where

$f_3 = 1-\rho_g h'_g$; $f_4 = \frac{\rho_g}{\rho_l}h'_g - h'_f$ are thermodynamic properties,

$$\Pi_{M,\dot{Q},k} = \frac{\dot{Q}_{k,o}}{h_{fg,o}}\frac{t_r}{\Delta M_{\ell,r}}$$

$$\Pi_{M,W,i} = W_{\ell,i,o}\frac{t_r}{\Delta M_{\ell,r}}$$

$$\Pi_{M,sub,i} = \frac{\Delta h_{sub,i,o}}{h_{fg,o}}\frac{W_{\ell,i,o}t_r}{\Delta M_{\ell,r}} \quad (6.1\text{-}2)$$

$$\Pi_{M,\dot{P}1} = \frac{V_{RPV,o}f_{3,o}}{h_{fg,o}}\frac{\Delta P_r}{\Delta M_{\ell,r}}$$

$$\Pi_{M,\dot{P}2} = \frac{f_{4,o}\Delta P_r}{h_{fg,o}}\frac{M_{\ell,o}}{\Delta M_{\ell,r}}$$

are PI numbers, and

$$\Delta M_{\ell}^{+} = \frac{M_{\ell}-M_{\ell,o}}{\Delta M_{\ell,r}};\quad t^{+} = \frac{t}{t_r};\quad \dot{Q}_{k}^{+} = \frac{\dot{Q}_{k}}{\dot{Q}_{k,o}};\quad W_{\ell,i}^{+} = \frac{W_{\ell,i}}{W_{\ell,i,o}};\quad h_{sub,i}^{+} = \frac{\Delta h_{sub,i}}{\Delta h_{sub,i,o}};$$

$$M_{\ell}^{+} = \frac{M_{\ell}}{M_{\ell,o}};\quad P^{+} = \frac{P-P_o}{\Delta P_r};\quad h_{fg}^{+} = \frac{h_{fg}}{h_{fg,o}};\quad f_3^{+} = \frac{f_3}{f_{3,o}};\quad f_4^{+} = \frac{f_4}{f_{4,o}};\quad V_{RPV}^{+} = \frac{V_{RPV}}{V_{RPV,o}} = 1$$

are the nondimensional variables. A standard nomenclature for the Π groups is adopted where the first subscript indicates the equation to which the term applies (i.e. mass, energy or pressure), the second one indicates the phenomenon represented and the third one indicates the flow path or source.[29]

The reference value for the differential ΔP_r is the reference pressure change from the pressure rate equation (6.1-5). The reference time, t_r, is determined by the reference time for the phase as defined in Section 7.3. By using a common reference time across all model equations for a given phase, distortions in timing of different processes will be identified. The reference value for

[29] RAI 280

mass change is determined by making the dominant Π group equal to 1. For the late blowdown and GDCS transitions phases the dominant cause for liquid mass *loss* is flashing. [[

]] we set the second nondimensional flashing term $\Pi_{M,\dot{P}2}$ equal to 1,

$$\Pi_{M,\dot{P}2} = \frac{f_{4,o}\Delta P_r}{h_{fg,o}} \frac{M_{\ell,o}}{\Delta M_{\ell,r}} = 1$$

or

$$\Delta M_{\ell,r} = \frac{f_{4,o}\Delta P_r}{h_{fg,o}} M_{\ell,o}$$

For the reflood phase, the liquid mass *increase* is dominated by GDCS flow so that the reference change in mass is given by

$$\Delta M_{\ell,r} = W_{\ell,GDCS}\, t_r$$

The remaining reference values are the values at the beginning of the phase.

The summation signs in Equation 6.1-1 indicate that there can be multiple sources for many of the phenomena. For example, mass change due to liquid flows can result from break flow, SLCS flow, GDCS flow and IC condensation drain line flow. In applying this equation the relevant flow path or source would replace the subscript i.

Temperature (Energy) Equation:

The temperature of the suppression pool is important to the steam partial pressure in the WW gas space. The temperature change is of course dependent on the energy in the pool. The nondimensional form of the full equation is

$$M^+ \frac{de^+}{dt^+} = -\Pi_{e,\dot{V}} P^+ \frac{d\Delta V^+}{dt^+} + \sum_k \Pi_{e,\dot{Q},k} \dot{Q}_k^+ + \sum_i \Pi_{e,Wh,i} W_i^+ h_i^+ + P^+/\rho^+ \sum_i \Pi_{e,mech,i} W_i^+ \qquad (6.1\text{-}3)^{30}$$

where:

$$\Pi_{e,\dot{V}} = \frac{P_o \Delta V_r}{M_o \Delta e_r} \; ; \; \Pi_{e,\dot{Q},k} = \frac{\dot{Q}_{k,o} t_r}{M_o \Delta e_r} \; ; \; \Pi_{e,Wh,i} = \frac{W_{i,o} \Delta h_{i,o} t_r}{M_o \Delta e_r} \; ; \; \Pi_{e,mech,i} = \frac{P_o W_{i,o} t_r}{M_o \Delta e_r \rho_o} \qquad (6.1\text{-}4)$$

[30] RAI 281

and

$$e_i^+ = \frac{e - e_o}{\Delta e_r}; \quad P^+ = \frac{P}{P_o}; \quad \Delta V^+ = \frac{V - V_o}{\Delta V_r}; \quad t^+ = \frac{t - t_o}{t_r};$$

$$\dot{Q}_k^+ = \frac{\dot{Q}_k}{\dot{Q}_{i.o}}; \quad W_i^+ = \frac{W_i}{W_{i.o}}; \quad h_i^+ = \frac{h_i - h}{\Delta h_{i.o}};$$

$$\rho^+ = \frac{\rho}{\rho_o}; \quad M^+ = \frac{M}{M_o}$$

are nondimensional variables.

Time Rate of Pressure Change

An additional parameter that is important for the Late Blowdown/GDCS phase is the RPV pressure. It is important because it determines the time at which injection of GDCS flow to the RPV can begin as well as influencing the two-phase level and quantity of liquid changed to vapor due to flashing. The pressure rate equation is developed in the SBWR scaling report [3-1, Eq. 2.5-3].

The right side of the equation contains terms for energy increase due to heat and enthalpy additions, pressurization due to volume changes and fluid addition and changes in constituent fractions. The nondimensional form of the equation is

$$f_2^+ V^+ \frac{dP^+}{dt^+} = \sum_k \Pi_{P,\dot{Q},k} Q_k^+ - \Pi_{P,V} P^{*+} \frac{d\Delta V^+}{dt^+} + \sum_i \Pi_{P,Wh,i} W_i^+ h_j^+ + \frac{P^{*+}}{\rho^+} \sum_i \Pi_{P,\,mech,\,i} W_i^+ - V^+ \sum_j \Pi_{P,yj} \left(f_{1,j}^+ \frac{dy_j^+}{dt^+} \right) \tag{6.1-5}$$

where

$$P^* = P + \left. \frac{\partial e}{\partial v} \right|_{P,y_j}$$

$$f_{l,j} = \left. \frac{1}{v} \frac{\partial e}{\partial y_j} \right|_{P,v,y}$$

$$f_2 = \left. \frac{1}{v} \frac{\partial e}{\partial P} \right|_{v,y_j}$$

are thermodynamic properties, and

$$\Pi_{P,\dot{Q},k} = \frac{\dot{Q}_{k,o}}{V_o f_{2,o}} \frac{t_r}{\Delta P_r}$$

$$\Pi_{P,\dot{V}} = \frac{P_o^* \Delta V_r}{\Delta P_r V_o f_{2,o}} = 0 \qquad \text{(in this study)} \qquad (6.1\text{-}6)$$

$$\Pi_{P,Wh,i} = \frac{W_{i,o} \Delta h_{i,o}}{V_o f_{2,o}} \frac{t_r}{\Delta P_r}$$

$$\Pi_{P,mech,i} = \frac{W_{i,o} P_o^*}{V_o f_{2,o} \rho_o} \frac{t_r}{\Delta P_r}$$

$$\Pi_{P,y,j} = \frac{f_{1,j,o} \Delta y_{j,r}}{\Delta P_r f_{2,o}}$$

are PI numbers, and

$$P^+ = \frac{P - P_o}{\Delta P_r}; \quad V^+ = \frac{V}{V_o}; \quad \Delta V^+ = \frac{V - V_0}{\Delta V_r}; \quad t^+ = \frac{t - t_o}{t_r};$$

$$\dot{Q}_k^+ = \frac{\dot{Q}_k}{\dot{Q}_{k.o}}; \quad W_i^+ = \frac{W_i}{W_{i.o}}; \quad h_i^+ = \frac{h_i - h}{\Delta h_{i.o}}; \quad y_j^+ = \frac{y_j - y_{j,o}}{\Delta y_{i,r}};$$

$$P^{*+} = \frac{P^*}{P_o^*}; \quad \rho^+ = \frac{\rho}{\rho_o}; \quad f_{1,j}^+ = \frac{f_{1,j}}{f_{1,j,o}}; \quad f_2^+ = \frac{f_2}{f_{2,o}}$$

are nondimensional variables. This equation is used for the RPV for the late blowdown and GDCS transition phases and in the containment drywell and wetwell regions for the long-term phase.

RPV Reference Values

The reference values for the pressure differential for the RPV are determined by the pressures at the beginning and end of the phase as discussed in Section 7.3.[31] The reference times for the late blowdown and GDCS transition phase are governed by the pressure rate equation and are given by the time for the pressure to decrease from the phase beginning pressure to the final pressure as a result of the dominant phenomenon on the right hand side of the equation - in this case enthalpy flow through the ADS. From the PI-group for this term, $\Pi_{P,Wh,\,ADS}$, we see that this is given by

[31] RAI 284

$$t_r = \frac{\Delta P_r V_r f_{2,r}}{W_{i,ADS} \Delta h_{i,ADS}}$$

where the flow is based on the blowdown flow leaving the vessel for the late blowdown phase.

Containment Reference Values

For the long-term phase, the pressure of interest is the containment pressure. The reference pressure is the difference between the pressure at the beginning of the phase and the containment design limit as discussed in Section 7.3.[32] The reference volume change is zero since the volumes are set by fixed walls and the water level movement during a phase is negligible in the DW and WW. [[

]] The remaining reference values are the values at the beginning of the phase.

Momentum in Lines:

The equation for momentum in lines has not changed from the one used for general scaling criteria in Section 4,

$$\Pi_{in} \frac{dW^+}{dt^+} = \Pi_{pd} \Delta P^+ - \Pi_{loss} \frac{W^{+2}}{\rho^+} + \Pi_h \rho^+ H^+ \quad (6.1\text{-}7)$$

Where

$$\Pi_{in} \equiv \frac{W_r \left(\frac{L}{a}\right)_r}{\Delta P_r t_r} \quad (6.1\text{-}8)$$

$$\Pi_{pd} \equiv \frac{\Delta P_o}{\Delta P_r} \quad (6.1\text{-}9)$$

$$\Pi_{loss} \equiv \frac{W_r^2 \left(\frac{F}{a^2}\right)_r}{2 \Delta P_r \rho_r} \quad (6.1\text{-}10)$$

[32] RAI 284

$$\Pi_h \equiv \frac{\rho_r g H_r}{\Delta P_r} \tag{6.1-11}$$

are PI numbers, and

$$\Delta P^+ = \frac{P_1 - P_2}{\Delta P_o}; \quad t^+ = \frac{t}{t_r}$$

$$W^+ = \frac{W}{W_r}; \quad \rho^+ = \frac{\rho}{\rho_o}; \quad H^+ = \frac{H}{H_o}$$

are nondimensional variables. The reference time is determined by the acceleration time of the flow for the given driving force as described in Section 4.6. The reference change in mass flow rate, ΔW_r, is generally the quasi-steady flow rate in the pipe, W_r, since the initial value is zero in most cases. The reference pressure differential, ΔP_r, is the difference in initial pressure between the two volumes connected by the pipe. The remaining reference values are the initial values for the phase.

6.2 Global Momentum Scaling

In the SBWR scaling report [3-1] global momentum scaling was developed and applied. In this process, matrix equations for the entire system are developed and nondimensionalized. In addition, global reference values as well as local ones are used to nondimensionalize the equations. There are two main objectives of this type of scaling:

- identify any additional nondimensional numbers that may result
- identify any interactions between different flow paths that may occur

The results from the SBWR work showed that there are no significant interactions in the SBWR system or the related tests and no new PI numbers resulted.[33] In addition, the complexity added by using matrix momentum equations rather than individual equations for each system line made the conclusions that could be drawn regarding momentum scaling less clear.

The ESBWR configuration is similar enough to the SBWR that conclusions resulting from application of this method would be the same. Therefore global momentum scaling is not repeated for the ESBWR. Instead, the effects on momentum scaling of individual lines that may result from changes to the SBWR design are considered.

6.3 Summary

This section summarized the system specific nondimensionalization of the governing equations for determination of phenomena importance and quantification of distortions in test facilities. The equations are summarized below and the resulting PI numbers are summarized in table 6-1.

[33] RAI 286, Supp RAI 259 & Supp RAI 286

These equations are applied to the specific regions of the ESBWR in Section 7 and the test facilities in Section 8.

$$h_{fg}^{+}\frac{d\Delta M_{\ell}^{+}}{dt^{+}} = -\sum_{k}\Pi_{M,\dot{Q},k}\dot{Q}_{k}^{+} + h_{fg}^{+}\sum_{i}\Pi_{M,W,i}W_{\ell,i}^{+} + \sum_{i}\Pi_{M,sub,i}h_{sub,i}^{+}W_{\ell,i}^{+} - \left[\Pi_{M,\dot{P}1}V_{RPV}^{+}f_{3}^{+} + \Pi_{M,\dot{P}2}f_{4}^{+}M_{\ell}^{+}\right]\frac{dP^{+}}{dt^{+}} \quad (6.1\text{-}1)$$

$$M^{+}\frac{de^{+}}{dt^{+}} = -\Pi_{e,\dot{V}}P^{+}\frac{d\Delta V^{+}}{dt^{+}} + \sum_{k}\Pi_{e,\dot{Q},k}\dot{Q}_{k}^{+} + \sum_{i}\Pi_{e,Wh,i}W_{i}^{+}h_{i}^{+} + P^{+}/\rho^{+}\sum_{i}\Pi_{e,mech,i}W_{i}^{+} \quad (6.1\text{-}3)^{34}$$

$$f_{2}^{+}V^{+}\frac{dP^{+}}{dt^{+}} = \sum_{k}\Pi_{P,\dot{Q},k}Q_{k}^{+} - \Pi_{P,\dot{V}}P^{*+}\frac{d\Delta V^{+}}{dt^{+}} + \sum_{i}\Pi_{P,Wh,i}W_{i}^{+}h_{i}^{+} + \frac{P^{*+}}{\rho^{+}}\sum_{i}\Pi_{P,mech,i}W_{i}^{+} - V^{+}\sum_{j}\Pi_{P,y,j}\left(f_{1,j}^{+}\frac{dy_{j}^{+}}{dt^{+}}\right) \quad (6.1\text{-}5)$$

$$\Pi_{in}\frac{dW^{+}}{dt^{+}} = \Pi_{pd}\Delta P^{+} - \Pi_{loss}\frac{W^{+2}}{\rho^{+}} + \Pi_{h}\rho^{+}H^{+} \quad (6.1\text{-}7)$$

[34] RAI 281

Table 6-1 Summary of PI-groups

PI-group	Equation Where Used	Comment
$\Pi_{M,\dot{Q}_k} = \frac{\dot{Q}_{k,o}}{h_{fg,o}} \frac{t_r}{\Delta M_{l,r}}$	Liquid Mass (6.1-1)	Mass *loss* due to boiling from heat addition
$\Pi_{M,W,i} = W_{\ell,i,o} \frac{t_r}{\Delta M_{\ell,r}}$	Liquid Mass (6.1-1)	Mass change due to liquid flow in or out of control volume
$\Pi_{M,sub,i} = \frac{\Delta h_{sub,i,o}}{h_{fg,o}} \frac{W_{\ell,i,o} t_r}{\Delta M_{\ell,r}}$	Liquid Mass (6.1-1)	Mass change due to subcooling of inlet flow
$\Pi_{M,\dot{P}1} = \frac{V_{RPV,o} f_{3,o}}{h_{fg,o}} \frac{\Delta P_r}{\Delta M_{l,r}}$	Liquid Mass (6.1-1)	Mass *loss* due to flashing as a result of pressure changes (Part 1)
$\Pi_{M,\dot{P}2} = \frac{f_{4,o} \Delta P_r}{h_{fg,o}} \frac{M_{\ell,o}}{\Delta M_{\ell,r}}$	Liquid Mass (6.1-1)	Mass *loss* due to flashing as a result of pressure changes (Part 2)
$\Pi_{e,\dot{V}} = \frac{P_o \Delta V_r}{M_o \Delta e_r}$	Temperature (Energy) 6.1-3	Energy change due to changes of volume
$\Pi_{e,\dot{Q}_k} = \frac{\dot{Q}_{k,o} t_r}{M_o \Delta e_r}$	Temperature (Energy) 6.1-3	Energy change due to heat additions
$\Pi_{e,wh,i} = \frac{W_{i,o} \Delta h_{i,o} t_r}{M_o \Delta e_r}$	Temperature (Energy) 6.1-3	Energy change due to enthalpy additions
$\Pi_{e,mech,i} = \frac{P_o W_{i,o} t_r}{M_o \Delta e_r \rho_o}$	Temperature (Energy) 6.1-3	Energy changes due to mechanical work from incoming or outgoing fluid
$\Pi_{P,\dot{Q}_k} = \frac{\dot{Q}_{k,o}}{V_o f_{2,o}} \frac{t_r}{\Delta P_r}$	Pressure Rate (6.1-5)	Pressure change due to sensible heat additions
$\Pi_{P,\dot{V}} = \frac{P_o^* \Delta V_r}{\Delta P_r V_o f_{2,o}}$	Pressure Rate (6.1-5)	Pressure change due to volume change
$\Pi_{P,Wh,i} = \frac{W_{i,o} \Delta h_{i,o}}{V_o f_{2,o}} \frac{t_r}{\Delta P_r}$	Pressure Rate (6.1-5)	Pressure change due to enthalpy addition or subtraction
$\Pi_{P,mech,i} = \frac{W_{i,o} P_o^*}{V_o f_{2,o} \rho_o} \frac{t_r}{\Delta P_r}$	Pressure Rate (6.1-5)	Pressure change due to mechanical work from incoming or outgoing fluid
$\Pi_{P,y,j} = \frac{f_{1,j,o} \Delta y_{j,r}}{\Delta P_r f_{2,o}}$	Pressure Rate (6.1-5)	Pressure change due to changes in constituent mass fractions
$\Pi_{in} \equiv \frac{W_r \left(\frac{L}{a}\right)_r}{\Delta P_r t_r}$	Momentum (6.1-7)	Ratio of pressure drop due to acceleration to reference pressure drop

PI-group	Equation Where Used	Comment
$\Pi_{pd} \equiv \frac{\Delta P_o}{\Delta P_r}$	Momentum (6.1-7)	Ratio of pressure difference between end points to reference pressure drop
$\Pi_{loss} \equiv \frac{W_r^2\left(\frac{F}{a^2}\right)_r}{2\Delta P_r \rho_r}$	Momentum (6.1-7)	Ratio of pressure drop due to friction and form basis to reference pressure drop
$\Pi_h \equiv \frac{\rho_r g H_r}{\Delta P_r}$	Momentum (6.1-7)	Ratio of submergence or hydrostatic pressure difference to reference pressure drop

7.0 ESBWR RESULTS – PIRT VALIDATION

In this section the nondimensional forms of the governing equations summarized in Section 6 are applied to the ESBWR.[35] Sections 7.1 and 7.2 discuss the transient phases of a LOCA in the ESBWR and for what periods, ESBWR volumes, and parameters the scaling will be applied. Section 7.3 summarizes the method of selecting reference values that assures that the scaling results obtained are valid. In Sections 7.4 through 7.7 the results are presented and summarized for the equations as applied to the ESBWR. The details of the reference values used and detailed results can be found in Appendix A.

7.1 Transient Phases

Figure 1-1 shows the different periods or phases of a LOCA transient in the ESBWR. Key variables are represented schematically in the figure (RPV, DW and WW pressures; decay heat and PCC heat removal; GDCS flow and RPV mass). The figure shows how the magnitudes of the different parameters vary from phase to phase. Four transient phases were considered for scaling: (1) Late Blowdown, (2) Transition to GDCS Flow, (3) Full GDCS (or Reflood), and (4) Long Term PCCS. The breaks between phases were selected based on when a significant change in the magnitude of one or more of the key variables occurred. Within each phase, the important variables maintain a similar magnitude and/or the same phenomena remain important. Breaking the transient into phases is necessary to assure that the nondimensional variables remain of order one over the range of application, which is a necessary condition for validity of the top-down scaling methodology as has been discussed in [7-1]. Scaling provides a snapshot of the system behavior at a single point in time. By breaking the transient into phases where the magnitudes of variables do not change significantly the scaling done at a single point in time is representative of the entire phase. Therefore continuous time dependent scaling is neither needed nor desirable.

The beginning of phase 1 corresponds to late blowdown where the LOCA transient was picked up in the GIST and GIRAFFE/SIT tests. The beginning of phase 2 corresponds to the beginning of GDCS injection when the RPV to WW or DW (depending on containment configuration) pressure difference is equal to the hydrostatic head in the GDCS drain system (P_{rpv}-P_{ww} = ρgL or P_{rpv}–P_{dw} = ρgL). Phase 3 represents the quasi-steady period when GDCS is flowing into RPV at a high rate primarily governed by the hydrostatic head in the GDCS system and piping pressure losses. Phase 4 represents a quasi-steady period when the PCCS is removing decay heat.

7.2 Important System Parameters[36]

Table 7-1 summarizes the specific applications of the scaling equations to different regions of the ESBWR. The water level in the RPV is of prime interest during the first three phases. Therefore, the RPV liquid mass equation is evaluated for these phases. Additionally, the RPV depressurization is important, since it controls the flashing rate and time of GDCS initiation. Thus, the RPV pressure is also considered for these phases.

In the long-term phase, the liquid level has recovered in the RPV and the containment pressure is of primary interest. The containment pressure is set by the pressure in the WW. The initial

[35] RAI 285
[36] RAI 294

increase in containment pressure occurs during the blowdown phase when most of the noncondensibles are moved to the WW. The long-term pressure is controlled by the quantity of noncondensibles in the WW and the energy balance for the WW gas space. Therefore, the pressure equation is evaluated for the WW in the long-term PCCS phase. The DW acts primarily as a conduit for steam to flow to the PCCS and WW during all phases. To assure that this is the case and that none of the sources and sinks of energy in the DW are important relative to the PCCS heat removal, the pressure equation is also evaluated for the DW during the long-term phase.

Table 7-1 Application of Scaling Equations to ESBWR Phases and Regions[37]

		Plant Region		
		RPV [5]	**DW[2]**	**WW gas[3]**
Transient Phase	**Late Blowdown (7.5.1)[1,4]**	M, P	-	-
	GDCS Transition (7.5.1)[1,4]	M, P	-	-
	Full GDCS (7.5.1) [1,4]	M	-	-
	Long Term PCCS (7.5.2) [1,4]	-	P	P

1 M = liquid mass equation, P = pressure equation.
2 DW and RPV gas act as one volume during reflood and long-term phases
3 Includes GDCS gas volume for 4000 MWt ESBWR containment design
4 Number in parenthesis is section where results are shown
5 The limiting breaks are used for each region: GDCS Line break for the RPV and MSLB or FWLB for the containment

7.3 Reference Parameters

The reference values are carefully calculated in order to assure that the nondimensional variables in the equations of Section 6.3 are of order 1. In this way the magnitudes of the different PI numbers on the right hand side of the equation indicate the relative importance of each phenomenon affecting the parameter on the left hand side of the equation. The important parameters then become the ones that are important to match well in the test facilities. The methods for calculating the reference parameters are summarized below. The complete set of reference parameters is given in Appendix A.

[37] RAI 294

7.3.1 Transient Phase Boundaries

One reference time is selected for each transient phase. By normalizing each model equation during a transient phase with a common reference time, distortions resulting from timing differences become transparent.[38] The reference time is selected to represent the time associated with the dominant process during the phase.

Late blowdown phase

The late blowdown phase begins at the point of test initiation for the GIRAFFE/SIT and GIST tests, 1.03 and 0.79 MPa, respectively. The phase ends when the RPV pressure is low enough for the GDCS flow to start given that the level in the RPV is below the GDCS nozzle. This will be true when the pressure difference between the GDCS gas space and the RPV dome is equal to the hydrostatic head in the GDCS line and pool (see Figure 4.2-1). The pressure difference between the RPV dome and GDCS gas space is given by

$$P_{RPV} - P_{GDCSgas} = \frac{1}{2\rho_g} W_{ADS}^2 \left(\frac{F}{a^2}\right)_{ADS} + \frac{1}{2\rho_g} W_{ADS}^2 \left(\frac{F}{a^2}\right)_{MV} + \rho_l g h_{sub,MV} \qquad (7.3\text{-}1a)$$

where equation 3.2-3 has been specialized to the flow paths of interest by adding subscripts to identify the local flow path and substituting the main vent submergence, $h_{sub,MV}$, for the generic term H in eq. 3.2-3. Here we are assuming that all of the ADS flow goes through the MV to the SP (a reasonable approximation given the much lower press drop through the main vent path compared to the PCCS vent). Additionally, the form losses are small compared to the submergence of the main vent so this can be further simplified to

$$P_{RPV} - P_{GDCSgas} \cong \frac{1}{2\rho_g} W_{ADS}^2 \left(\frac{F}{a^2}\right)_{ADS} + \rho_l g h_{sub,MV} \qquad (7.3\text{-}1b)$$

The pressure at the end of the late blowdown phase comes from setting the transient term and the flow rate in the line momentum equation (3.2-3) equal to zero[40]

$$0 = P_{GDCSgas} - P_{RPV} + \rho g H_{GDCS} \qquad (7.3\text{-}2)$$

In Eqn. 7.3-2, H_{GDCS} is the vertical height of the liquid filled GDCS line. Note that the submergence is also zero since the water level in the RPV is assumed to be below the GDCS injection nozzle. Since the ADS flow rate is a function of the RPV pressure also, equations 7.3-1b and 7.3-2 can be used to solve for the RPV pressure when the GDCS flow begins.

The dominant process controlling this transient period is the depressurization of the vessel. Therefore the reference time is selected to be the blowdown time constant. This comes from balancing the dominant depressurization driving force against the depressurization rate in the nondimensional RPV pressure rate equation (6.1-5). The dominant term controlling the

[38] RAI 287
[39] RAI 288

blowdown rate (as is shown later in Figure 7-4) is the loss of energy through the ADS flow paths. Therefore the reference time is obtained by setting the corresponding PI-group, $\Pi_{P,Wh,ADS}$ equal to 1 (the multiplier on the left hand side of the equation). The resulting relationship is

$$t_r = \frac{\Delta P_r V_r f_{2,r}}{W_{i,ADS} \Delta h_{i,ADS}} \tag{7.3-3}$$

where the reference pressure difference is the RPV pressure at the beginning of the late blowdown phase minus the DW pressure.[40]

GDCS Transition

The GDCS transition phase ends when the GDCS flow rate reaches its maximum value, which occurs when the RPV and DW have equalized in pressure (i.e. blowdown is over). It was shown in the SBWR scaling report [3-1] that the driving pressure rather than the line inertia controls the GDCS flow.

Since this process is controlled by RPV depressurization also, the blowdown time constant is again used for the reference time. The process above is repeated but the reference values are taken from the conditions at the beginning of the GDCS transition phase (corresponding to saturated conditions at the pressure given by equation 7.3-2). The reference pressure difference is the RPV pressure at the beginning of the GDCS transition phase minus the DW pressure.

Reflood Phase

The reflood phase continues until the GDCS pool has drained or the water level is in equilibrium with the level in the RPV. The period of primary interest, however, is during the initial water level increase when the water level is still near its minimum value. Therefore the reflood period is considered to end when 2 meters of water have been added to the RPV water level. The selection of 2 meters is arbitrary as long as the same value is used for the ESBWR and tests a consistent comparison results. The resulting reference time will be

$$t_r = \frac{\Delta M_{\ell,r}}{W_{\ell,GDCS,o}} = \frac{\Delta V_r \rho_r}{W_{\ell,GDCS,o}} \tag{7.3-4}$$

where the mass and volume changes refer to the free space in the 2 meters above the core.

Long-term phase

The long-term phase is a quasi-steady period where the pressures and levels are approximately constant. As such, there is no obvious beginning or end to the period. The parameter of interest is that the containment pressure , to assure that it does not exceed the design limit. Therefore this phase is defined by the time it will take for the containment pressure to reach the design limit due to VB leakage with no mitigating heat or mass losses from the WW gas space. The start of the

[40] RAI 289

phase is taken at 6 hours to assure that the subcooling in the RPV has been eliminated by decay heat. The phase duration is set by the pressurization time constant as shown in the next section.

7.3.2 Reference Times

As described above the reference times for the four phases are:

Late blowdown: time for RPV to depressurize from the GIRAFFE or GIST starting pressure to the pressure at which GDCS flow can begin, given by equation 7.3-3.

GDCS Transition: time for RPV to depressurize from the pressure at the end of late blowdown phase to the DW pressure, again given by equation 7.3-3 with values for flow, enthalpy, pressure, etc..

Reflood: time for GDCS flow to increase vessel collapsed water level by two meters, given by V/Q where V is the free volume in two meters of the RPV and Q is the maximum GDCS volumetric flow rate from the GDCS momentum equation,

$$0 = -\rho_m g h_{sub,MV} + \rho_m g L_m - \left(\frac{F}{a^2}\right)_m \frac{W_m^2}{2\rho_m}$$

Long-term Phase: time to pressurize WW to the design limit as a result of VB leakage, given by equation 7.3-3 with appropriate values for the reference parameters.

7.3.3 Pressure

For the RPV, the reference pressure differences are defined by the phase boundaries as described in the previous two sections. The reference pressures are the pressures at the beginning of each phase. The RPV pressure is not calculated after the first two phases.

The tests considered as part of this work start in the late blowdown phase, after the RPV pressure has dropped to ~10% of its initial value and the majority of noncondensibles have been moved from the DW to the WW, pressurizing the containment. There is a large uncertainty about the fraction of noncondensibles that remain in the DW at this stage, since it is dependent on noncondensible gas hideout and the specific location of the broken pipe. As discussed elsewhere stratification and hideout will be treated in a bounding manner rather than best estimate prediction since TRACG is not designed to do CFD calculations. [[

]]

The actual value is not significant. As long as the tests and prototype are treated in the same manner, scaling distortions, such as differences in the DW to WW volume ratio will be uncovered by this methodology.

At later stages the containment pressure will change due to increases in the WW volume due to GDCS drain down and an increase in the steam partial pressure. The last 5% of the noncondensibles are assumed to move to the WW during the long-term phase, providing the noncondensible source for the bubble term and the constituent fraction term shown in Figure 7-7. For the long-term phase, the reference pressure difference is the difference between the pressure at the beginning of the phase and the design limit as described above.

7.3.4 Flow rates

Reference flow rates are set based on quasi-steady flow rates for the given pressures and water levels at the beginning of each phase. Flow rates from the RPV are based on choked flow when pressure exceeds the critical pressure. Bernoulli flow is used when the pressure is below the critical pressure. The reference GDCS flow for the GDCS transition phase is ¼ of the maximum flow, which occurs at the end of the phase. The purpose of the analysis during this period it to look at the balance between heating, depressurization and GDCS subcooling as it affects the RPV liquid mass. The maximum flow is used in the next phase (Reflood) and zero flow is used in the previous phase (Late Blowdown). Therefore some intermediate flow is useful to look at the balance during this period. A value closer to the low end is selected because the minimum water level in the RPV is reached at about this point. By using this value it is easy to visually estimate the effect of maximum flow by quadrupling the resulting pi-group or setting it to zero, respectively.

7.4 Format of Results

The figures show the results for 4500 MWt ESBWR in a compact and informative format (see Figure 7-1, for example). The results for 4500 MWt and 4000 MWt ESBWR designs are compared with test facilities in Section 8. In each figure, the equation being evaluated is shown in the upper right hand corner. The equation contains multiple terms of the same type as indicated by the summations and subscript "i". These account for multiple mass or energy flow paths. The picture at the left of each figure indicates the control volume being considered. The specific phenomena being considered are indicated schematically and by the PI-groups shown in the figure. The PI-groups correspond to those in the equation with the subscript "i" replaced by a specific flow path name. For example the generic mass addition term, $\Pi_{M,W,i}$, is replaced by the specific one, $\Pi_{M,W,Break}$, for the break flow.

The results are shown in the graph in the bottom right hand corner of the figure. The bar chart indicates the magnitude, and therefore importance, of each phenomenon being considered for the parameter of interest. The results are grouped by flow path or process rather than by phenomena since it is usually the process or structure that is scaled rather than the individual phenomena. For example the mass addition and subcooling effects of the IC return line are grouped into a single bar (see Figure 7-1). The bars are subdivided, however, so that the magnitudes of the individual phenomena are still discernable. The color of the bar section indicates which phenomenon is represented. For example the yellow section of the "ICreturn" bar indicates the portion due to mass addition ($\Pi_{M,W,ICr}$) and the smaller light blue section indicates the

contribution from subcooling ($\Pi_{M,sub,ICr}$). Many flow paths will not have all forms of energy and mass transfer present. For example, there is only sensible heat transfer from the core and structures. Detailed results can be found in the tables of Appendix A.

The equations are scaled so that the dominant phenomenon (PI-group) will be of order one. Therefore PI-groups with magnitude less than about 0.2 do not contribute much to the overall behavior of the system. Also, it is desirable to have phenomena with magnitude greater than 0.2 scaled well, as will be discussed in Section 8.1.

7.5 Top-Down Results

7.5.1 RPV Behavior

The calculations for the RPV for 4500 MWt ESBWR are summarized in Figures 7-1 through 7-5. The primary variable of interest is the water level in the RPV since our goal is to keep the core covered. The RPV pressure is also of interest since it controls the timing of GDCS initiation and therefore influences the minimum water level. The liquid mass equation is evaluated for the late blowdown, GDCS transition and reflood phases as indicated in Table 7-1. New terms for the SLCS injection have been included for the 4500 MWt ESBWR. The pressure rate equation is evaluated for the late blowdown and GDCS transition periods. It is not necessary to evaluate the pressure during the reflood period since the vessel is completely depressurized by then. For the RPV liquid mass evaluation, a GDCS line break is considered, since this break results in the lowest RPV water level.

The results for RPV liquid mass during the late blowdown, GDCS transition and reflood phases are shown in Figures 7-1, 7-2 and 7-3, respectively. The effective control volume for the evaluation is the liquid in the vessel. Therefore, the phenomena considered are at the boundaries of the liquid. The mass and energy flows considered are: break flow; GDCS inlet flow; IC return line flow (if present); stored energy release from core and structures; decay heat; and flashing due to depressurization.[41] ADS flows do not act directly on the liquid mass because they are steam flows. They indirectly influence the mass strongly through the flashing term, however. All of the fluid in the RPV is considered to be in thermal equilibrium. There are no noncondensibles present in the vessel during this phase. Although no credit is taken for the IC in licensing analyses for LOCAs, the IC is included in the scaling analysis to assess its importance and therefore potential to interact with other systems.

The loss of vessel liquid inventory is dominated by flashing due to depressurization as indicated by the large bar for this process in Figure 7-1 and relatively large bar in Figure 7-2. The boil-off due to decay heat and stored energy release also provide significant contributions. The majority of mass decrease occurs during the blowdown period. During the GDCS transition period there is a small amount of mass loss until the GDCS flow and subcooling overcomes the mass loss due to flashing, boiling and break flow. It is interesting to look at the GDCS transition period by itself because it is a short period where many phenomena are of similar magnitude and is the point when the minimum water level occurs. However, the mass change during this period is small. Therefore, to put the phenomena magnitudes for this period in perspective, relative to their overall contribution to the change in liquid mass, an additional bar is added to the left-hand

[41] RAI 290

side of the Figure 7-2. This bar is the ratio of mass loss during the late blowdown period compared to the mass loss during the GDCS transition period. It has the effect of showing the importance of the phenomena in Figure 7-2 on a scale comparable to what is shown in Figure 7-1.

As indicated in Figure 7-2, several phenomena are of similar importance. Flashing due to depressurization, boiling due to energy input and break flow have similar contributions to inventory loss. The GDCS flow and condensate returned from the IC are increasing the inventory. [[

]] The flow transitions from zero to full flow during this phase but the period of interest is the first part of the phase when the minimum water level is achieved. Over the full period the GDCS bar height would range from zero to 4 times the height shown. Similarly the flashing magnitude would range from the height shown to zero since the depressurization is basically complete at the end of this phase. The contribution by the IC to liquid mass is small but favorable to the mass in the vessel.

For consideration of the RPV pressure, the control volume is the entire vessel since the gas space is what controls the pressure in the vessel. The RPV depressurization is dominated by the energy removal through the ADS system as indicated by the large bar at the left end of Figure 7-4. The depressurization rate is reduced by steam generation resulting from energy input from decay heat and stored energy release. The IC and break have a very small impact on RPV pressure compared to the dominant terms.

For the GDCS transition phase in Figure 7-5, a bar indicating the ratio of the overall pressure change to the pressure change during the transition is included in order to put the phenomena magnitudes in perspective. As shown, the phenomena magnitudes are more in balance but all of the phenomena are relatively unimportant to the overall behavior of the system when the previous phase is considered. The small magnitude of the IC bar indicates that its presence or absence would not be expected to change the character of the system behavior and therefore no interactions with other systems would be expected. This was indeed proven to be the case in the GIRAFFE/SIT test where transients were run with and without the condenser present.

The reflood phase (Figure 7-3) is very straightforward; the liquid mass is dominated by the GDCS flow with all other parameters being insignificant. The subcooling indicated by the blue portion of the GDCS bar is more than sufficient to offset the energy input from decay heat and stored energy release, so no widespread boiling should occur. Predicting the RPV behavior during this phase is essentially a tank filling problem.

Due to the large margin in the plant design, the core never uncovers. Therefore localized phenomena such as dryout and rewet do not occur. This eliminates the importance of localized (bottom-up) phenomena that may be distorted in small scale tests. Scaling of internal flows and flashing in various regions of the RPV are analyzed and documented in response to RAI 290.

7.5.2 Containment behavior

For the containment, pressure is the variable of primary importance. As has been discussed elsewhere the long-term containment pressure is controlled by the wetwell pressure and

specifically the contributions due to moving the noncondensible gas into the wetwell plus the partial pressure of steam.

7.5.2.1 Drywell Pressure Rate

Figure 7-6 shows the evaluation for the drywell. The volume considered is the free gas space of the drywell (DW). For the PCCS phase, the large connecting paths between the RPV and the DW regions results in a very small pressure drop. Therefore, the pressures remain approximately equal. Uniform distribution of constituents is assumed in the top down scaling. The flows entering and exiting the RPV and DW volumes are: (1) IC inlet and drain; (2) steam generated in the RPV by decay heat and stored energy release; (3) PCC inlet; (4) main vent flow; and (5) vacuum breaker leakage.

The top-down scaling used assumes a uniform distribution of noncondensibles, so the enthalpy of flows leaving the DW is the same as the average enthalpy, rendering h^+ equal to zero. Therefore, h^+_{PCC} and h^+_{IC} are zero. The primary effect of these terms is the mechanical work of adding or removing mass from the volume. The condensation or evaporation flows will be at the enthalpy for saturated steam, which is different from the average enthalpy, so they are retained. Also, the enthalpy of mass flows entering the DW may be quite different from the average DW enthalpy, so in-flow enthalpy terms are retained.

The bar graph shows that the response is dominated by the steam flow from decay heat and the PCC inlet flow. In addition, these phenomena magnitudes are very large (on the order of 400). This indicates that the flows are sufficient to change the DW pressure very rapidly relative to the reference time of interest. These characteristics are similar to those of a pipe and in fact, the DW behaves like a large pipe as far as predicting its behavior is concerned. The important aspect of the DW is the amount of noncondensible that it holds during normal operation since noncondensibles will be pushed into the wetwell during an accident. Additionally, the particular characteristics of the hideout regions of the DW can effect the timing of noncondensible release and therefore the timing of pressure changes in the containment from gas moving to the WW.

It is noteworthy that the heat removal in the DW is completely unimportant as is the PCC heat removal. The PCC inlet flow would be approximately the same with or without heat removal in the PCC. The PCC heat removal is important to the suppression pool since without it uncondensed steam would reach the SP and heat up the pool region above the vent exit.

The enthalpy term in the pressure rate equation is based on the enthalpy difference between the flow and the volume. Therefore, with the uniform distribution assumption the enthalpy contribution of all exiting flows is zero. This was not true for the RPV depressurization where flows were considered to be either liquid or vapor so that the associated enthalpy was less than or greater than the mixture average, respectively.

It should be noted that there is a very short-term period during the vent clearing stage when the drywell is of more relevance to the containment pressure. Prior to the liquid being cleared out of the main vents [[ ]]the blowdown energy cannot be passed to the WW, and the DW behaves as a dead end volume. This transient period is before the start of the tests considered here. The loads during that period are not predicted using TRACG and have been licensed previously. Therefore the test program and scaling do not cover that period.

7.5.2.2 Wetwell Pressure Rate

Figure 7-7 shows the WW evaluation. As noted above the WW controls the containment pressure for the ESBWR after the first few minutes of blowdown. Due to the large DW to WW connection paths via the main vents and VBs, the DW pressure is always within a small band above or below the WW pressure after the initial blowdown. The WW gas space is the control volume for the WW calculations, as shown in the figure. Although the gas space is in equilibrium with the top suppression pool layer (above the PCC vent) for most of the accident, the heat and mass transfer rates at the pool surface are not sufficient to keep them in constant equilibrium. Therefore they must be treated separately and the exchange rate between them considered as a boundary flow for each. The mass and energy flows entering and exiting the WW control volume are: (1) main vent flow; (2) PCC vent flow; (3) vacuum breaker leakage flow; and (4) wall structure stored energy. The flows through the main vents and PCC vents pass through the SP and reach equilibrium with the pool by the time they exit the pool as bubbles reaching the surface; i.e. the temperature is approximately the same as the pool and the steam partial pressure in the bubble is approximately the saturation pressure corresponding to the pool temperature (there are slight differences due to the increased pressure inside the bubble due to surface tension).

The right side of the equation contains terms for enthalpy additions, mechanical compression from mass additions, sensible heat additions, compression due to volume changes and changes in component mass fractions. The pool level does not change measurably during the long-term phase so the volume change term is zero. [[

]]

The top-down scaling used assumes a uniform distribution of noncondensibles, thus, the enthalpy of flows leaving the WW is the same as the average enthalpy, rendering h^+ equal to zero. Therefore, h^+_{VB} will be zero for normal VB flow from the WW to the DW. The primary effect of this term is the mechanical work of adding or removing mass from the volume. The condensation or evaporation flows will be at the enthalpy for saturated steam, which is different than the average enthalpy, so they are non-zero. Also, the enthalpy of flows entering the WW may be quite different from the average WW enthalpy. For the cases considered, the main vent does not open during this phase. The main vent and PCC vent flows are combined in the bubble term as discussed above.

As was done for the RPV pressure during the GDCS transition phase, a bar representing the ratio of the total pressure change to the pressure change during the long-term phase has been added to the left end of the bar chart in Figure 7-7. As shown the dominant pressure change occurs during the blowdown phase when noncondensibles are purged from the DW to the WW. The rather steady pressure during this phase is the result of a balance between heat and mass input from VB leakage and pool surface evaporation and energy removal to the walls. The walls provide a significant heat sink for the WW since the energy inputs are small. The heat transfer to the walls is conduction limited so the detailed modeling of the convection to the walls is not important. The WW is considered to be at saturated conditions for the estimates of heat and mass transfer to the pool surface. The conditions in the WW change during the long-term phase but eventually settle at a condition near equilibrium with the pool surface.

7.5.2.3 Passive Containment Cooling System (PCCS)

The PCCS could be considered as another volume for top down scaling. However, it has flows similar in magnitude to the DW but a smaller volume and therefore will responds like a connecting pipe between the DW and WW. It has a very short time constant and therefore rapidly adjusts itself to an equilibrium condition between the DW and WW pressure. The details of the heat removal through the PCC are addressed through bottom-up scaling.

7.5.3 Summary of Top-down Results

Application of top-down scaling to the ESBWR has yielded the following results:

For the RPV the blowdown period is dominated by ADS flow and flashing. There is a short transition period where several phenomena are of similar magnitude but the significant mass change has already occurred during the blowdown phase. The reflood phase is dominated by the GDCS flow. Because the core does not uncover, only the liquid mass is important.

For the containment, the pressure change is dominated by movement of noncondensibles from the DW to the WW. The DW pressure just follows WW pressure. Hide-out of noncondensibles in the DW can change the timing of pressure changes due to hold up of noncondensibles but other than that the DW behavior is largely unimportant to the containment pressure behavior. The PCC is only important in controlling amount of energy that goes into the suppression pool. It does not influence the DW response or pressure directly. The long-term changes in containment pressure are small compared to the initial pressurization due to noncondensibles moving from the DW to the WW.

7.6 Bottom-up Scaling

Bottom up scaling is used to look at specific processes important to system behavior in more detail. Based on the results of the top-down scaling several processes are of potential interest: ADS flow, void distribution in the RPV, PCCs behavior, and stratification and mixing in gas spaces and pools. However, for reasons discussed below only the PCCs behavior is of significant interest.

ADS FLOW

The ADS flow is controlled by a combination of the pressure evolution in the RPV and the critical flow area in the pipes, since the flow is choked for most of blowdown. The pressure evolution has been covered by the top-down scaling above. The only scaling needed for the critical flow area is to assure that the ratio of flow areas between the ESBWR and tests facilities is at the system scale, R, as determined by the general scaling criteria in Section 4.

VOID DISTRIBUTION

The void distribution is of some interest but not critically important because of the large quantity of water left in the vessel. Bottom-up analyses in the SBWR scaling report [3-1, Section 3.8] showed that the important parameters for void fraction were: the vertical scale, L, the vapor generation rate, Γ, and the flow regime. The vapor generation rate is controlled by parameters evaluated in the top-down scaling (primarily flashing), covered above. The facilities are at full

vertical scale. The fuel height has changed a small amount from the SBWR to the ESBWR but is still similar in length. Also, since the bundle cross-sectional geometry has not changed from the SBWR the flow regime will be the same for the same boundary conditions.

PCC AND IC

The bottom-up behavior of the PCC and IC can be important during periods where the steam supply is equal to or greater than the condenser capacity.[42] For periods where the steam supply is less than this, the PCC self regulates and the amount of noncondensible gas stored in the PCC compensates for any differences in heat removal capacity.[43] The multiple tube design of the condensers allows each tube to be full scale, only the number of tubes is changed. This allows them to satisfy both top-down and bottom-up scaling simultaneously, even at small system scales. Details of the bottom-up scaling for the PCCs was provided in Sections 3.6 and 4.4 of the SBWR scaling report [3-1]. The ESBWR tube dimensions and range of conditions are the same as the SBWR so the scaling has not changed. There are, however, more tubes per PCC and more PCCs in the ESBWR, which has been reflected in the top-down scaling. The same findings are true for the pool-side heat transfer since the tube geometry and pitch have not changed. A detailed analysis of the phenomena involved in bottom-up scaling of the PCCS is documented in response to RAI 259.1, and self-regulation within the PCCS System is considered in RAI 283.

STRATIFICATION, HIDEOUT AND MIXING

As described previously, stratification and mixing can result in variations in the system behavior. Stratification or hideout can shift the rate and timing of noncondensible release from the DW to the WW. Reduced scale facilities with simplified geometry can not simulate the details of an actual DW with all of its complexities: isolated regions such as around the thermal shield or above the RPV head; large quantities of piping and equipment at different operating temperatures; non-smooth walls due to bracing; etc... In addition, the unlimited number of possible break locations and sizes, which will result in different stratification and hideout conditions, cannot all be simulated in a test program.

Fortunately, the only strong effect of these varying conditions is the timing of the pressure increases due to noncondensibles moving from the DW to the WW. The PCC behavior does not reflect the details of stratification, only the noncondensible fraction at the PCC inlet. Therefore, to bound the effects of the multitude of possible stratification conditions, parametric tests were done in the PANDA facility to cover a range of timing and rate of noncondensible release in the DW. This was done through a variety of forced stratification and delayed noncondensible injection tests.[44]

[42] RAI 259.1
[43] RAI 283
[44] RAI 291

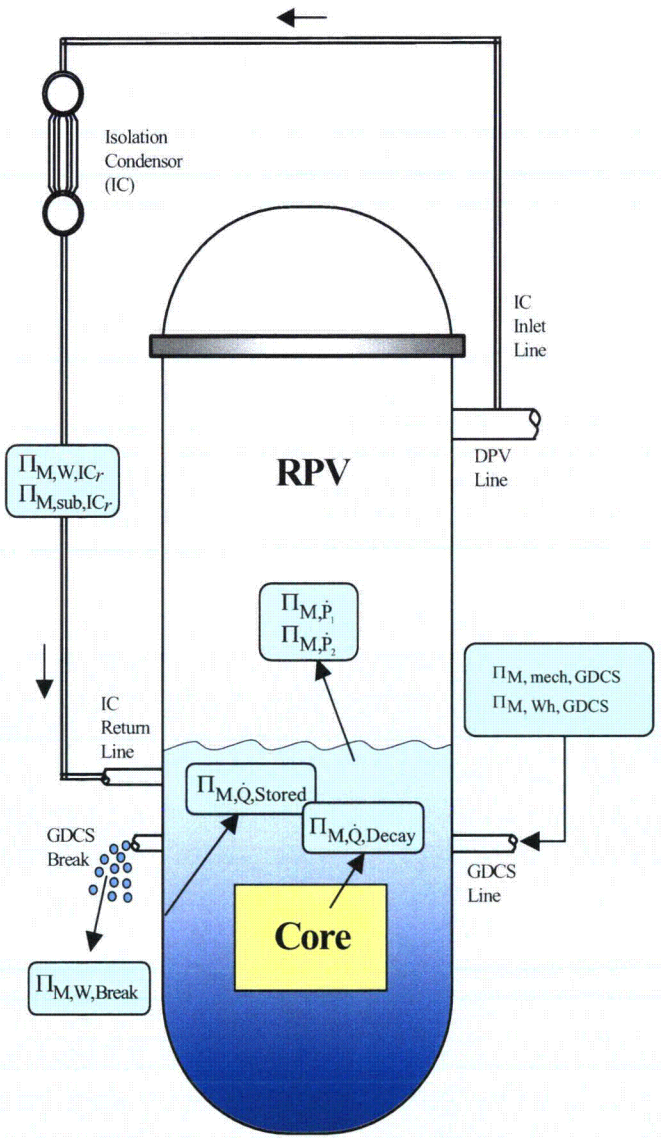

Equation

$$h_{fg}^{+}\frac{d\Delta M_{\ell}^{+}}{dt^{+}} = -\sum_{i}\Pi_{M,\dot{Q},i}\dot{Q}_{i}^{+} + h_{fg}^{+}\sum_{i}\Pi_{M,W,i}W_{\ell,i}^{+} + \sum_{i}\Pi_{M,sub,i}h_{sub,i}^{+}W_{\ell,i}^{+} - \left[\Pi_{M,\dot{P}1}V_{RPV}^{+}f_{3}^{+} + \Pi_{M,\dot{P}2}f_{4}^{+}M_{\ell}^{+}\right]\frac{dP^{+}}{dt^{+}}$$

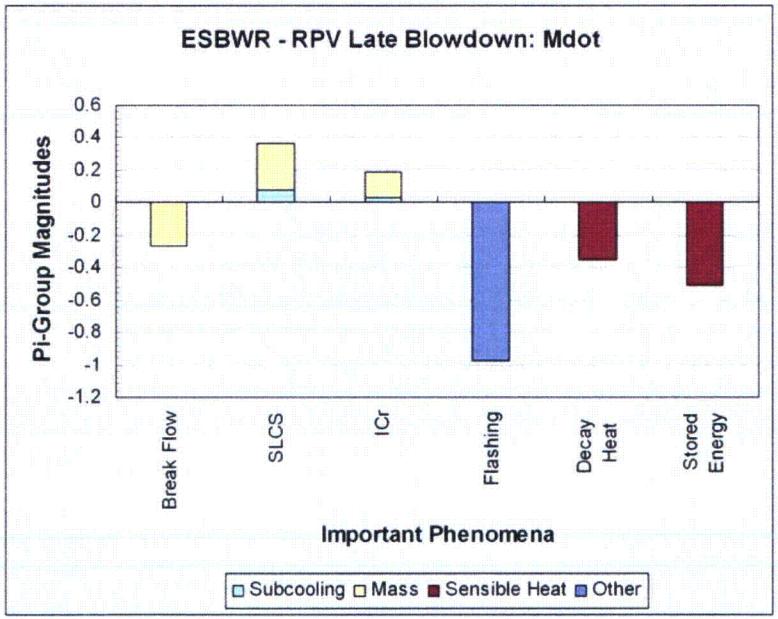

Figure 7-1. ESBWR - RPV Late Blowdown: Time Rate of Liquid Mass Change (Mdot)

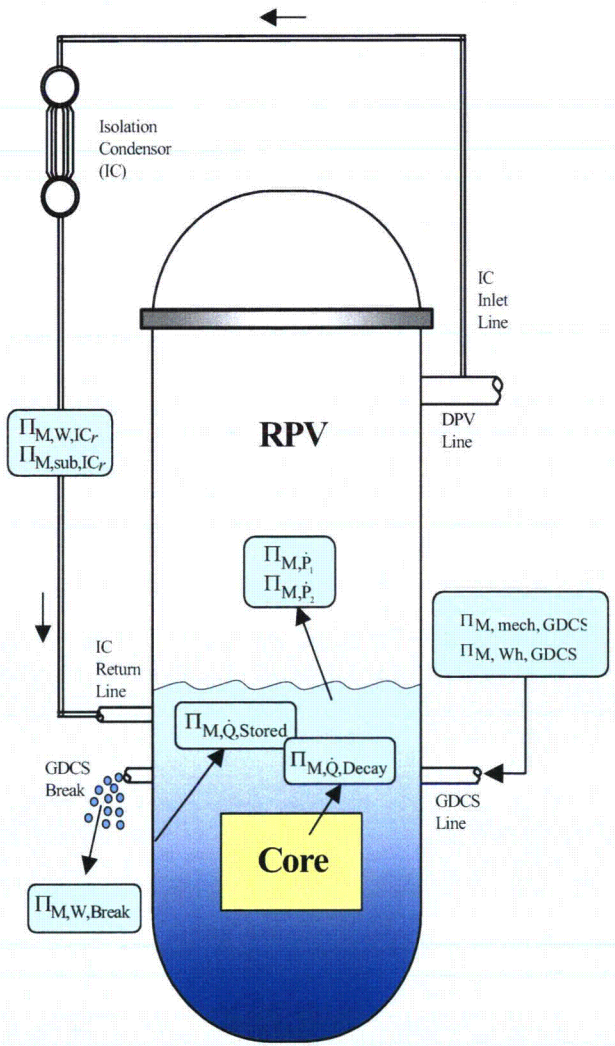

Equation

$$h_{fg}^{+}\frac{d\Delta M_{\ell}^{+}}{dt^{+}} = -\sum_{i}\Pi_{M,\dot{Q},i}\dot{Q}_{i}^{+} + h_{fg}^{+}\sum_{i}\Pi_{M,W,i}W_{\ell,i}^{+} + \sum_{i}\Pi_{M,sub,i}h_{sub,i}^{+}W_{\ell,i}^{+} - \left[\Pi_{M,\dot{P}1}V_{RPV}^{+}f_{3}^{+} + \Pi_{M,\dot{P}2}f_{4}^{+}M_{\ell}^{+}\right]\frac{dP^{+}}{dt^{+}}$$

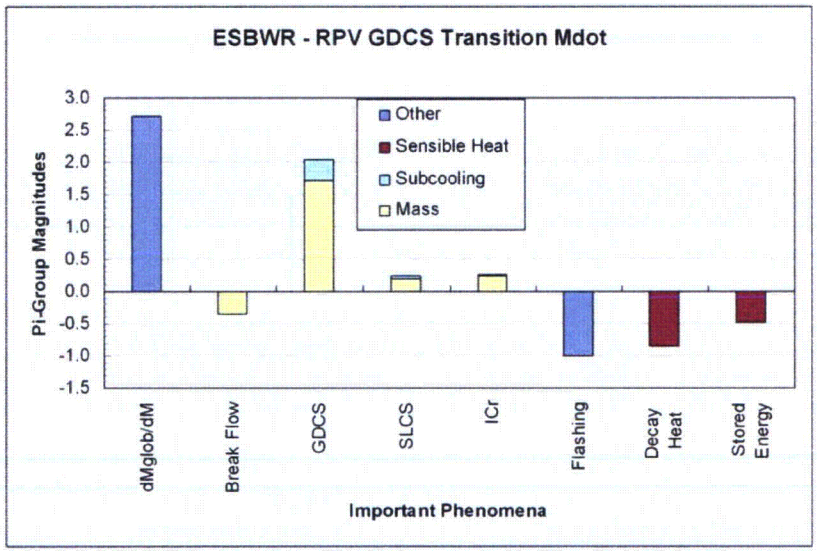

Figure 7-2. ESBWR - RPV GDCS Transition: Time Rate of Liquid Mass Change (Mdot)

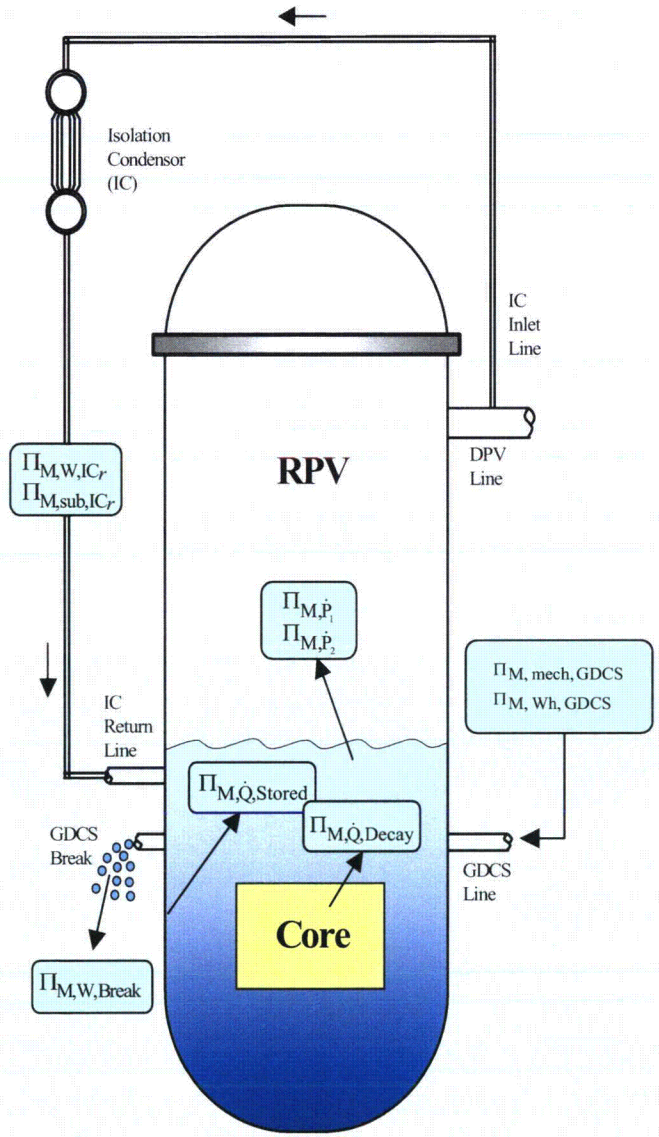

Equation

$$h_{fg}^{+}\frac{d\Delta M_{\ell}^{+}}{dt^{+}} = -\sum_{i}\Pi_{M,\dot{Q},i}\dot{Q}_{i}^{+} + h_{fg}^{+}\sum_{i}\Pi_{M,W,i}W_{\ell,i}^{+} + \sum_{i}\Pi_{M,sub,i}h_{sub,i}^{+}W_{\ell,i}^{+} - \left[\Pi_{M,\dot{P}1}V_{RPV}^{+}f_{3}^{+} + \Pi_{M,\dot{P}2}f_{4}^{+}M_{\ell}^{+}\right]\frac{dP^{+}}{dt^{+}}$$

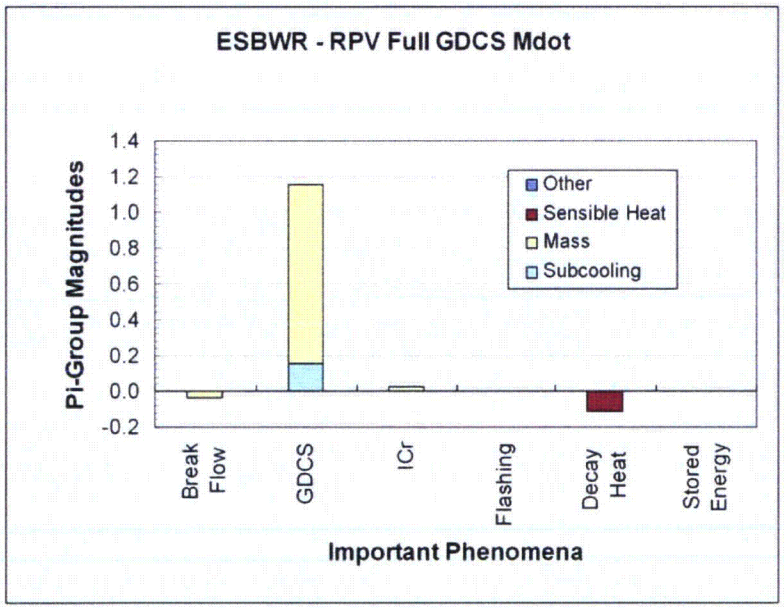

Figure 7-3. ESBWR – RPV Full GDCS (Reflood): Time Rate of Liquid Mass Change (Mdot)

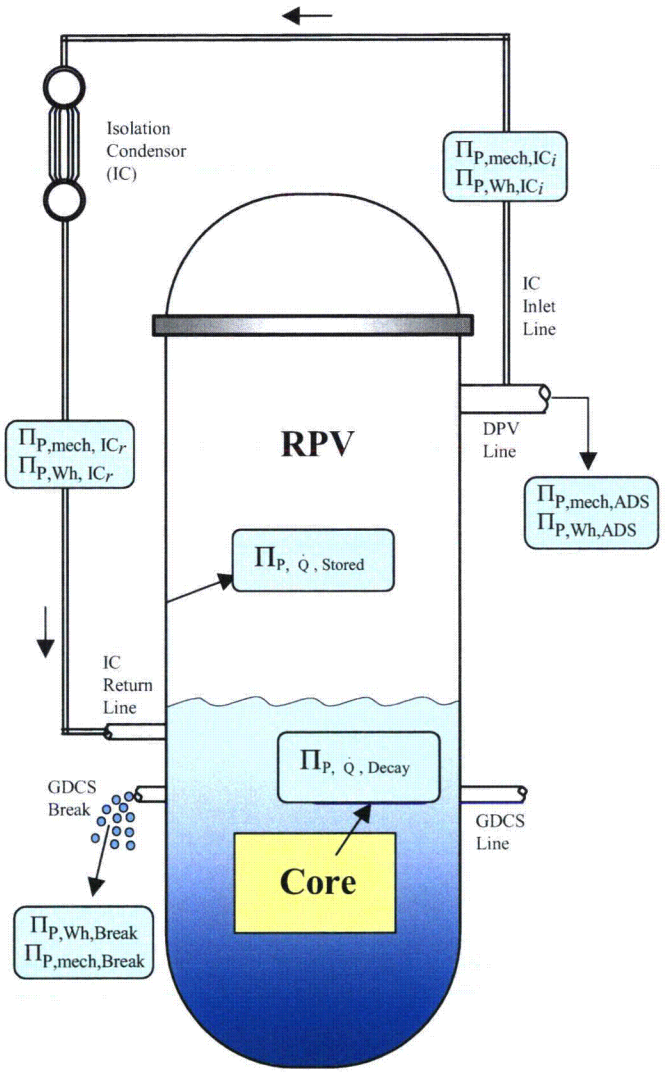

Equation

$$f_2^+ V^+ \frac{dP^+}{dt^+} = \sum_i \Pi_{P,\dot{Q},i} Q_i^+ - \Pi_{P,\dot{V}} P^{*+} \frac{dV^+}{dt^+} + \sum_i \Pi_{P,Wh,i} W_i^+ h_i^+ + \frac{P^{*+}}{\rho^+} \sum_i \Pi_{P,mech,i} W_i^+ - V^+ \sum_j \Pi_{P,y,j} \left(f_{1,j}^+ \frac{dy_j^+}{dt^+} \right)$$

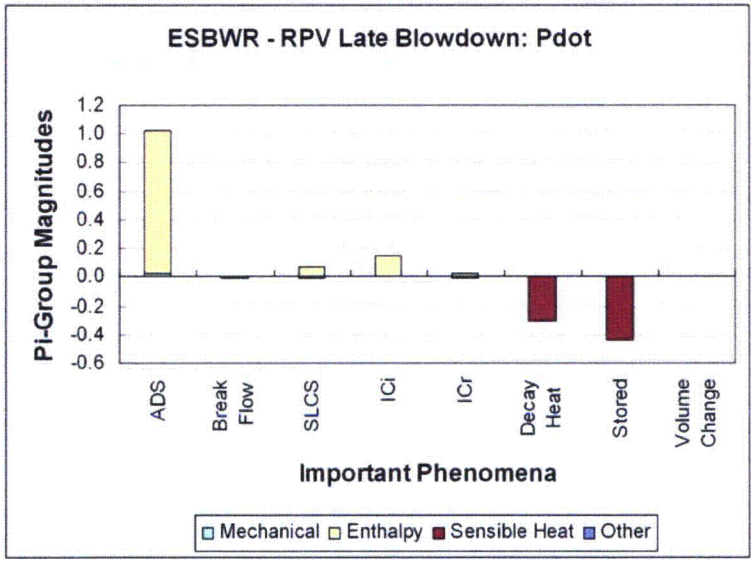

Figure 7-4. ESBWR – RPV Late Blowdown: Time Rate of Pressure Change (Pdot)

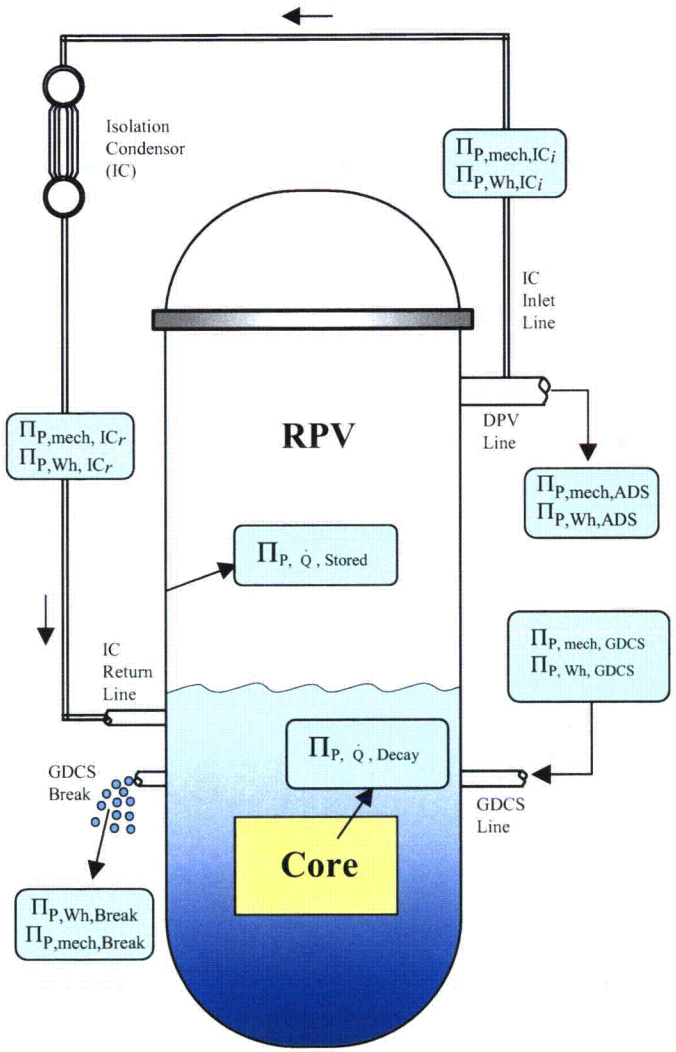

Equation

$$f_2^+ V^+ \frac{dP^+}{dt^+} = \sum_i \Pi_{P,\dot{Q},i} Q_i^+ - \Pi_{P,\dot{V}} P^{*+} \frac{dV^+}{dt^+} + \sum_i \Pi_{P,Wh,i} W_i^+ h_i^+ + \frac{P^{*+}}{\rho^+} \sum_i \Pi_{P,mech,i} W_i^+ - V^+ \sum_j \Pi_{P,y,j} \left(f_{l,j}^+ \frac{dy_j^+}{dt^+} \right)$$

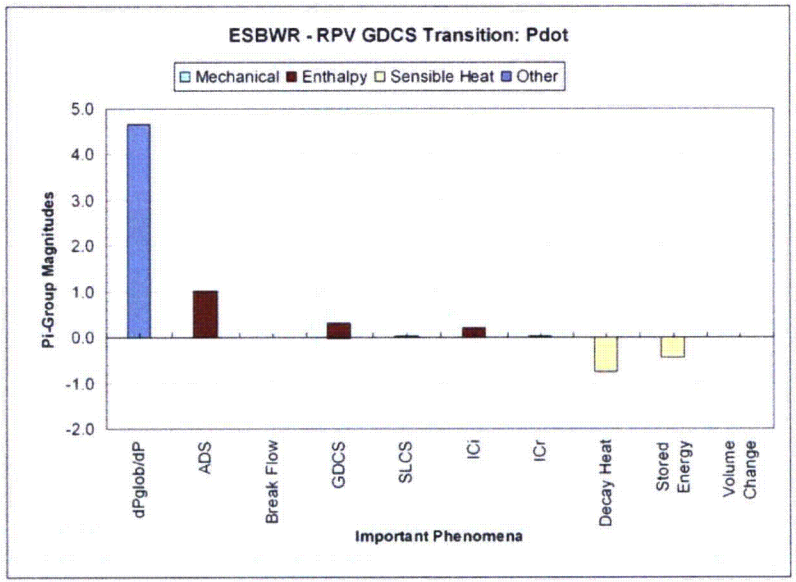

Figure 7-5. ESBWR – RPV GDCS Transition: Time Rate of Pressure Change (Pdot)

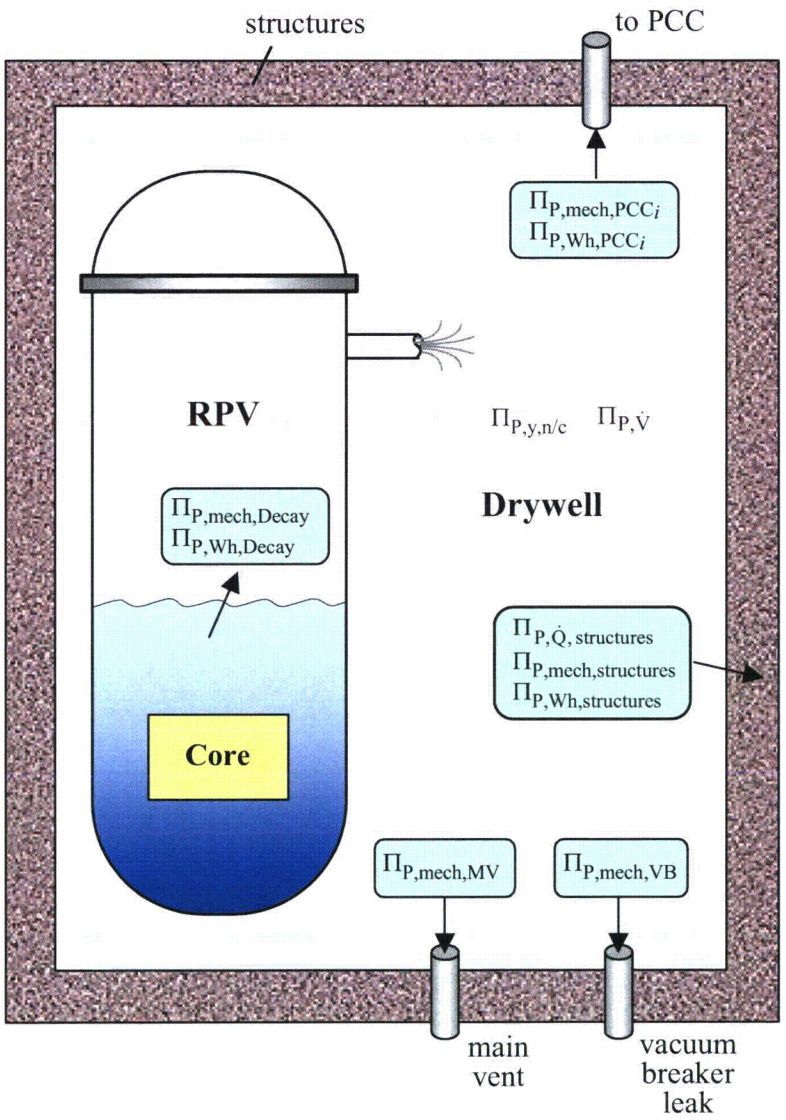

Equation

$$f_2^+ V^+ \frac{dP^+}{dt^+} = \sum_i \Pi_{P,\dot{Q},i} Q_i^+ - \Pi_{P,\dot{V}} P^{*+} \frac{dV^+}{dt^+} + \sum_i \Pi_{P,Wh,i} W_i^+ h_i^+ + \frac{P^{*+}}{\rho^+} \sum_i \Pi_{P,mech,i} W_i^+ - V^+ \sum_j \Pi_{P,y,j} \left(f_{1,j}^+ \frac{dy_j^+}{dt^+} \right)$$

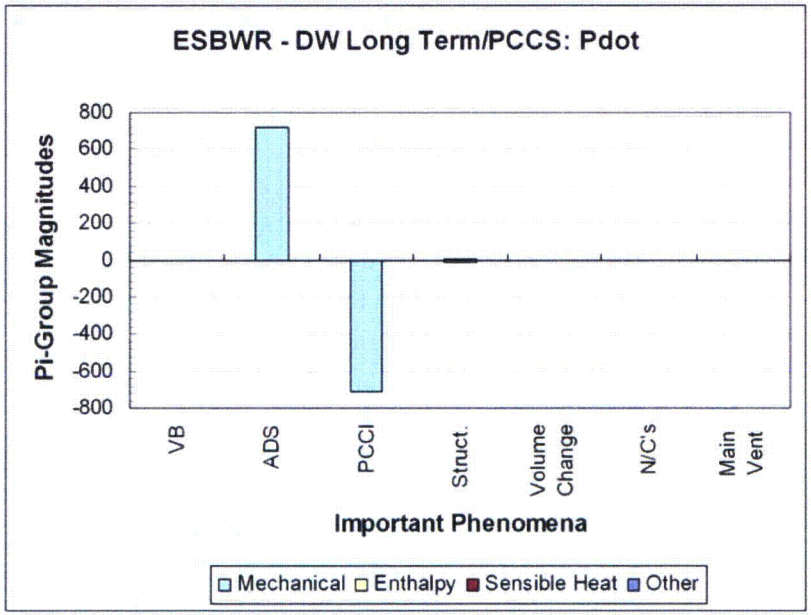

Figure 7-6. ESBWR – Drywell Long Term/PCCS: Time Rate of Pressure Change (Pdot)

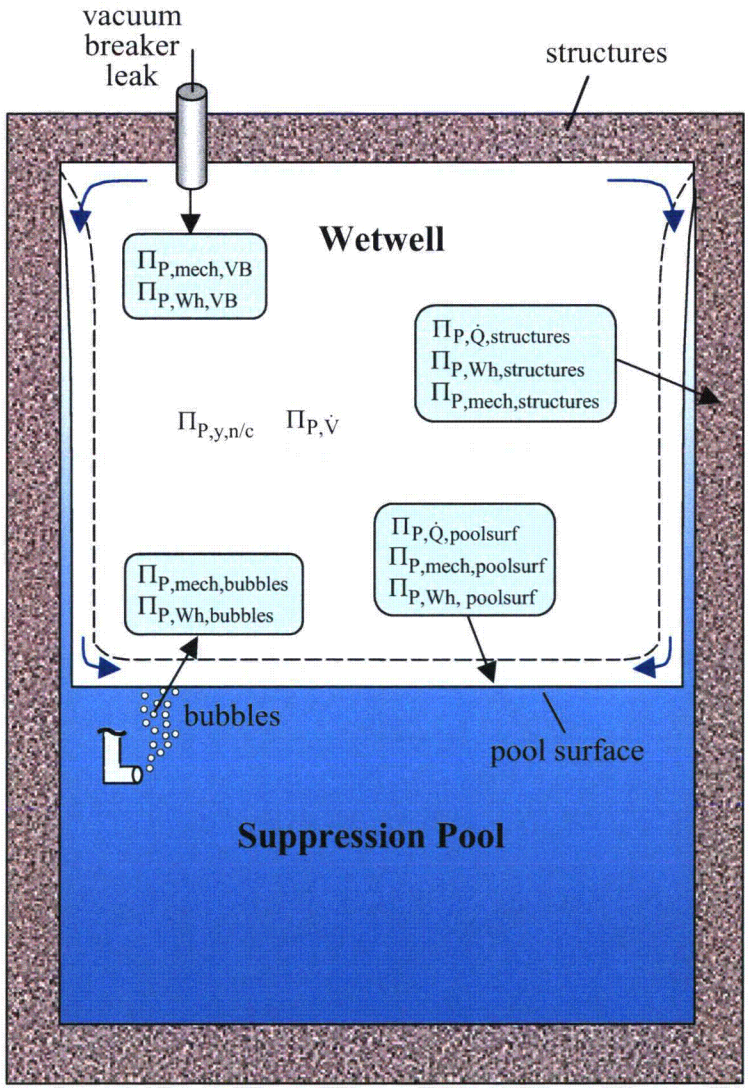

Equation

$$f_2^+ V^+ \frac{dP^+}{dt^+} = \sum_i \Pi_{P,\dot{Q},i} Q_i^+ - \Pi_{P,\dot{V}} P^{*+} \frac{dV^+}{dt^+} + \sum_i \Pi_{P,Wh,i} W_i^+ h_i^+ + \frac{P^{*+}}{\rho^+} \sum_i \Pi_{P,mech,i} W_i^+ - V^+ \sum_j \Pi_{P,y,j} \left(f_{1,j}^+ \frac{dy_j^+}{dt^+} \right)$$

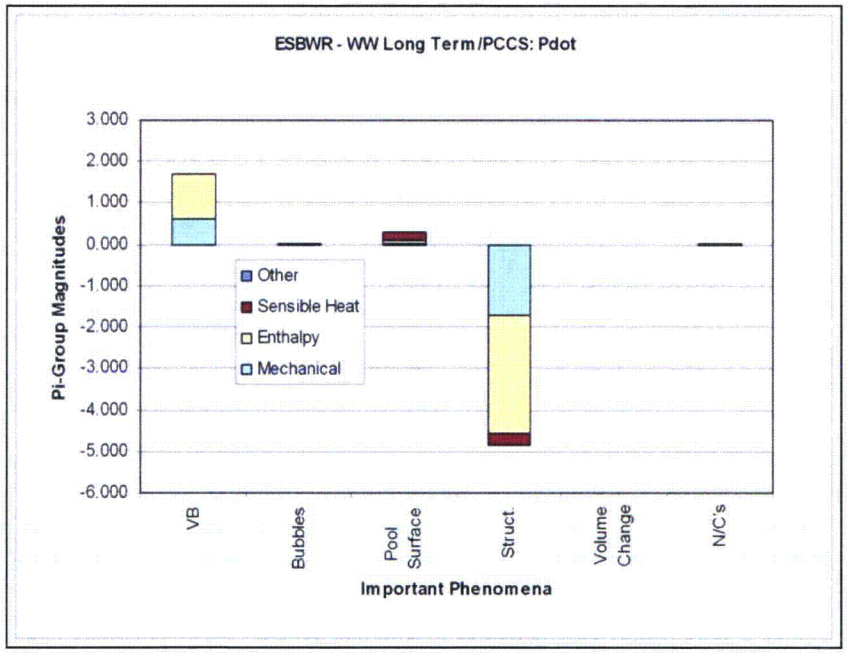

Figure 7-7. ESBWR – Wetwell Long Term/PCCS: Time Rate of Pressure Change (Pdot)

8.0 TEST FACILITY SCALING

In Section 7, the specific top-down scaling method was applied to the ESBWR to identify parameters of importance to the system behavior. In this section, the same method is applied to test facilities to confirm that the facilities, which were designed according to the general scaling criteria (developed in Section 4), adequately represented the ESBWR for use in qualifying TRACG.

The GIRAFFE/SIT and GIST test series were focused on the RPV behavior during the first three transient phases - late blowdown, GDCS transition and reflood. Therefore, the scaling of these facilities for the RPV liquid mass and RPV pressure rate during these phases is evaluated.

The GIRAFFE/He and PANDA test series were focused on the behavior of the containment during the PCCS phase. Therefore, the scaling of the containment pressure rate responses during the PCCS phase is evaluated for these facilities. Table 8-1 summarizes the specific applications of the scaling equations to different test facilities.

Table 8-1 Numerical Scaling Evaluations

Volume	ESBWR	GIST	GIRAFFE /SIT	GIRAFFE/He	PANDA-M	PANDA-P
Late Blowdown Phase (8.3) [1, 4, 5]						
RPV	M, P	M, P	M, P			
DW						
WW						
GDCS Transition Phase (8.3) [1, 4, 5]						
RPV	M, P	M, P	M, P			
DW						
WW						
Full GDCS Phase (8.3) [1,4, 5]						
RPV	M	M	M			
DW						
WW						
Long Term PCCS Phase (8.4) [1, 4, 5]						
RPV						
DW [2]	P			P	P	P
WW [3]	P			P	P	P

1 M = mass equation P = pressure equation
2 DW and RPV gas act as one volume during reflood and long-term phases
3 Includes GDCS gas volume as appropriate
4 Number in parenthesis is section where results are shown
5 The limiting breaks are used for each region: GDCS Line break for the RPV and MSLB or FWLB for the containment

8.1 Criteria for Well Scaled Facility

The goal of tests is to represent phenomena important to system behavior at scaled magnitudes similar to the prototype so that models can be qualified for predicting important phenomena over a range of conditions similar to those expected in the prototype. Breaking this down, it means the following criteria should be met:

- Important phenomena should be represented in tests at similar magnitudes to those expected in the prototype
- Phenomena not important in prototype should not be important in test

On the other hand, unimportant phenomena need not be modeled well or necessarily at all in the tests.

No specific quantitative criterion exists to define what constitutes a well-scaled test. A reasonable criterion that we adopt here is to maintain important phenomena within factor of around three of the prototype.[45] That is for PI-groups identified as important to the system behavior the ratio of the ESBWR value to the test value should fall [[ ]] The justification for selecting this criterion is that it ensures that the phenomena are well within the same order of magnitude in both the prototype and test, and it provides separation from the criterion for identifying phenomena as unimportant.

8.2 Reference Parameters

The reference parameters for the test facilities were determined in a manner similar to that used for the ESBWR (Sections 6.1 and 7.3). Reference values are supplied using a combination of test data, where possible, and simulation results to render the nondimensional variables of order one. The results obtained for the test facilities are compared with the 4000 MWt and 4500 MWt ESBWRs in Figures 8-1 through 8-5 for short-term RPV behavior. New terms for the SLCS injection have been included for the 4500 MWt ESBWR. Figures 8-6 and 8-7 show the results for long-term containment behavior. The detailed results are tabulated in Appendix A. As before the magnitudes of the PI groups indicate the importance of the phenomena to the system response. Comparing the height of the bars for the ESBWR and test facilities one can see how well each phenomenon was represented in the tests.

8.3 Short-term RPV Behavior

This period encompasses the Late Blowdown, Transition to GDCS Flow and the Reflood stages of a LOCA. The primary variable of interest during this period is RPV level. Since there is no direct measurement of the two-phase level, the water mass in the RPV and void fraction are used for evaluation. The minimum water level occurs as the GDCS flow begins and collapses the voids. Therefore, the mass, which is indicative of the collapsed level, is a good variable for evaluation. In addition, pressure is an important variable in determining the RPV mass transient, since it determines when the GDCS can begin to inject fluid into the RPV.

[45] RAI 295

The GIRAFFE/SIT Test GS1 and GIST Test C01a were selected for analysis in this period because they represent a similar set of conditions. Both tests are GDCS line breaks, and neither has ICs or PCCs available. This case results in the lowest RPV mass and water level as discussed in Reference [3-1].

The beginning of the Late Blowdown phase is defined as the time when the pressure is equal to the pressure at the beginning of the late blowdown tests, GIST and GIRAFFE/SIT as described earlier. Figure 8-1 through 8-3 show the results of the liquid mass evaluations for each of the three early phases, while Figures 8-4 and 8-5 show the results for the pressure rate during the late blowdown and GDCS transition periods. The ESBWR results are the same as those shown in Section 7. From these figures we can see which PI-groups are important and how they compare in the tests and the ESBWR.

All of the parameters are well scaled for both tests during the late blowdown period, as shown in Figures 8-1 and 8-4. The heights of the bars for the ESBWR and tests are similar and well within the factor of 3 difference stated as the criterion for good scaling. The IC bars are zero for the test facilities since the tests considered did not use an IC. The main purpose of including the IC in the ESBWR was to show that its impact was small compared to the dominant processes and should not lead to any system interactions with other safety systems. This result was indeed confirmed in GIRAFE/SIT tests which included the IC as detailed in the GIRAFFE/SIT test report [8-1].

The results are normalized to the flashing and ADS flow for the liquid mass and pressure rate, respectively, since these are the dominant processes. As stated earlier the depressurization time constant due to ADS flow sets the reference time for both equations. Differences in other bars are relative to the dominant flows. For example, the larger stored energy bar in GIST shown in Figure 8-4 indicates that the stored energy release is large relative to the ADS flow when compared to the ESBWR relative strengths. There is no indication as to whether this is due to small ADS flow or large stored energy release in the GIST facility. In fact, it is unimportant which is the case in a scaling sense since it is the relative comparison of processes and geometrical considerations that are important. It would be possible to for instance to have all three of the important parameters in Figure 8-4, ADS, decay heat and stored energy, be small relative to the facility scale and still have a good scaling result for the RPV pressure. The floating parameter would be an increased time scale for the GIST facility since the important processes happen at a slower rate. This would be a perfectly acceptable result. However, since the facilities were not designed for altered time scale distortions in some phenomena that could not be scaled at reduced time scales would show up. The above discussion is just to identify what the scaling results do and do not indicate. That is, the magnitudes of the bars do indicate if the scaling is adequate or not but do not indicate the ratios of specific process magnitudes relative to the ESBWR since the process magnitudes are normalized through scaling. The specific magnitudes can be found in the tables of Appendix A.

The GDCS transition results shown in Figures 8-2 and 8-5 show a little more variation between the ESBWR and test facilities phenomena scaling. However, the important phenomena still fall within approximately a factor of three of the ESBWR values. As indicated by the leftmost bar in Figure 8-5, the majority of depressurization occurs prior to this phase so that all of the

phenomena are of relatively low importance to the RPV pressure. This is somewhat true for the RPV mass as well, since the majority of mass loss occurs during blowdown (Figure 8-2). [46]

It is seen that the Pi-group values for the 4500 MWt ESBWR for various phenomena are in the same order of magnitude as the Pi-group values for the 4000 MWt ESBWR, the GIRAFFE-SIT test and the GIST test. In other words, the scaling "distortion" among these four entities or "scales" is minimal. Also, as expected, the Pi-group for the SLCS injection is important for the M-dot equation or the vessel liquid inventory for the late blowdown phase of the 4500 MWt ESBWR, but its magnitude is less than 0.4 making the flashing term still the most dominant one.

The liquid mass results during the reflood phase are shown in Figure 8-3. The RPV pressure is not calculated since depressurization is complete so the pressure has no effect on the RPV mass. The important parameters are again well scaled.

8.4 Long-term

This period encompasses the long-term PCCS period of a LOCA. The water level has been recovered in the RPV and the primary variable of interest is the containment pressure. The system must remove decay heat while maintaining the temperature and pressure below the design limits.

The GIRAFFE/He Test H1, PANDA M-series Test M3 and PANDA P-series Test P1 were selected for analysis in this period because they represent a similar set of conditions. All three tests are main steam line breaks with no ICs available and no VB leakage. This case results in the highest containment pressure as discussed in Reference [8-2].

The beginning of the Long-term phase is taken at 6 hours into the LOCA transient for scaling purposes of both 4000 MWt and 4500 MWt ESBWRs. Figure 7 of Reference [8-3] shows that the Pi-group values for the 4500 MWt ESBWR long-term phase are relatively insensitive to the initial DW/WW conditions, e.g., 6 hours vs. 14 hours. By this time, any lingering effects of earlier transient phases have died out and the system has settled into its quasi-steady long-term behavior. Figure 8-6 and 8-7 show the results for the pressure in the DW and WW, respectively. The 4500 MWt ESBWR results are the same as those shown in Section 7. From these figures we can see which PI-groups are important and how they compare in the tests and the ESBWR.

As indicated in the figures, the important parameters are well matched for both the DW and WW. As discussed earlier, the primary function of the DW is to pass steam generated in the RPV by decay heat to the PCCs: other aspects of the DW are unimportant. The mass and energy flows in the WW during this phase are small compared to contribution of the influx of noncondensible gas that occurs in earlier transient stages.

The WW gas space is considered to be near saturation for the estimates of the heat and mass transfer to the walls and pool. Sufficiently detailed test data is not available to estimate the heat and mass transfer rates in the tests. Therefore the heat and mass transfer are estimated analytically using heat and mass transfer correlations. The important aspect of this is that the heat lost into or through the walls is controlled by the wall rather than the gas space. Therefore

[46] RAI 293

the total rate of heat transfer to the wall is set by well known parameters (conduction for the ESBWR and heat losses for the tests) and analytical estimates are used to partition the energy flows in the gas space between sensible heat transfer and latent heat transfer. The sum is set by the conduction in walls. The rates and partitioning of heat and mass flow will vary minimally over the long-term phase as they depend on the humidity and input flows.

The bubble term in the WW results represents the transfer of remaining noncondensible gas from the DW to the WW. As discussed above, the timing of this movement is uncertain and can vary. [[

]] When the bubbles enter the WW gas space they bring with them noncondensible gas and steam at the pressure corresponding to the surface temperature of the pool. The "VB" term is zero for the tests since there is no VB leakage in the tests selected for consideration. Later tests in the PANDA P-series of tests included VB leakage to assess its effect.

8.5 PCC Scaling

The PCCs are primarily important in controlling how much energy goes into the top layer of the suppression pool – one of the key parameters influencing the long-term containment pressure. The maximum PCC capacity determines at what time the PCC capacity is sufficient to remove all of the decay heat thus stopping it from being deposited in the SP. The PANDA tests were run with different numbers of PCC in operation providing a range of capacities that bounds the heat removal capacity of the ESBWR PCCs.

As mentioned in Section 5, the PCCs are implemented as full-scale slices of the prototype PCC. Therefore tubes in the PANDA facility are full scale and there are no scaling distortions in the tubes. The numbers of tubes are reduced to properly scale the total heat removal from the condensers to the system scale, R, as shown by the top-down scaling results. The headers are reduced in size according to the system scale, thus maintaining the proper power to volume scaling. The flow into the header is sufficient to provide good mixing and the pressure drop along the header is small compared to the tubes as evidenced in the full scale PCC testing in the PANTHERS facility. Therefore no localized (bottom-up) effects are expected in the headers. Because the surface area to volume ratio is increased for the reduced length headers the heat removal through the header walls is increased. The heat loss in the headers is much less than the tubes, however, so it does not result in a significant distortion.[47]

8.6 Summary for Test Facility Comparison

The primary variables of importance to ESBWR safety during a LOCA are the RPV water level and containment pressure. The scaling analyses in Section 7 showed that these parameters are influenced by a limited number of "important" processes. These important processes for both 4000 MWt and 4500 MWt ESBWRs are well scaled in the test facilities as shown in this section.

The processes important to the RPV water level are; initial mass, inventory lost during the blowdown period and the timing of GDCS initiation. The results above show that the

[47] RAI 14

phenomena important to these processes are well scaled in the GIST and GIRAFEE/SIT tests used to provide data for TRACG qualification.

The containment pressure response is also dominated by a small set of processes. The primary contributions to pressure changes are the movement of noncondensibles between the DW and WW and initial heat-up of the SP, which results in a steam partial pressure in the WW. The phenomena important to these processes are well scaled in the tests as shown above. In addition, the noncondensible movement is represented for a wide range of conditions in the tests series by using varying configuration, amounts of noncondensible gas and release timings. The PCCs which play the major role in influencing the amount of energy deposited in the top layer of the SP are well scaled, as described in Section 8.5. The PCCs are very scalable since the tubes can be represented at full scale and the conditions in the headers are nearly homogenous, so that length changes do not introduce significant scaling distortions.

In, summary the phenomena important to the plant system behavior are well scaled in the test facilities thus providing useful date for TRACG qualification. Although not essential, phenomena of lesser importance are well scaled also. In addition, no new phenomena were identified in the tests.

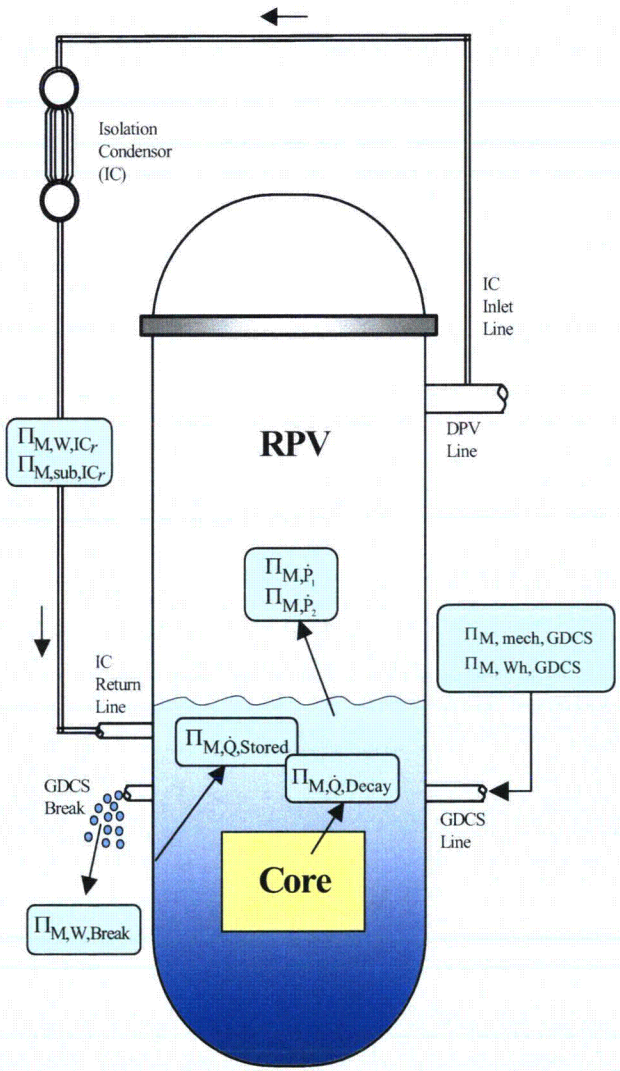

Equation

$$h_{fg}^{+}\frac{d\Delta M_{\lambda}^{+}}{dt^{+}} = -\sum_{i}\Pi_{M,\dot{Q},i}\dot{Q}_{i}^{+} + h_{fg}^{+}\sum_{i}\Pi_{M,W,i}W_{\lambda,i}^{+} + \sum_{i}\Pi_{M,sub,i}h_{sub,i}^{+}W_{\lambda,i}^{+}$$
$$-\left[\Pi_{M,\dot{P}1}V_{RPV}^{+}f_{3}^{+} + \Pi_{M,\dot{P}2}f_{4}^{+}M_{\lambda}^{+}\right]\frac{dP^{+}}{dt^{+}}$$

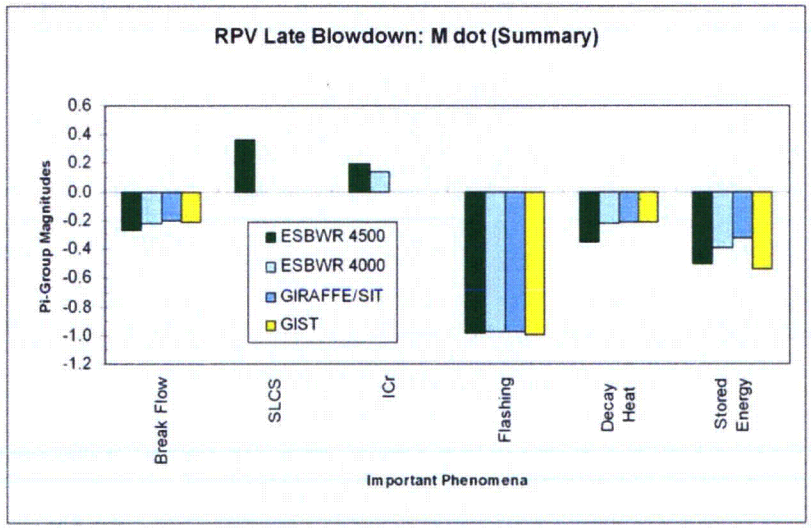

Figure 8-1. RPV Late Blowdown: Time Rate of Liquid Mass Change (Mdot) - Summary

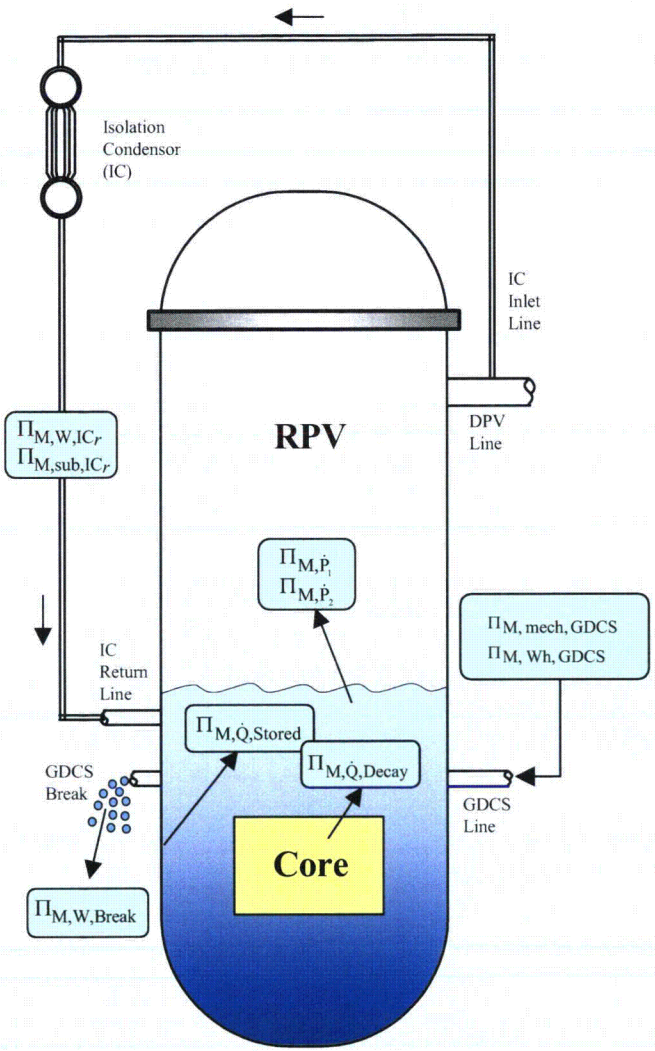

Equation

$$h_{fg}^{+}\frac{d\Delta M_{\lambda}^{+}}{dt^{+}} = -\sum_{i}\Pi_{M,\dot{Q},i}\dot{Q}i^{+} + h_{fg}^{+}\sum_{i}\Pi_{M,W,i}W_{\lambda,i}^{+} + \sum_{i}\Pi_{M,sub,i}h_{sub,i}^{+}W_{\lambda,i}^{+}$$
$$-\left[\Pi_{M,\dot{P}1}V_{RPV}^{+}f_{3}^{+} + \Pi_{M,\dot{P}2}f_{4}^{+}M_{\lambda}^{+}\right]\frac{dP^{+}}{dt^{+}}$$

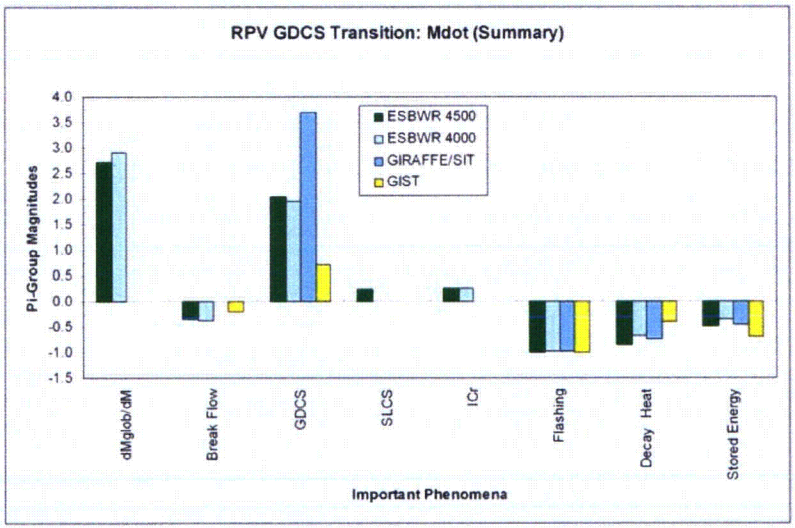

Figure 8-2. RPV GDCS Transition: Time Rate of Liquid Mass Change (Mdot) - Summary

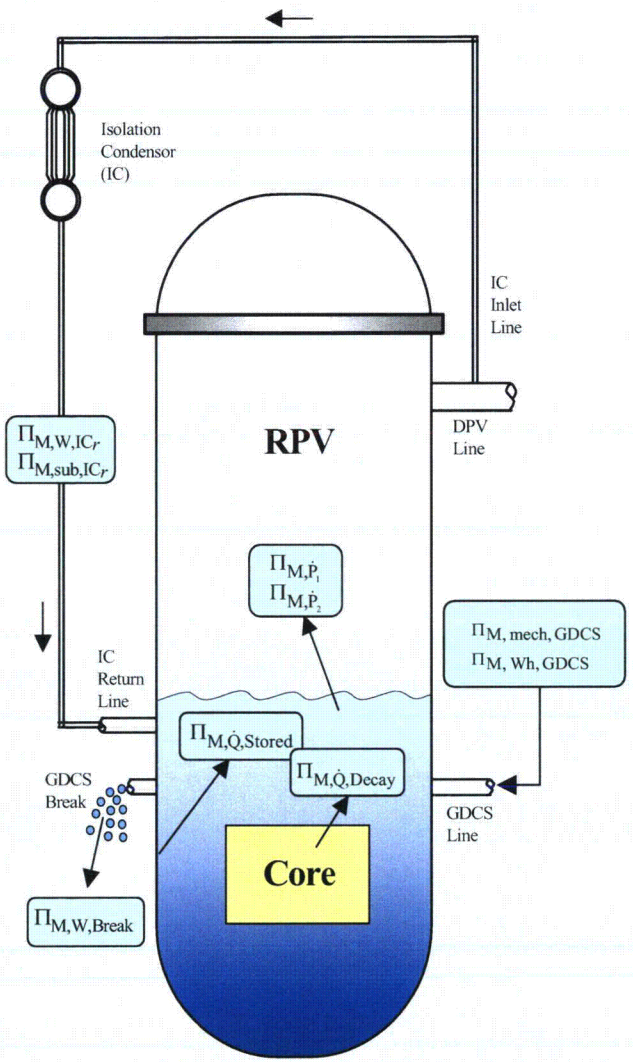

Equation

$$h_{fg}^{+}\frac{d\Delta M_{\lambda}^{+}}{dt^{+}} = -\sum_{i}\Pi_{M,\dot{Q},i}\dot{Q}_{i}^{+} + h_{fg}^{+}\sum_{i}\Pi_{M,W,i}W_{\lambda,i}^{+} + \sum_{i}\Pi_{M,sub,i}h_{sub,i}^{+}W_{\lambda,i}^{+}$$
$$-\left[\Pi_{M,\dot{P}1}V_{RPV}^{+}f_{3}^{+} + \Pi_{M,\dot{P}2}f_{4}^{+}M_{\lambda}^{+}\right]\frac{dP^{+}}{dt^{+}}$$

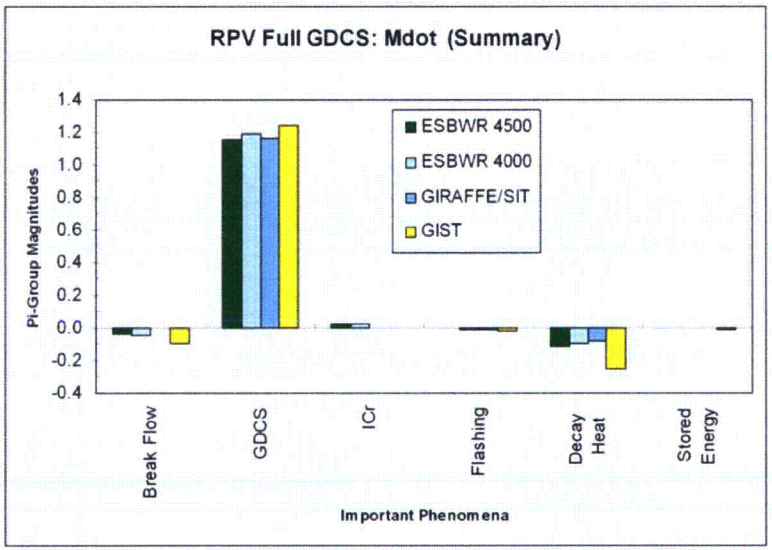

Figure 8-3. RPV Full GDCS (Reflood): Time Rate of Liquid Mass Change (Mdot) – Summary

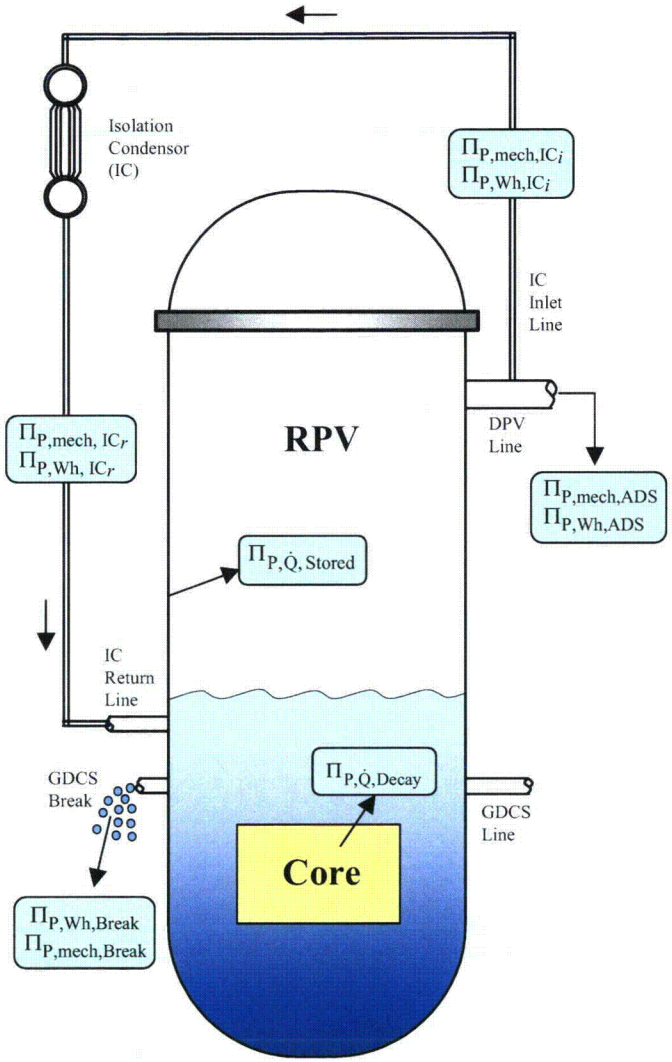

Equation

$$f_2^+ V^+ \frac{dP^+}{dt^+} = \sum_i \Pi_{P,\dot{Q},i} Q_i^+ - \Pi_{P,\dot{V}} P^{*+} \frac{dV^+}{dt^+} + \sum_i \Pi_{P,Wh,i} W_i^+ h_i^+ + \frac{P^{*+}}{\rho^+} \sum_i \Pi_{P,mech,i} W_i^+ - V^+ \sum_j \Pi_{P,y,j} \left(f_{1,j}^+ \frac{dy_j^+}{dt^+} \right)$$

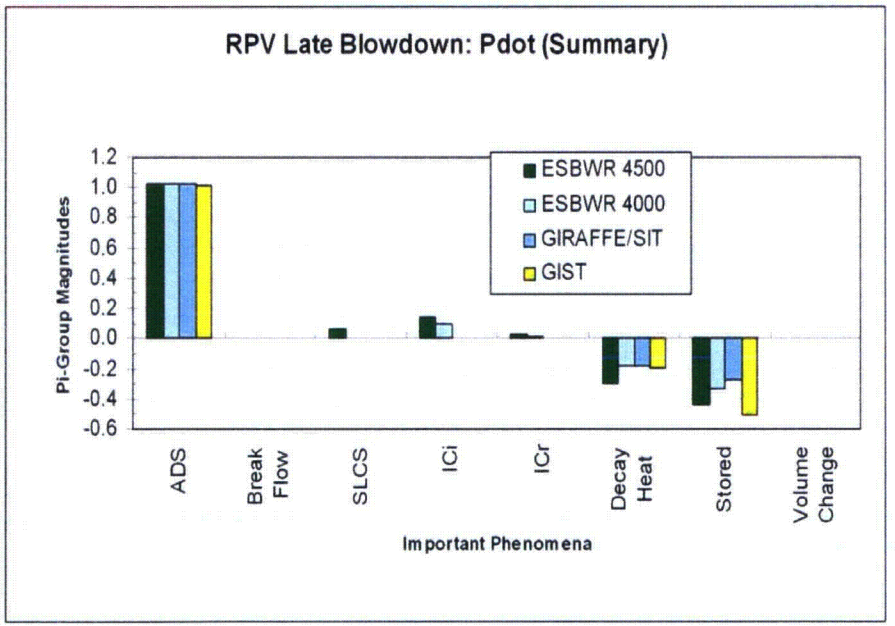

Figure 8-4. RPV Late Blowdown: Time Rate of Pressure Change (Pdot) – Summary

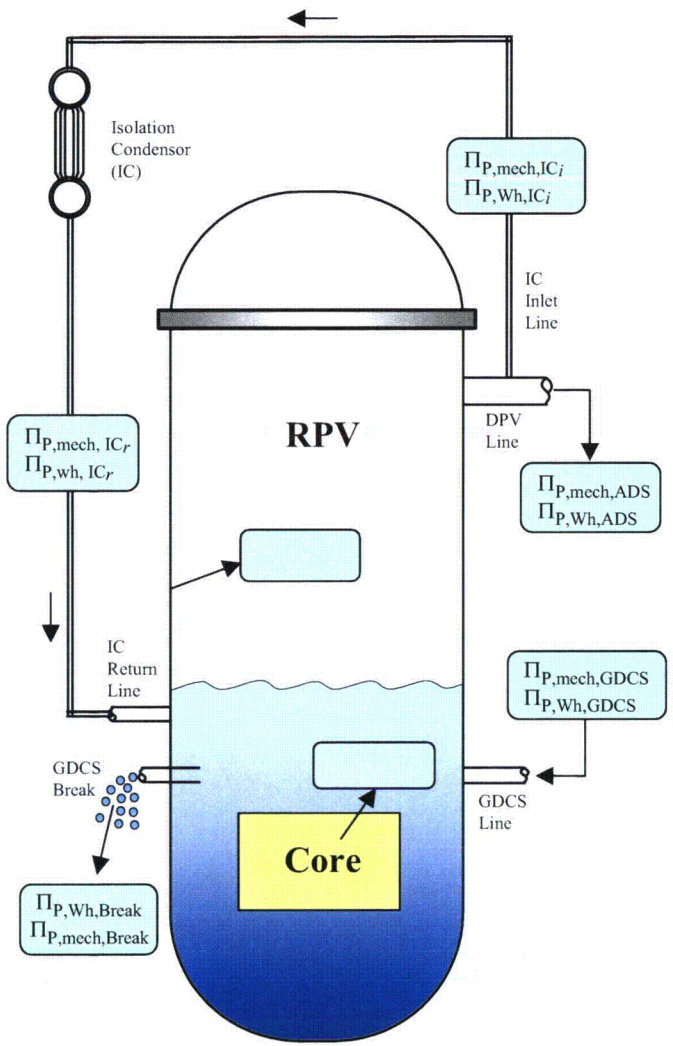

Equation

$$f_2^+ V^+ \frac{dP^+}{dt^+} = \sum_i \Pi_{P,\dot{Q},i} Q_i^+ - \Pi_{P,\dot{V}} P^{*+} \frac{dV^+}{dt^+} + \sum_i \Pi_{P,Wh,i} W_i^+ h_i^+ + \frac{P^{*+}}{\rho^+} \sum_i \Pi_{P,mech,i} W_i^+ - V^+ \sum_j \Pi_{P,y,j} \left(f_{1,j}^+ \frac{dy_j^+}{dt^+} \right)$$

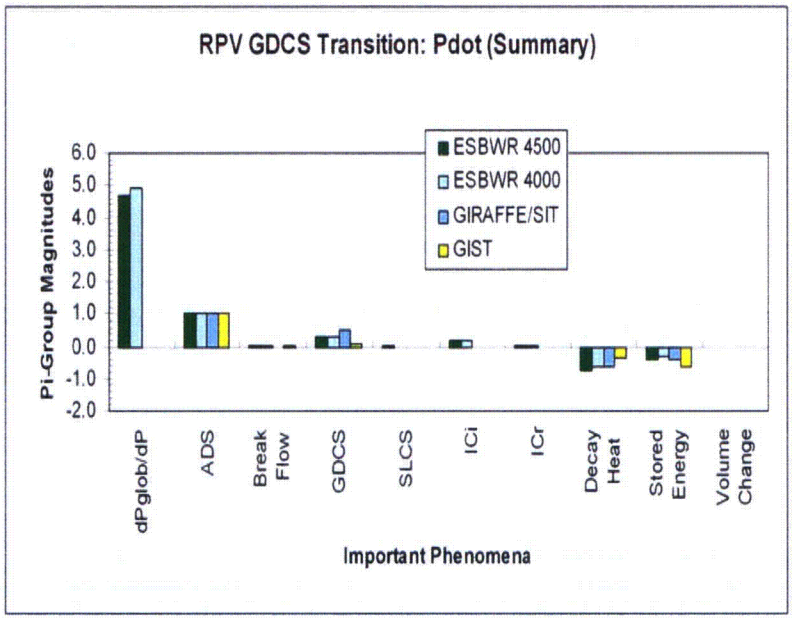

Figure 8-5. RPV GDCS Transition: Time Rate of Pressure Change (Pdot) – Summary

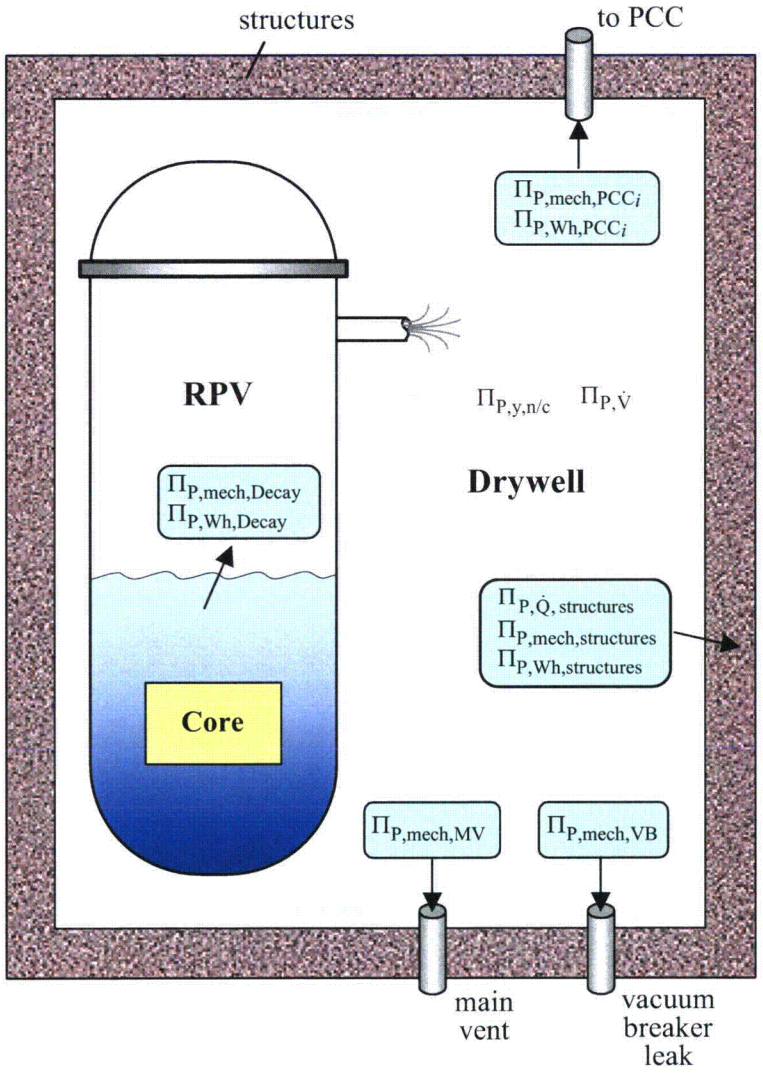

Equation

$$f_2^+ V^+ \frac{dP^+}{dt^+} = \sum_i \Pi_{P,\dot{Q},i} Q_i^+ - \Pi_{P,\dot{V}} P^{*+} \frac{dV^+}{dt^+} + \sum_i \Pi_{P,Wh,i} W_i^+ h_i^+ + \frac{P^{*+}}{\rho^+} \sum_i \Pi_{P,mech,i} W_i^+ - V^+ \sum_j \Pi_{P,y,j} \left(f_{I,j}^+ \frac{dy_j^+}{dt^+} \right)$$

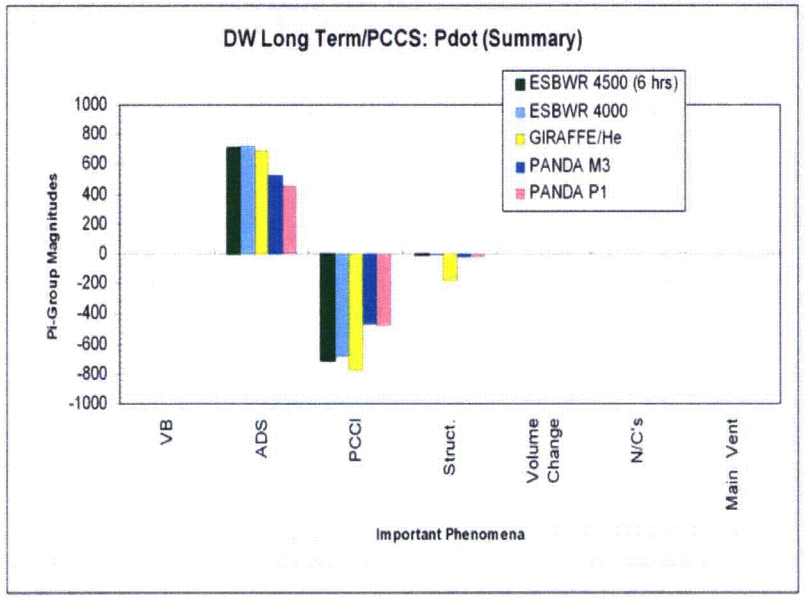

Figure 8-6. Drywell Long Term/PCCS: Time Rate of Pressure Change (Pdot) – Summary

9.0 EFFECT OF SCALE

There are limitations to the application of scaling theory for complex systems such as a nuclear power plant. Perhaps the most convincing argument for concluding that the effects of scale distortions are unimportant in the ESBWR test program are comparisons of the system behavior at different scales. The figures below show comparisons of the key aspects of the system behavior from facilities with significantly different system scales as well as simulation results for the SBWR.

Figures 9-1 and 9-2, taken from the SBWR Testing Summary Report [3-2], show comparisons of the normalized pressure and RPV liquid mass for the SBWR, GIRAFFE/SIT test and GIST test plotted against non-dimensional time, t^+.[48] The curves indicate a very similar behavior for the three facilities at very different scales, indicating that there are no significant distortions or scale effects for the RPV water level.

Figure 9-3 shows the variation in containment pressure with variations in the noncondensible gas pressure. As discussed earlier, the figure shows that the primary contribution to containment pressure is the movement of noncondensible gas from the DW to the WW. The small deviations from the solid line in the figure can be attributed to uncertainties in the gas concentration measurements and variations in the steam partial pressure resulting from differences in the SP temperature for the wide range of test conditions represented. Even for the wide range of test conditions, the variation is small indicating that the contribution from SP temperature, while important, is small compared to the noncondensible gas contribution.

Figures 9-4 and 9-5 show the performance of the PCC and IC at different scales and conditions. As shown the PCCs and ICs are very scalable. The behavior is very similar over a wide range of scales and conditions for both pure steam conditions and mixtures of steam and noncondensible gas.

[48] RAI 13

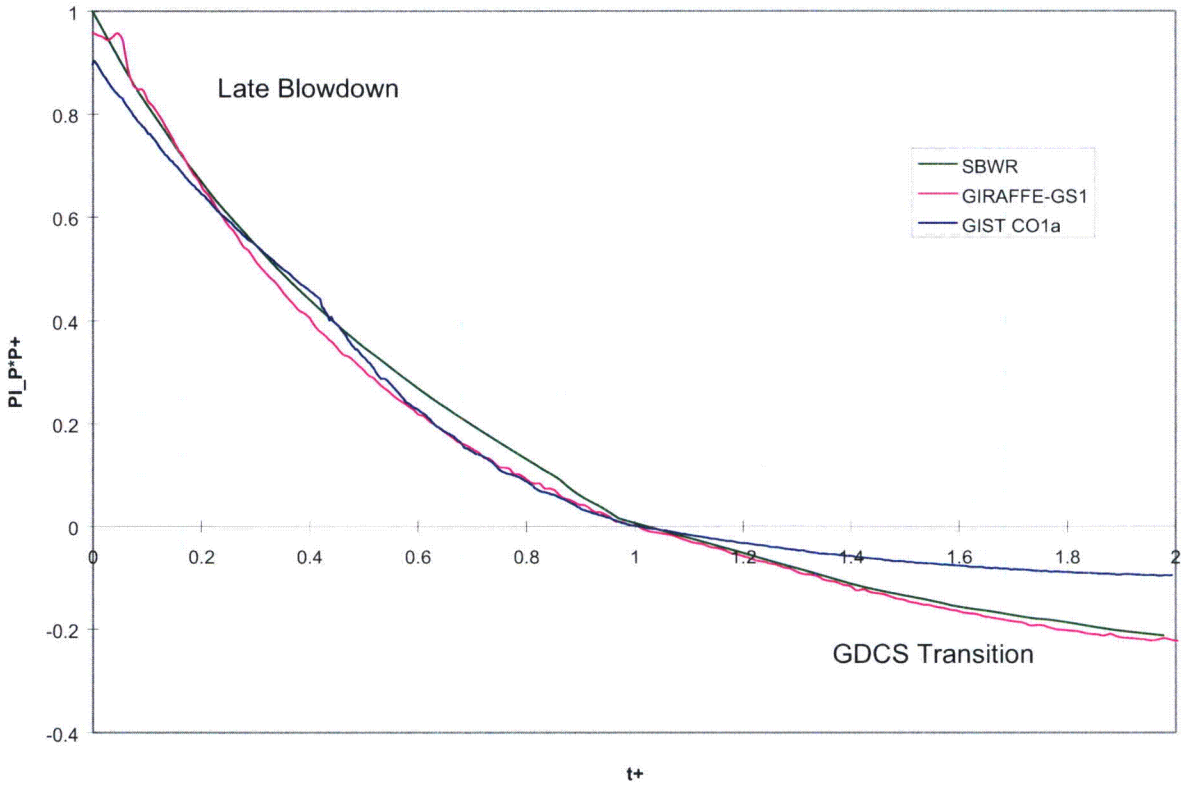

Figure 9-1 Nondimensional RPV Pressure Comparison for SBWR, GIRAFFE/SIT and GIST

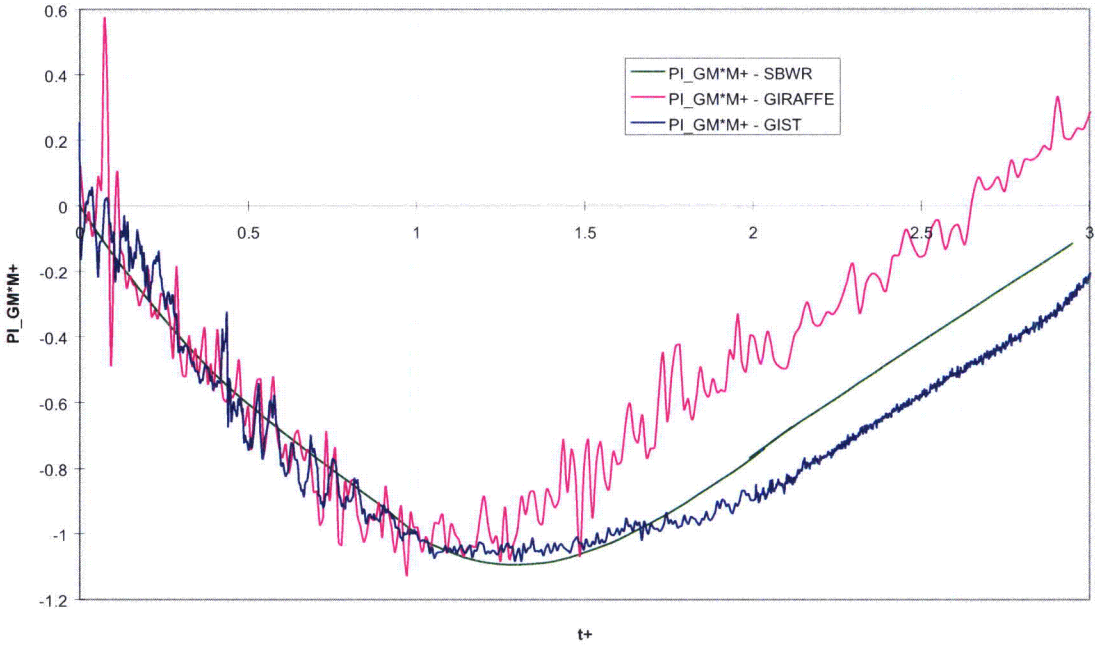

Figure 9-2 Nondimensional RPV Liquid Mass Comparison for SBWR, GIRAFFE/SIT and GIST

[[

]]

Figure 9-3 Comparison of WW Pressure Increases with Noncondensible Partial Pressures for Giraffe/He, PANDA-M and PANDA-P tests

[[

]]

Figure 9-4 Comparison of PCC and IC Behavior for Pure Steam at Different Scales

[[

]]

Figure 9-5 Comparison of PCC Behavior for Steam-Noncondensible Mixtures at Different Scales

10.0 CONFIRMATORY SCALING ANALYSIS

10.1 Short-term RPV Behavior

To substantiate the results presented in Section 8.3 further, a simplified continuous analysis in the non-dimensional time domain was carried out. di Marzo [10-1] proposed a simplified model, in a dimensional form, to determine the RPV pressure and water inventory in BWRs during depressurization transients. Following the formulation of [10-1], we use the Clausius – Clapeyron relation and other simplifying assumptions such as treating the steam as a perfect gas, and no vapor accumulation in the RPV. These assumptions, as employed in [10-1], are justified during the low-pressure late blowdown and GDCS transition periods of our confirmatory scaling analysis of the short-term RPV behavior. The analysis also assumes a break in the liquid line such as GDCS injection line close to the RPV.

The final simplified equations for the RPV pressure change rate, dP/dt, and the water inventory change rate, dI/dt, neglecting the small mechanical energy terms (Supplemental Response to RAI 292 in [8-2]) in comparison to the more dominant thermal energy terms, are as follows:

$$\frac{dP}{dt} = \left[-\frac{RT}{V_o}\left(\sum_i \frac{\Delta h_i}{h_{fg}} W_{i,l} + W_D \right) + \frac{RT}{h_{fg} V_o} Q_{decheat} + \frac{RT}{h_{fg} V_o} Q_{stored} \right] \div \left[\left(\frac{a-1}{a} \right)\left(1 - \frac{M_o I}{\rho_l V_o} \right) + \frac{M_o c_{pl} T}{V_o a^2} \frac{I}{P} \right] \quad (10.1\text{-}1)$$

and

$$\frac{dI}{dt} = \frac{1}{M_o}\left[\sum_i W_{i,l} - W_D \right] \quad (10.1\text{-}2)$$

where the following variables are used

P = Pressure in vessel
t = Time
I = M_l/M_o = Liquid inventory in vessel divided by initial total inventory
M_l = Liquid inventory
$W_{i,,l}$ = Liquid inflow/outflow (GDCS, SLCS, break, etc) rates (inflow is +ve)
W_D = Steam discharge rate through ADS (outflow is +ve)
$Q_{decheat}$ = decay heat
Q_{stored} = stored energy release from vessel wall

In addition, the following values are held constant

M_o = Initial inventory in vessel (steam and liquid)
ρ_l = Liquid density
V_o = RPV non-solid or free volume
R = Gas constant for steam
T = Temperature in vessel (since the saturation temperature drops at a much slower rate compared to the pressure)
Δh_i = Liquid subcooling relative to RPV condition
h_{fg} = Latent heat of vaporization
$a = h_{fg}/RT$
c_{pl} = Specific heat of liquid or water

Equations (10.1-1) and (10.1-2) are non-dimensionalized following the procedure used in Section 6. The IC and CRD flows have been neglected, as in our earlier work (Supplemental Response to RAI 292 in [8-2]), because they are small compared to the break, ADS, SLCS and GDCS flows. The final non-dimensional forms of Equations (10.1-1) and (10.1-2) are as follows:

$$\frac{dP^+}{dt^+} = \left[\Pi_{P\_GDCS} W^+_{GDCS} + \Pi_{P\_SLCS} W^+_{SLCS} - \Pi_{P\_ADS} P^+ A^+_{ADS} + \Pi_{P\_decheat} Q^+_{decheat} + \Pi_{P\_stored} Q^+_{stored}\right] \div \left[\left(\frac{a_o - 1}{a_o}\right)\left(1 - \Pi_{mi} I^+\right) + \Pi_{cp} \frac{I^+}{P^+}\right] \quad (10.1\text{-}3)$$

and

$$\frac{dI^+}{dt^+} = \Pi_{I\_GDCS} W^+_{GDCS} + \Pi_{I\_SLCS} W^+_{SLCS} - \Pi_{I\_ADS} A^+_{ADS} P^+ - \Pi_{I\_break} \sqrt{P^+} \quad (10.1\text{-}4)$$

The non-dimensional variables in Equations (10.1-3) and (10.1-4) are all in the form,

$$X^+ = \frac{X}{X_o} \quad (10.1\text{-}5)$$

where X is the variable of interest and X_o is the reference value for the variable. For all variables except time, area and the GDCS flow rate and subcooling, the initial values at the start of the late blowdown phase are used as the reference values. For the ADS area, which may vary with time, the maximum area is used as the reference value. The rated GDCS flow rate, discussed later, is used as the reference value for non-dimensionalizing the GDCS flow rate. The "characteristic time," t_r, used to non-dimensionalize time, t, is obtained from the consideration of time required to drop the RPV pressure from P_o to the pressure at which GDCS injection begins only due to enthalpy discharge through the ADS. This characteristic time was defined in Sections 6.1 and 7.3.1:

$$t_r = (\Delta P_r V_o f_{2,o})/(W_{ADS,av} \Delta h_{ADS,o}) \quad (10.1\text{-}6)$$

where,

$\Delta P_r = P_o - P_l$ (P_l being the RPV pressure at which GDCS injection starts)

Other symbols have the usual meaning.

Following Supplemental Response to RAI 292 in [8-2], it has been assumed that the steam flow rate through the ADS, W_{ADS}, is proportional to the RPV pressure, P, and the break flow rate through the liquid line is proportional to the square root of RPV pressure, P. These assumptions are substantiated from the equations and figures given in Section 2.13 (Critical Flow) of Reference [10-2].

The GDCS flow rate can be given by

$$W_{GDCS} = W_{GDCS_{rated}} \sqrt{\frac{\rho_l g H_{GDCS} + P_{DW} - P_{RPV}}{\rho_l g H_{GDCS}}} \quad (10.1\text{-}7)$$

where

P_{RPV} = RPV pressure (P in the equations above)
P_{DW} = Drywell pressure (held constant)
H_{GDCS} = Hydrostatic head for the GDCS line
$W_{GDCSrated}$ = Rated GDCS flow when the RPV and drywell are at the same pressure
g = Acceleration due to gravity

Note that Equation (10.1-7) smoothly increases the GDCS flow rate from zero (when P_{RPV} becomes equal to P_l or ($P_{DW} + \rho_l g H_{GDCS}$)) to the rated value as P_{RPV} approaches P_{DW}. Also, the component interconnection between the GDCS pool and the RPV has been considered. This is the only relevant component interconnection in the late blowdown and GDCS transition phases.

The PI groups that appear in Equations (10.1-3) and (10.1-4) are defined as,

$$\Pi_{mi} = \frac{M_o I_o}{\rho_{lo} V_o}$$

$$\Pi_{cp} = \frac{M_o c_{pl} T_o I_o}{V_o a_o^2 P_o}$$

$\prod_{P\_GDCS} = \prod_{P,Wh,\,GDCS} \prod_{fa} (\Delta P_r/P_o) = (W_{GDCS,rated} \Delta h_{GDCS,1} t_r)/(V_o a_o P_o)$

$\prod_{P\_SLCS} = \prod_{P,Wh,\,SLCS} \prod_{fa} (\Delta P_r/P_o) = (W_{SLCS,o} \Delta h_{SLCS,o} t_r)/(V_o a_o P_o)$

$\prod_{P\_ADS} = \prod_{P,Wh,\,ADS} \prod_{fa} (\Delta P_r/P_o) \prod_{ha} \prod_{DwADS} = (RT D_o A_{o,ADS} t_r)/V_o$

$\prod_{P\_decheat} = \prod_{P,Q,decay} \prod_{fa} (\Delta P_r/P_o) = (Q_{decay,o}\ t_r)/(\ V_o\ a_o\ P_o)$

$\prod_{P\_stored} = \prod_{P,Q,stored} \prod_{fa} (\Delta P_r/P_o) = (Q_{stored,o}\ t_r)/(\ V_o\ a_o\ P_o)$

$$\Pi_{P,Wh,i} = \frac{W_{i,o}\Delta h_{i,o}}{V_o f_{2,o}} \frac{t_r}{\Delta P_r}$$ where i = GDCS, SLCS and ADS

$$\Pi_{P,\dot{Q},k} = \frac{\dot{Q}_{k,o}}{V_o f_{2,o}} \frac{t_r}{\Delta P_r}$$ where k = decay heat and stored heat

$$\Pi_{fa} = \frac{f_{2,o}}{a_o}$$

$$\Pi_{ha} = \frac{h_{fg}}{\Delta h_{ADS}}$$

$$\Pi_{DwADS} = \frac{D_o A_{o,ADS} P_o}{W_{ADS,av}}$$ (D_o being the "discharge" coefficient for steam – sec/m)

$\prod_{I\_GDCS} = \prod_{M,W,GDCS} \prod_{dmi} = (W_{GDCS,rated}\ t_r)/(M_o\ I_o)$

$\prod_{I\_SLCS} = \prod_{M,W,SLCS} \prod_{dmi} = (W_{SLCS,o}\ t_r)/(M_o\ I_o)$

$\prod_{I\_ADS} = \prod_{M,W,ADS} \prod_{dmi} \prod_{DwADS} = (D_o\ A_{o,ADS}\ P_o\ t_r)/(\ M_o\ I_o)$

$\prod_{I\_break} = \prod_{M,W,break} \prod_{dmi} \prod_{DwBreak} = (F_o\ A_{o,break}\ P_o^{0.5}\ t_r)/(\ M_o\ I_o)$

$$\Pi_{dmi} = \frac{\Delta M_{Io}}{M_o I_o}$$

$$\Pi_{M,W,i} = W_{I,i,o} \frac{t_r}{\Delta M_{Io}}$$ where i = GDCS, SLCS, ADS and Break

$$\Pi_{DwBreak} = \frac{F_o A_{o,break} \sqrt{P_o}}{W_{break,av}}$$ F_o being the "discharge" coefficient for saturated liquid,

[[ ]]

Note that the parameters ΔP_r, $f_{2,o}$, ΔM_{Io} and Δh_{ADS} cancel out in the Pi-groups that appear in Equations (10.1-3) and (10.1-4). For this confirmatory analysis, the Pi-groups are defined as combinations of other Pi-groups to have direct correspondence with the Pi-groups introduced in

the formal scaling analysis in Section 6. However, for the sake of convenience, the final expressions of the Pi-groups have also been shown above.

To account for the stored heat release from the vessel structure, Q_{stored}, di Marzo [10-1] increased the value of water specific heat, c_{pl}, somewhat arbitrarily by a factor of 1.5. In reality, the vessel is comprised of metals of various thicknesses – some "thin" such as vessel internals, and some "thick" like the vessel wall. The "thin" structures would be fast responding and would quickly follow the vessel water temperature whereas the "thick" structures would be slow responding and there would be some delay in following the water temperature. In this analysis, a sensitivity study was performed for the 4500 MWt ESBWR. Three cases were considered:

Case 1: No heat transfer from metal (vessel structure) to water
Case 2: Metal to water heat transfer only due to the "thin" vessel internals
Case 3: Metal to water heat transfer due to both "thin" and "thick" vessel structures.

The factor ($F\text{-}c_{pl}$) for increasing the water specific heat is calculated based on the vessel metal heat capacity, participating in the metal to water heat transfer, as shown below:

$$F\text{-}c_{pl} = (M_{lo}\, c_{pl} + M_{metal} c_{p,steel})/(M_{lo} c_{pl})$$

The values of this factor for the three cases of the 4500 MWt ESBWR are:

[[

]]

The real situation is somewhere between Case 2 and Case 3. However, to be conservative from the RPV water inventory point of view, the Case 3 has been considered as the base-case. The same assumption was also used for calculation of Q_{stored} in the formal scaling analysis presented in Sections 7 and 8.

So the best estimate factor ($F\text{-}c_{pl}$) for increasing the water specific heat for the various ESBWR and test cases are as follows:
[[

]]

As a result, the last term in the numerator of Equation (10.1-3) is dropped and the value of water c_{pl} is multiplied by the factor $F\text{-}c_{pl}$.

Since the GDCS injection line break was used in Sections 7 and 8, the same GDCS injection line break has also been used in the present confirmatory analysis.

The base-case for the 4500 MWt ESBWR includes (a) F-c_{pl} equal to [[ ]] to account for the metal-to-water heat transfer, (b) SLCS injection flow rate of [[ ]] into the late blowdown phase which starts when the RPV pressure drops to [[ ]] and (c) GDCS injection through all three intact GDCS lines. As mentioned earlier, the IC and CRD flows have been neglected, because they are small compared to the break, ADS, SLCS and GDCS flows.

The Runga-Kutta integration method is used to solve the ordinary differential Equations (10.1-3) and (10.1-4). Figure 10-1 shows the results of the 4500 MWt ESBWR for the base-case (with SLCS flow) and another case without the SLCS injection during the late blowdown and the GDCS transition phases. It is seen that the SLCS injection helps keeping the water inventory at a higher level until the GDCS injection begins. However, the SLCS injection has only a small effect on the vessel depressurization rate, and thus on the timing of the GDCS initiation which occurs when P+ reaches the value of P_l/P_o. It was shown previously in Figure 8-4 that for the P-dot equation, contribution due to the SLCS flow rate is small compared to the ADS flow rate that dominates the RPV depressurization rate. However, the SLCS flow rate is significant from the RPV liquid inventory or M-dot viewpoint as seen in Figure 8-1.

Similar analyses with no SLCS, IC and CRD flows have been performed for the 4000 MWt ESBWR, GIRAFFE-SIT GS1 and GIST C01A tests. (In the 4000 MWt ESBWR design, the SLCS injection was not contemplated during a LOCA.) The calculated results along with the test data are compared with the calculated base-case results of the 4500 MWt ESBWR in Figure 10-2. The figure shows that the trends and even the values of the non-dimensional pressure and liquid inventory for the 4000 MWt and 4500 MWt ESBWR designs and the three different scales represented by the full-scale ESBWRs and the two test facilities are very similar. Comparison between the calculated results and the test data for the two different scales represented by the GIRAFFE and GIST tests are also very good. A summary comparison of all the Pi-group values that enter into the non-dimensional pressure and liquid inventory equations for the confirmatory analysis is presented in Table 10-1. In general, the values for the two ESBWR designs and the test facilities compare well and this agreement is reflected in the consistency of the results shown in Figure 10-2. [[

]]
However, this does not have a significant effect on the non-dimensional pressure response because it is not a dominant Pi-group for this phase of the transient.

Finally, Figure 10-3 shows the comparison of the four best-estimate confirmatory calculations for the 4500 MWt ESBWR, 4000 MWt ESBWR, GIRAFFE-SIT Test GS1 and GIST Test C01A along with the data of GIRAFFE-SIT Test GS1 and GIST Test C01A on the non-dimensional pressure (P+) vs. non-dimensional liquid inventory (I+) plane as per the NRC request (RAI 6.3 - 1).

It can be seen that the behavior of the 4500 MWt ESBWR during the late blowdown and GDCS injection phases is expected to be very similar to that observed in the GIRAFFE-SIT and GIST tests, and therefore, no additional tests are required for scaling of the 4500 MWt ESBWR for short-term RPV behavior. This is in agreement with the results presented in Section 8.3.

Table 10-1 Comparison of Pi-Group Values

[[

]]

10.2 Long-term Containment Cooling Phase

The purpose of the confirmatory analysis for the late blowdown and GDCS transition phases discussed in Section 10.1 is to show that the pair of differential equations that govern the RPV transient pressure and liquid inventory can be simplified and solved numerically to directly demonstrate similar responses for the ESBWR and the test facilities. In the process, the key phenomena that govern the relatively rapid changes in the RPV pressure and liquid inventory during these phases of the LOCA transient are identified and clarified. This situation is in marked contrast to the long term cooling (PCCS) phase of the LOCA transient where pressures in the RPV, DW and WW are essentially equal and changes are occurring in a quasi-static manner.

Figure 10-4 shows a schematic of the 4500 MWt ESBWR containment systems during the long term cooling phase. The steam generation rate inside the RPV is directly proportional to the decay heat and the entire amount of steam discharges into the Drywell (DW) through the break (MSLB or FWLB) and the ADS. The steam discharge rate is independent of the type of break and the RPV and the drywell are effectively uncoupled. The decay heat steam along with a small amount of residual DW noncondensable flows into the PCC, which is submerged in the PCC pool above and outside the containment. The steam is condensed in the PCC tubes and the condensate flows into the GDCS pool. The residual DW noncondensable eventually moves to the WW gas space and causes a small pressure increase. Section 6.2 of Reference [10-3] shows that during the long-term cooling phase, the PCCS is capable of transferring all the decay heat to the PCCS pool outside the containment. Therefore, there is no further heat up of the WW pool and no WW gas space pressure increase due to steam generated in the RPV because of decay heat. [[

]]The minimal coupling between the different regions means that the Pi groups for the wetwell and the drywell can be evaluated separately without reference to the other regions. Based on these considerations, we believe that no additional or confirmatory scaling analysis is required for the long-term cooling phase. Results presented in Section 8.4 are sufficient.

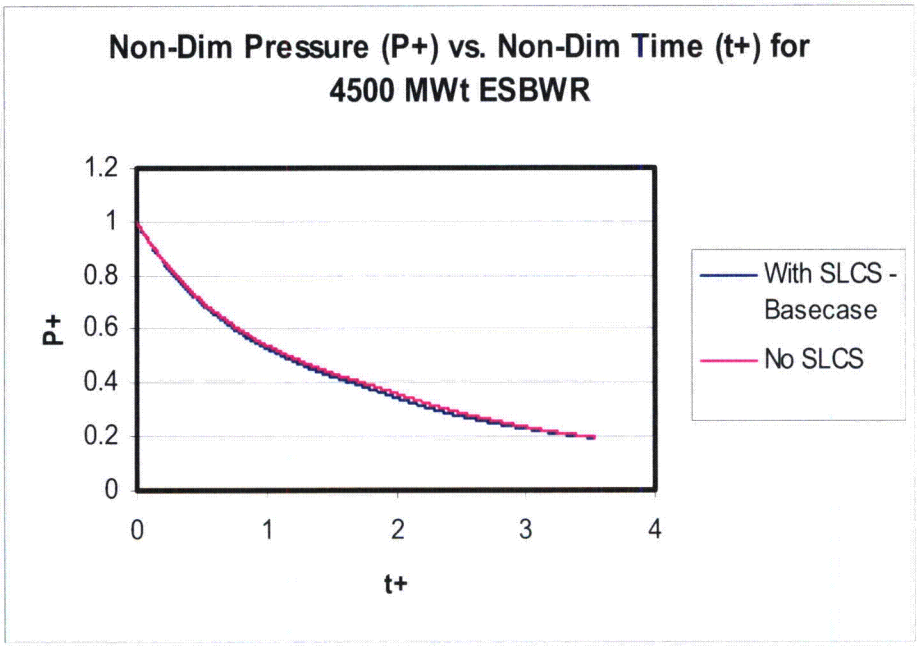

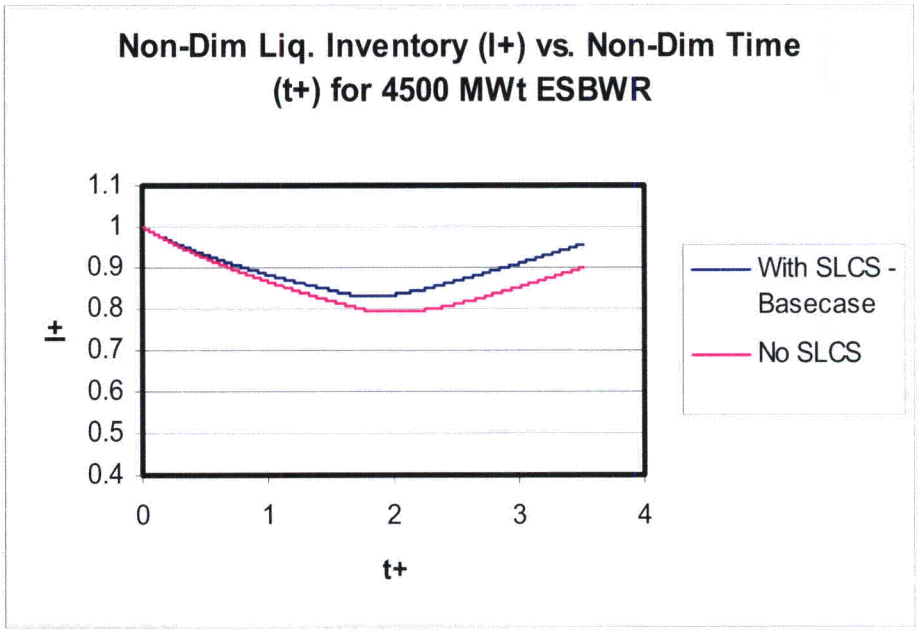

Figure 10-1. Calculated P^+ and I^+ for 4500 MWt ESBWR With and Without SLCS Injection

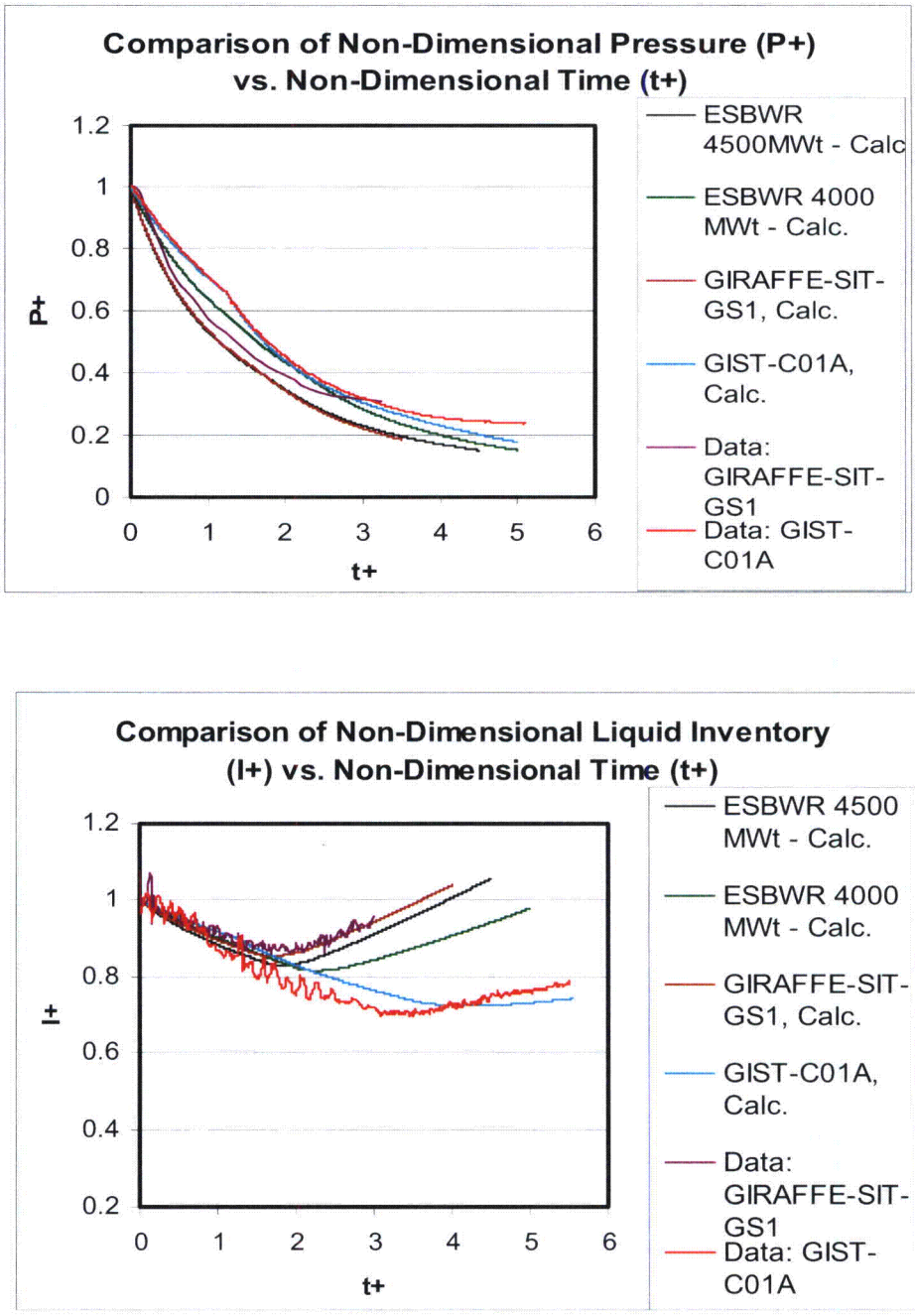

Figure 10-2. Comparison of Calculated P^+ and I^+ for 4500 MWt ESBWR, 4000 MWt ESBWR, GIRAFFE-SIT Test GS1 and GIST Test C01A With the Test Data

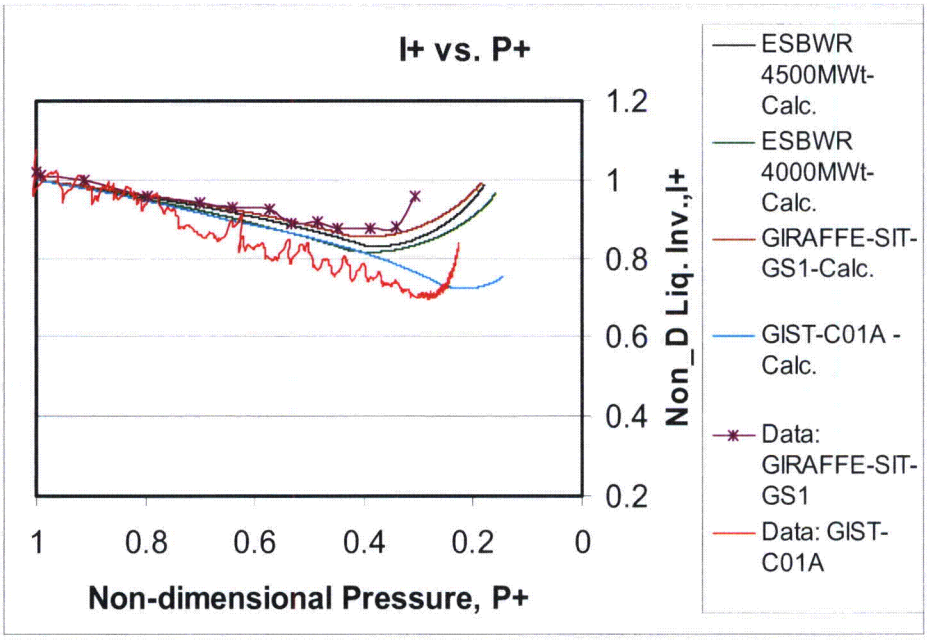

Figure 10-3. Comparison of All Confirmatory Best-estimate Calculations with Experimental Data of GIRAFFE-SIT Test GS1 and GIST Test C01A

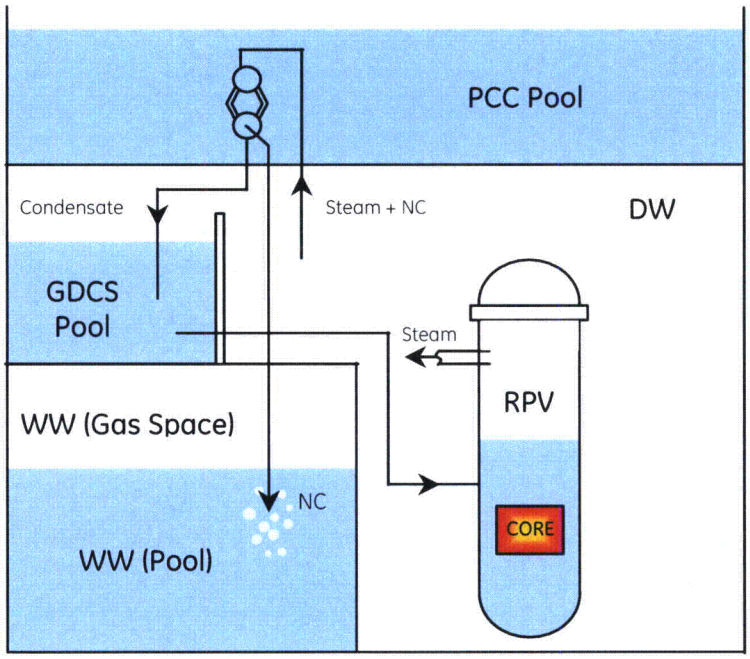

Figure 10-4. Schematic of the 4500 MWt ESBWR Containment Systems during the Long Term PCCS Phase

11.0 SUMMARY AND CONCLUSIONS

The **objective** of this scaling report is to show that the test facilities properly "scale" the important phenomena and processes identified in the ESBWR PIRT and/or provide assurance that the experimental observations from the test programs are sufficiently representative of ESBWR behavior for use in qualifying TRACG for ESBWR licensing calculations. This objective is met through a series of steps described below.

Section 2 provides an overview of the methodology used. The scaling methodology follows the hierarchical two-tiered scaling methodology composed of top-down scaling, which identifies processes important to the system behavior and a bottom-up, or phenomena level, scaling that looks at the characteristics of the processes identified as important from the top-down scaling

Section 3 describes the equations that govern the behavior of parameters important to the behavior and safety of the ESBWR, namely: RPV liquid mass, pressure and void fraction; containment pressure; and suppression pool energy. These equations are normalized in subsequent sections to provide scaling laws and evaluate the ESBWR and test facilities.

In **Section 4** the system governing equations are normalized using general reference parameters in order to arrive at a set of **general scaling criteria** that can be used for test facility design. These are the criteria that were used for the design of the test facilities included in this report. Brief **descriptions of the test facilities** are provided in **Section 5** as well as references to where the details of the test facilities can be found. In general the design of the experimental facilities and the conduct of the various tests were guided by consideration of the proper modeling and simulation of the key phenomena governing the performance of the passive safety systems. The implications of the scaling adjustments for the ESBWR are minimized by the fact that all of the tests were performed at prototypical temperature and pressure and with prototypical or near-prototypical elevations and elevation differences. These are the key variables and parameters governing the performance of the passive safety systems.

It should be noted that the general scaling criteria are very useful for facility design but do not provide a measure of what phenomena are important to the system behavior, nor are they useful in identifying distortions in the test facilities once they are completed. Instead this is accomplished with a more detailed nondimensionalization of the governing equations as described in **Section 6**. The nondimensionalization developed in Section 6 provides detailed scaling equations that can be used to identify which phenomena are important to the system behavior and therefore should be well scaled in the test facilities. Additionally these equations can be used to assess if this goal had been achieved in the tests.

In **Section 7** the detailed scaling equations from Section 6 are applied to the ESBWR (4500 MWt) to identify the processes important to the system behavior. The parameters important to safety are identified as: the RPV liquid mass that ensures that the core remains covered; the RPV pressure which is important in determining the timing of the GDCS injection; and the containment pressure which is important to assure that the containment is not breached during an accident. The LOCA transient is broken down into four temporal phases – late blowdown, GDCS transition, reflood, and long-term decay heat removal – within which the dominant phenomena remain unchanged and the phenomena magnitudes are relatively constant.

The **results for the ESBWR** indicate that a small number of processes are important to the behavior of the system parameters of interest (liquid mass and pressure). For the RPV liquid mass the important processes are flashing due to depressurization, boiling due to energy input from stored energy and decay heat, and GDCS flow (Figures 7-1 through 7-3). Although other parameters influence the behavior of the liquid mass during the short GDCS transition phase, the mass change during this phase is very small and therefore not very significant to the overall mass loss in the vessel. For the RPV pressure the dominant phenomenon is energy flow through the ADS system (Figures 7-4 and 7-5).

The wetwell pressure controls the containment pressure and the drywell is found to be unimportant to the containment response during the transient period considered (late blowdown onward). The drywell is found to act in a manner similar to a large pipe that transfers steam from the RPV to the main vents and PCCs (Figure 7-6). The time constant for the DW pressure is very short compared to the wetwell and the pressure in the DW therefore rapidly adjusts to the boundary condition presented by the WW pressure. The primary contribution of the DW is that its volume determines the quantity of noncondensible gas that must be accommodated by the WW in the long term. The important process for the containment pressure is the movement of noncondensible gas from the DW to the WW (Figure 7-7).

In **Section 8**, the same scaling method is applied to the test facilities to evaluate if the phenomena identified as important to the ESBWRs (both 4500 MWt and 4000 MWt) are scaled properly in the test facilities. Figures 8-1 through 8-7 show that all of the important phenomena magnitudes are well scaled in the test facilities.

Proper bottom-up scaling is a common problem with reduced scale facilities, where aspect ratio, surface to volume ratio and other geometric considerations make it difficult to simulate local effects. A review of the processes important to the system behavior concludes that they are either well scaled from the bottom-up perspective (ADS flow, PCC heat removal, SP mixing) or can be addressed through parametric studies and a bounding approach with TRACG (stratification in gas space, SP mixing). The bottom-up results are, for the most part, borrowed from the SBWR scaling report [3-1] rather than repeating them in this report. [49]

Although it does not constitute scaling analyses, **absence of significant distortions is confirmed** by comparing key parameters from tests done at a wide variety of scales in **Section 9**. The comparisons shown in Figures 9-1 through 9-5 show a similar behavior at all scales indicating that the important processes were well represented in the tests and that no significant scale distortions occurred.

Results of confirmatory scaling analysis, based on continuous calculation in non-dimensional time domain, for short-term RPV behavior are presented in Section 10.1. The results are in agreement with those presented in Section 8.3. As discussed in Section 10.2, similar confirmatory analysis is not required for the long-term cooling phase; results presented in Section 8.4 are sufficient for the scaling purposes.

[49] RAI 15

The conclusions drawn from this report and results of the tests are:

- There are only a small number of phenomena important to ESBWR system behavior
- Important phenomena are well scaled in the tests
- No unexpected phenomena were observed in the tests*
- Distortions in localized phenomena (bottom-up) due to reduced scale facilities were not significant
- Comparison of test results at different scales confirm these results

Overall the test facilities are demonstrated to adequately simulate the phenomena important to the ESBWR. Although there are distortions in the facilities, they are found to be in areas that do not affect significant parameters for the system behavior. As such, the test data obtained from these facilities are suitable for qualification of TRACG.

* Some non prototypic heat leakage from the main vent pipe to the WW gas space for portions of the PANDA P tests resulted in non representative phenomena for short periods. Once observed, they were eliminated by closing the main vent valve (see the ESBWR Test Report [11-1] for details.

12.0 REFERENCES

[1-1] GE Nuclear Energy, *ESBWR Design Description*, NEDC-33084P, Rev 1, August 2003.

[1-2] B. S. Shiralkar and R. E. Gamble, *ESBWR Test and Analysis Program Description*, NEDC-33079P, August 2002.

[2-1] N. Zuber, *Hierarchical, Two-Tiered Scaling Analysis Appendix D to An Integrated Structure and Scaling Methodology for Severe Accident Technical Issue Resolution,* Nuclear Regulatory Commission Report NUREG/CR-5809, EGG-2659, November 1991.

[3-1] R. E. Gamble, et al., *Scaling of the SBWR Related Tests*, NEDC-32288P, Revision 1, October 1995.

[3-2] P. F. Billig, et al., *SBWR Testing Summary Report,* NEDC-32606P Revision 0, August 2002.

[4-1] T. J. Boucher, M. diMarzo, and L. M. Shotkin, *Scaling Issues for a Thermal-Hydraulic Integral Test Facility*, 19th Water Reactor Safety Information Meeting, Washington, DC, October 30, 1991.

[4-2] M. Ishii and I. Kataoka, *Similarity Analysis and Scaling Criteria for LWR's Under Single-Phase and Two-Phase Natural Circulation*, NUREG/CR-3267, ANL-83-32, 1983.

[4-3] R. L. Kiang, *Scaling Criteria for Nuclear Reactor Thermal Hydraulics*, Nuclear Science and Engneering, 89, 207-216, 1985.

[4-4] G. Kocamustafaogullari and M. Ishii, *Scaling Criteria for Two-Phase Flow Loops and their Application to Conceptual 2x4 Simulation Loop Design*, Nuclear Technology, 65, 146-160, 1984.

[4-5] G. Yadigaroglu, *Derviation of General Scaling Criteria for BWR Containment Tests* 4th International Conference on Nuclear Engineering, New Orleans, LA, March 13-14, 1996.

[5-1] GE Nuclear Energy, *TRACG Qualification for SBWR*, NEDC-32725P, Rev. 1, August 2002.

[5-2] GE Nuclear Energy, *TRACG Qualification for ESBWR*, NEDC-33080P, August 2002.

[5-3] J. G. M. Andersen et al., *TRACG Qualification,* Licensing Topical Report, NEDE-32177P, Rev. 3, August 2007.

[5-4] *Mark III LOCA-Related Hydrodynamic Load Definition,* Nuclear Regulatory Commission Report NUREG 0978, August 1984.

[5-5] P. F. Billig, *Simplified Boiling Water Reactor (SBWR) Program Gravity-Driven Cooling System (GDCS) Integrated Systems Test – Final Report,* GE Nuclear Energy Report GEFR-00850, October 1989.

[5-6] P. F. Peterson, V. E. Schrock., and R. Greif., *Scaling for Integral Simulation of Mixing in Large, Stratified Volumes*, NURETH 6, Proc. Sixth Int. Topical Meeting on Nuclear Reactor Thermal Hydraulics, 5-8 Oct. 1993, Grenoble, France, Vol. 1, pp. 202-211.

[5-7] S. Lomperski, *PANDA Facility Characterization Vessel Heat Loss Measurements*, ALPHA-519-0, November 1997.

[5-8] K. M. Vierow and V. E. Schrock, *Condensation in a Natural Circulation Loop with Noncondensable Gases-Part I – Heat Transfer*, Proc. Of the Int. Conf. On Multiphase Flows, V. 1, pp. 183-190, Tsukuba, Japan, September 1991.

[7-1] W. Wulff and U.S. Rohatgi, *System Scaling for the Westinghouse AP600 Pressurized Water Reactor and Related Test Facilities,* NUREG-SS-11, BNL-NUREG-52550, September 1997.

[8-1] *GIRAFFE SBWR System Interaction Test Report*, NEDC-32504P, June 1996.

[8-2] B. S. Shiralkar and Y. K. Cheung, *TRACG Application for ESBWR*, NEDC-33083P-A, March 2005.

[8-3] GE Nuclear Energy, *Response to NRC Request for Additional Information Letter No. 4 Related to ESBWR Design Certification Application – ESBWR Scaling Analysis RAI Number 6.3-1,* MFN 06-225, Enclosure 1, July 18, 2006.

[10-1] M. di Marzo, *A Simplified Model of the BWR Depressurization Transient*, Nuclear Engineering and Design, 205, 107-114, 2001.

[10-2] F. J. Moody, *Introduction to Unsteady Thermofluid Mechanics*, John Wiley & Sons, New York, 1990.

[10-3] GE Hitachi Nuclear Energy, *ESBWR Design Control Document*, Tier 2, Revision 4, September 2007.

[11-1] J. R. Fitch, et al, *ESBWR Test Report*, NEDC-33091P, August 2002.

Appendix A – Detailed Results[9]

Table A-1 Reference Values for RPV Liquid Mass During Late Blowdown

[[

]]

[9] The absence of any potential inflow or outflow quantity, or any parameter, in Tables A-1 through A-14 implies that the value of the variable/parameter equals zero for the ESBWR and the associated tests.

Table A-2 RPV Liquid Mass PI-Groups During Late Blowdown

Π Groups	ESBWR (4500 MWt)	ESBWR (4000 MWt)	GIRAFFE/ SIT	GIST
$\Pi_{M,\dot{Q},decayheat}$	0.348	0.218	0.212	0.207
$\Pi_{M,\dot{Q},storedenergy}$	0.506	0.391	0.320	0.537
$\Pi_{M,W,Break}$	-0.268	-0.219	-0.199	-0.214
$\Pi_{M,W,GDCS}$	0	0	0	0
$\Pi_{M,sub,GDCS}$	0	0	0	0
$\Pi_{M,W,SLCS}$	0.283	0	0	0
$\Pi_{M,sub,SLCS}$	0.080	0	0	0
$\Pi_{M,\dot{P}1}$	-0.020	-0.024	-0.024	-0.011
$\Pi_{M,\dot{P}2}$	1	1	1	1
$\Pi_{M,W,ICreturn}$	0.164	0.120	0	0
$\Pi_{M,sub,ICreturn}$	0.029	0.021	0	0

Table A-3 Reference Values for RPV Liquid Mass During GDCS Transition

[[

]]

Table A-4 RPV Liquid Mass PI-Groups During GDCS Transition

Π Groups	ESBWR (4500 MWt)	ESBWR (4000 MWt)	GIRAFFE/ SIT	GIST
$\Pi_{M,\dot{Q},decayheat}$	0.841	0.679	0.736	0.392
$\Pi_{M,\dot{Q},storedenergy}$	0.479	0.355	0.451	0.687
$\Pi_{M,W,Break}$	-0.355	-0.366	0	-0.205
$\Pi_{M,W,GDCS}$	1.71	1.64	3.08	0.626
$\Pi_{M,sub,GDCS}$	0.325	0.325	0.610	0.095
$\Pi_{M,W,SLCS}$	0.198	0	0	0
$\Pi_{M,sub,SLCS}$	0.038	0	0	0
$\Pi_{M,\dot{P}1}$	-0.010	-0.013	-0.013	-0.010
$\Pi_{M,\dot{P}2}$	1	1	1	1
$\Pi_{M,W,ICreturn}$	0.238	0.236	0	0
$\Pi_{M,sub,ICreturn}$	0.021	0.023	0	0

Table A-5 Reference Values for RPV Liquid Mass During Full GDCS

[[

]]

Table A-6 RPV Liquid Mass PI-Groups During Full GDCS

Π Groups	ESBWR (4500 MWt)	ESBWR (4000 MWt)	GIRAFFE/ SIT	GIST
$\Pi_{M,\dot{Q},decayheat}$	0.113	0.098	0.079	0.256
$\Pi_{M,\dot{Q},storedenergy}$	0	0	0.002	0.009
$\Pi_{M,W,Break}$	-0.037	-0.040	0	-0.099
$\Pi_{M,W,GDCS}$	1	1.01	1.00	1.10
$\Pi_{M,sub,GDCS}$	0.160	0.175	0.166	0.147
$\Pi_{M,\dot{P}1}$	0.0	-0.0001	-0.0001	-0.0002
$\Pi_{M,\dot{P}2}$	0.0	0.007	0.010	0.021
$\Pi_{M,W,ICreturn}$	0.024	0.028	0	0
$\Pi_{M,sub,ICreturn}$	0.000	0.002	0	0

Table A-7 Reference Values for RPV Pressure During Late Blowdown

[[

]]

Table A-8 RPV Pressure Rate PI-Groups During Late Blowdown

Π Groups	ESBWR (4500 MWt)	ESBWR (4000 MWt)	GIRAFFE/SIT	GIST
$\Pi_{P,\dot{Q},decayheat}$	-0.302	-0.184	-0.180	-0.194
$\Pi_{P,\dot{Q},storedenergy}$	-0.439	-0.331	-0.272	-0.503
$\Pi_{P,\dot{V}}$	0	0	0	0
$\Pi_{P,Wh,ADS}$	1	1.00	1.00	1.00
$\Pi_{P,mech,ADS}$	0.024	0.030	0.029	0.013
$\Pi_{P,Wh,Break}$	-0.004	-0.004	-0.004	-0.002
$\Pi_{P,mech,Break}$	0.005	0.005	0.005	0.003
$\Pi_{P,Wh,ICinlet}$	0.140	0.099	0	0
$\Pi_{P,mech,ICinlet}$	0.003	0.003	0	0
$\Pi_{P,Wh,ICreturn}$	0.027	0.020	0	0
$\Pi_{P,mech,ICreturn}$	-0.003	-0.003	0	0
$\Pi_{p,\ Wh,\ SLCS}$	0.073	0	0	0
$\Pi_{p,\ mech,\ SLCS}$	-0.006	0	0	0

Table A-9 Reference Values for RPV Pressure During GDCS Transition

[[

]]

Table A-10 RPV Pressure Rate PI-Groups During GDCS Transition

Π Groups	ESBWR (4500 MWt)	ESBWR (4000 MWt)	GIRAFFE/SIT	GIST
$\Pi_{P,\dot{Q},decayheat}$	-0.764	-0.605	-0.653	-0.373
$\Pi_{P,\dot{Q},storedenergy}$	-0.435	-0.316	-0.400	-0.653
$\Pi_{P,\dot{V}}$	0	0	0	0
$\Pi_{P,Wh,ADS}$	1	1.00	1.00	1.00
$\Pi_{P,mech,ADS}$	0.011	0.015	0.015	0.006
$\Pi_{P,Wh,GDCS}$	0.309	0.307	0.575	0.093
$\Pi_{P,mech,GDCS}$	-0.017	-0.021	-0.041	-0.004
$\Pi_{P,Wh,Break}$	-0.003	-0.004	0	-0.001
$\Pi_{P,mech,Break}$	0.004	0.005	0	0.001
$\Pi_{P,Wh,ICinlet}$	0.214	0.208	0	0
$\Pi_{P,mech,ICinlet}$	0.002	0.003	0	0
$\Pi_{P,Wh,ICreturn}$	0.021	0.023	0	0
$\Pi_{P,mech,ICreturn}$	-0.002	-0.003	0	0
$\Pi_{p,\ Wh,\ SLCS}$	0.036	0	0	0
$\Pi_{p,\ mech,\ SLCS}$	-0.002	0	0	0

Table A-11 Reference Values for WW Pressure During Long Term/PCCS

[[

]]

Table A-12 WW Pressure Rate PI-Groups During Long-Term/PCCS

Π Groups	ESBWR (4500 MWt)	ESBWR (4000 MWt)	GIRAFFE/ He	PANDA M1	PANDA P3
$\Pi_{P,Wh,VB}$	1.068	0.884	1.07*	1.03*	1.07*
$\Pi_{P,mech,VB}$	0.613	0.683	0.649*	0.654*	0.623*
$\Pi_{P,Wh,Bubbles}$	0.0003	0.001	0.014	0.019	0.0001
$\Pi_{P,mech,Bubbles}$	0.039	0.118	0.181	0.249	0.002
$\Pi_{P,Wh,poolsurf}$	0.056	1.24	0	1.09	0.887
$\Pi_{P,mech,poolsurf}$	0.034	0.903	0	0.600	0.516
$\Pi_{P,\dot{Q},poolsurf}$	0.195	0.193	0	0.092	0.074
$\Pi_{P,Wh,structures}$	-2.855	-4.25	0	-2.95	-2.31
$\Pi_{P,mech,structures}$	-1.725	-3.09	0	-1.63	-1.40
$\Pi_{P,\dot{Q},structures}$	-0.250	-0.264	0	-0.267	-0.213
$\Pi_{P,\dot{V}}$	0	0	0	0	0
$\Pi_{P,y,n/c}$	0.030	0.085	0.153	0.212	0.001

* The PI parameter value is based upon the use of a $W_{VB,o}$ value that is geometrically-proportioned to the corresponding ESBWR value. The test facilities did not simulate a vacuum breaker operation.

Table A-13 Reference Values for DW Pressure During Long Term/PCCS

[[

]]

Table A-14 DW Pressure Rate PI-Groups During Long Term/PCCS

Π Groups	ESBWR (4500 MWt)	ESBWR (4000 MWt)	GIRAFFE/ He	PANDA M3	PANDA P1
$\Pi_{P,Wh,decayheat}$	-6.712	56.0	71.5	77.6	0.776
$\Pi_{P,mech,decayheat}$	723.571	670	590	425	440
$\Pi_{P,Wh,PCCinlet}$	0	0	0	0	0
$\Pi_{P,mech,PCCinlet}$	-714	-682	-744	-442	-457
$\Pi_{P,Wh,structures}$	0.095	-0.993	-19.0	-3.07	-0.042
$\Pi_{P,mech,structures}$	-9.579	-11.9	-154	-16.5	-17.7
$\Pi_{P,\dot{Q},structures}$	-0.002	-0.004	-0.141	-0.018	-0.0002
$\Pi_{P,\dot{V}}$	0	0	0	0	0
$\Pi_{P,y,n/c}$	-0.034	-0.166	-0.143	-0.202	-0.001
$\Pi_{P,mech,MV}$	-0.054	-0.141	-0.191	-0.261	-0.002
$\Pi_{P,mech,VB}$	-0.946	-0.993	-0.763	-0.760	-0.900

Enclosure 5

MFN 08-419

Affidavit

James C. Kinsey

GE Hitachi Nuclear Energy

AFFIDAVIT

I, James C. Kinsey, state as follows:

(1) I am the Vice President, ESBWR Licensing, GE Hitachi Nuclear Energy ("GEH") and have been delegated the function of reviewing the information described in paragraph (2) which is sought to be withheld, and have been authorized to apply for its withholding.

(2) The information sought to be withheld is contained in Enclosure 3 of GEH letter MFN 08-419, Mr. James C. Kinsey to U.S. Nuclear Regulatory Commission, *Response to Portion of NRC Request for Additional Information Letter No. 120 Related to ESBWR Design Certification Application - Emergency Core Cooling Systems - RAI Number 6.3-1 S01,* dated May 1, 2008. GEH proprietary information is identified in Enclosure 3, *NEDC-33082P, Revision 2 - ESBWR Scaling Report, April 2008 - GEH Proprietary Information,* by a dotted underline inside double square brackets. The electronic version includes a dark red font inside the brackets. For black-grayscale printed copies, the red font and dotted underline appears similar to normal text. [[This sentence is an example. {3}]] Figures and large equation objects are identified with double square brackets before, and after the object. In each case, the superscript notation {3} refers to paragraph (3) of this affidavit, which provides the basis of the proprietary determination. Specific information that is not so marked is not GEH proprietary. A non-proprietary version of this information is provided in Enclosure 4, *NEDO-33082, Revision 2 - ESBWR Scaling Report, April 2008 - Non-Proprietary Information.*

(3) In making this application for withholding of proprietary information of which it is the owner, GEH relies upon the exemption from disclosure set forth in the Freedom of Information Act ("FOIA"), 5 USC Sec. 552(b)(4), and the Trade Secrets Act, 18 USC Sec. 1905, and NRC regulations 10 CFR 9.17(a)(4), and 2.790(a)(4) for "trade secrets" (Exemption 4). The material for which exemption from disclosure is here sought also qualify under the narrower definition of "trade secret", within the meanings assigned to those terms for purposes of FOIA Exemption 4 in, respectively, Critical Mass Energy Project v. Nuclear Regulatory Commission, 975F2d871 (DC Cir. 1992), and Public Citizen Health Research Group v. FDA, 704F2d1280 (DC Cir. 1983).

(4) Some examples of categories of information which fit into the definition of proprietary information are:

a. Information that discloses a process, method, or apparatus, including supporting data and analyses, where prevention of its use by GEH's competitors without license from GEH constitutes a competitive economic advantage over other companies;

b. Information which, if used by a competitor, would reduce his expenditure of resources or improve his competitive position in the design, manufacture, shipment, installation, assurance of quality, or licensing of a similar product;

c. Information which reveals aspects of past, present, or future GEH customer-funded development plans and programs, resulting in potential products to GEH;

d. Information which discloses patentable subject matter for which it may be desirable to obtain patent protection.

The information sought to be withheld is considered to be proprietary for the reasons set forth in paragraphs (4)a., and (4)b, above.

(5) To address 10 CFR 2.390(b)(4), the information sought to be withheld is being submitted to NRC in confidence. The information is of a sort customarily held in confidence by GEH, and is in fact so held. The information sought to be withheld has, to the best of my knowledge and belief, consistently been held in confidence by GEH, no public disclosure has been made, and it is not available in public sources. All disclosures to third parties including any required transmittals to NRC, have been made, or must be made, pursuant to regulatory provisions or proprietary agreements which provide for maintenance of the information in confidence. Its initial designation as proprietary information, and the subsequent steps taken to prevent its unauthorized disclosure, are as set forth in paragraphs (6) and (7) following.

(6) Initial approval of proprietary treatment of a document is made by the manager of the originating component, the person most likely to be acquainted with the value and sensitivity of the information in relation to industry knowledge, or subject to the terms under which it was licensed to GEH. Access to such documents within GEH is limited on a "need to know" basis.

(7) The procedure for approval of external release of such a document typically requires review by the staff manager, project manager, principal scientist or other equivalent authority, by the manager of the cognizant marketing function (or his delegate), and by the Legal Operation, for technical content, competitive effect, and determination of the accuracy of the proprietary designation. Disclosures outside GEH are limited to regulatory bodies, customers, and potential customers, and their agents, suppliers, and licensees, and others with a legitimate need for the information, and then only in accordance with appropriate regulatory provisions or proprietary agreements.

(8) The information identified in paragraph (2), above, is classified as proprietary because it identifies the models and methodologies GEH will use in evaluating the consequences of design basis accidents (DBAs) for the ESBWR. GEH and its partners performed significant additional research and evaluation to develop a basis for these revised methodologies to be used in evaluating the ESBWR over a period of several years at a cost of over one million dollars.

The development of the evaluation process along with the interpretation and application of the analytical results is derived from the extensive experience database that constitutes a major GEH asset.

(9) Public disclosure of the information sought to be withheld is likely to cause substantial harm to GEH's competitive position and foreclose or reduce the availability of profit-making opportunities. The information is part of GEH's comprehensive BWR safety and technology base, and its commercial value extends beyond the original development cost. The value of the technology base goes beyond the extensive physical database and analytical methodology and includes development of the expertise to determine and apply the appropriate evaluation process. In addition, the technology base includes the value derived from providing analyses done with NRC-approved methods.

The research, development, engineering, analytical and NRC review costs comprise a substantial investment of time and money by GEH.

The precise value of the expertise to devise an evaluation process and apply the correct analytical methodology is difficult to quantify, but it clearly is substantial.

GEH's competitive advantage will be lost if its competitors are able to use the results of the GEH experience to normalize or verify their own process or if they are able to claim an equivalent understanding by demonstrating that they can arrive at the same or similar conclusions.

The value of this information to GEH would be lost if the information were disclosed to the public. Making such information available to competitors without their having been required to undertake a similar expenditure of resources would unfairly provide competitors with a windfall, and deprive GEH of the opportunity to exercise its competitive advantage to seek an adequate return on its large investment in developing these very valuable analytical tools.

I declare under penalty of perjury that the foregoing affidavit and the matters stated therein are true and correct to the best of my knowledge, information, and belief.

Executed on this 1st day of May 2008.

James C. Kinsey

James C. Kinsey
GE Hitachi Nuclear Energy